THE DEFORMATIONAL BEHAVIOR AND CONSTITUTIVE EQUATION OF CONCRETE BASED ON THE ELASTO-PLASTIC AND FRACTURE MODEL

A DISSERTATION

SUBMITTED TO UNIVERSITY OF TOKYO
IN PARTIAL FULFILLMENT OF THE REQUIREMENTS

for the degree

DOCTOR OF ENGINEERING

Field of Civil Engineering

by KOICHI MAEKAWA

Technological University of Nagaoka
Nagaoka, Niigata Pref. Japan

April, 1985

SYNOPSIS

Biaxial loading tests of concrete under compression-tension stress states were carried out for collecting the fundamental data to formulate the plane stress constitutive equations for concrete. The non-proportional stress paths were newly adopted to make clear the anisotropic behavior of concrete quantitatively.

According to the test results, the elasto-plastic and fracture constitutive equations which describe the progress of the plasticity and the fracture are formulated. A new system of flow rules, which define the directional correlations of the stress and strain vectors, is also proposed for formulating the anisotropy of concrete.

By organizing those constitutive equations, the plane stress constitutive law is derived, and its applicability is verified by the numerical analysis of the finite element method and the experimental data including stress paths where the principal stress direction continuously and intermittently rotates.

CONTENTS

1. Introduction

Many years have passed since Scordelis applied the finite element method (FEM) to the analysis of reinforced concrete beams in 1967(1). During the last few years, the numerical method of analyzing nonlinear problems has made a great advance and the studies for mathematical models necessary for the FEM analysis of reinforced concrete structures have been executed. Constitutive model and failure criteria of concrete, shear transfer across a cracking in concrete, bond between concrete and reinforcing bars are typical mathematical models.

The FEM analysis is used to simulate the behavior of large-scale structures for design purposes and the behavior of reinforced concrete members under various external actions for investigating the mechanics. The numerical method of predicting the behavior of structures based on the microscopic mechanical characteristics is attractive for researchers because it gives the unified analytical method. During the last ten years, a lot of studies concerning the numerical analysis have been carried out, however, unified analytical method is not yet completely established. It is because the mechanical characteristics of constituent materials are not completely investigated by experiments, and because there exist some problems in regard to the numerical method to represent the nonlinearity of the mathematical models. Especially, constitutive laws of concrete, shear transfer and dilatancy on cracked faces of concrete, bond and dowel actions between concrete and reinforcement are to be investigated, and modelling of crack in FEM analysis, nonlinear analytical method including strain-softening and the mathematical model to express the difference of stress-strain relations of concrete due to the size of the finite elements should be solved.

This paper deals with the constitutive equations of concrete under the plane stress condition, one of the most basic problems for the finite element analysis of reinforced concrete structures. The behavior of concrete under multiaxial stress states have been studied since an early age. Among these studies, the exerimental studies by Kupfer et al. in 1969(2) is wellknown. Since the study of Kupfer et al., biaxial and triaxial loading tests of concrete have been executed, and their main objective has been to get the failure envelope indicated by stresses. On the other side, a lot of multiaxial constitutive models of concrete have been reported such as the hypo-elastic model (isotropic nonlinear elastic model (3),(4),(5), anisotropic model(6), equivalent uniaxal model(7), etc.), the elasto-plastic model(8),(9),(10), Endocronic model(11), plastic fracturing model(12) and so on.

The behavior of the reinforced concrete structures often depends on the

deformation and failure of concrete element under high compression tension stress state(15). But the previously reported models and experiments are not careful enough for the characteristics of this state. The objectives of this research are to investigate the behavior of concrete under compression-tension stress states with an experimental approach and to formulate the constitutive equations for concrete with high accuracy.

In the previously reported biaxial loading tests(2),(13),(14),(16), the stress paths have been limited in the very special case, where the ratio of the principal stresses is constant and the principal direction is fixed in the loading hysteresis. If we adopt only this type of stress hysteresis, the anisotropic behavior of concrete and the path-dependent deformational characteristics of concrete can not be made clear.

Taking these situations into consideration, the author chose non-proportional stress paths, and for the first time in this research, the principal axis rotation tests were carried out.

According to the test results, the elasto-plastic and fracture constitutive equation is proposed. This equation describes the relation between the degree of the stress and strain vectors in taking the path-dependent deformational characteristics of concrete into account. A new system of flow rules which formulate the directional correlation of stress and strain vectors is also proposed. The proposed flow rule system is constructed by four equations and takes the anisotropy of concrete into account.

By solving the elasto-plastic and fracture equation and the four flow rule equations simultaneously, plane stress constitutive equations are derived and their applicability are verified by the experimantal data.

2. Deformational Behavior of Concrete under Biaxial Stress States (Compression-Tension Area)

2.1 Experiments

2.1.1 Difficulties in the test

In all the series of experiments, biaxial compressive and tensile forces were applied to concrete plates and strains were measured by strain guages. The precision and reliability of this kind of experiment depend very much on the creation of uniform stress and strain fields in concrete specimens. Actually it is quite difficult to create the uniform stress condition, therefore, it took more than one year to get the reliable data with reasonable accuracy.

In the first place, the friction between concrete specimens and loading plates must be eliminated as far as possible. To eliminate the friction at the contact faces where tensile forces were applied, authors sought for materials with higher tensile strength and lower stiffness than those of concrete. One-way fiber reinforced plastics were examined, but, finally natural wood was selected for the material to cut the friction.

In the second place, local splitting at the adhesive face must be avoided when the tensile force is transmitted to concrete through the wooden appalatus for eliminating the friction. It is not desirable to apply tensile forces to the face where the local tensile strength is lowered due to bleeding of concrete.

In the third place, it is important to make specimens with the precision of shape in a high order. Especially, corners of the specimens must be angled as right as possible. If the precision of test specimens is not guaranteed, it is impossible to create the uniform biaxial stress and strain fields within acceptable accuracy.

In the forth place, in order to eliminate the eccentricity, it is necessary to keep the axes of compressive and tensile forces through the center of the specimen at any time of loading.

Strictly speaking, it is impossible to solve these problems completely. However, within a certain acceptable limit from an engineering point of view, these problems have been solved.

2.1.2 Test specimens

Concrete plates 200mm x 200mm x 50mm were used for experiments. This concrete specimen has the same dimensions as Kupfer's experiment(2).

Therefore, experimental data may be compared with each other. To ensure the finishing precision of specimens, a special metal mould with finishing precision of 1/100mm were used. Fresh concrete was placed on the metal mould where cement powder was sprinkled on the inner faces of the metal mould to control the decrease of the tensile strength near the faces of the mould by bleeding of conrete.

During a week after placing, specimens were cured in water. Four or five weeks later, specimens were used for tests after drying in a laboratory. Mixture of concrete used are shown in Table 1. Uniaxial compressive strength was between 27 and 35 Mpa.

2.1.3 Cutting of friction

The compressive force was applied to concrete specimens through the loading plates. To reduce the contact friction, two sheets of teflons (0.1mm and 0.5mm thick) with silicon grease were set between the loading plate and concrete specimens. In order to prevent the injection of silicon grease into the specimen and the increase of conctact friction, paraffin was impregnated into B and D faces for coating as shown in Fig.1.

The tensile force was transmitted to concrete specimens through the wooden brushes as shown in Fig.2. This brush was placed between the concrete specimen (A and C faces in Fig.1) and the loading plates as shown in Fig.2 with epoxy type adhesive agent. The wooden brushes were designed with reference to the steel brushes by Kupfer et.al(2). The tensile strength of the wood used was about 60-70 Mpa and the modulus of the bending elasticity was $60\text{-}75 \times 10^2$ Mpa. To reduce the stiffness, cuttings were made as shown in Fig.2. The shape of the tooth section is 8.1mm x 11.0mm and the depth is 30mm. Faces A and C in Fig.1 were scraped by 1.5mm deep so that tensile force may be directly transmitted to the coase aggregates and mortar. Epoxy resin between the teeth of a brush was wiped out before hardening.

2.1.4 Loading system

The loading system of this experiment is shown in Fig.3. Two sheets of concrete specimens were used and biaxial compressive and tensile forces are simultaneously applied. Two center-hole type jacks introduced the tensile force to concrete specimens. In order to prevent the eccentricity of load, the same amount of oil was supplied to the two jacks. To follow the movement of the cylinder head of the compressive jack, two center-hole type jacks were fixed to the head of the compressive jack by the steel frames. The objective

Table 1. Mixtures of concrete used.

Type	W/C(%)	W(N)	C(N)	s/a(%)	G(N)	S(N)
A	50	1800	3620	47	9500	8270
B	60	1800	3000	48	9900	9130
C	50	1740	3480	47	9670	8420
D	45	1800	4000	47	9490	8260

High Early Strength Portland Cement used
Maximum Size of Coase Aggregates: 15mm

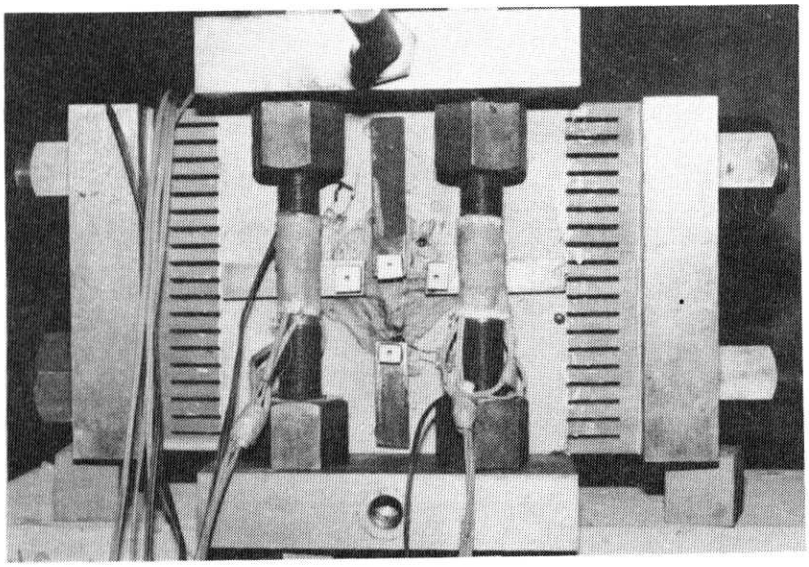

Fig.2. Wooden brush and test specimen.

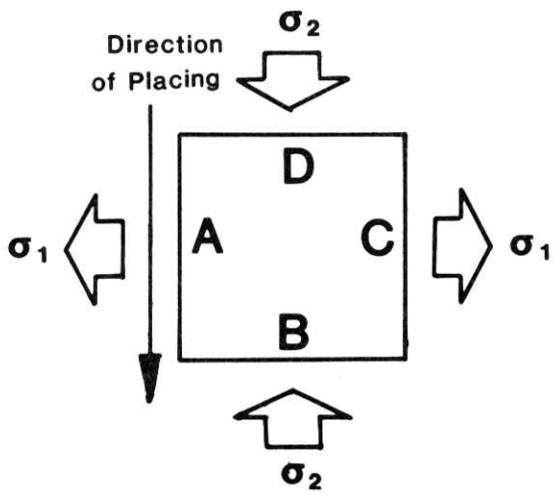

Fig.1. Directions of applied biaxial stresses.

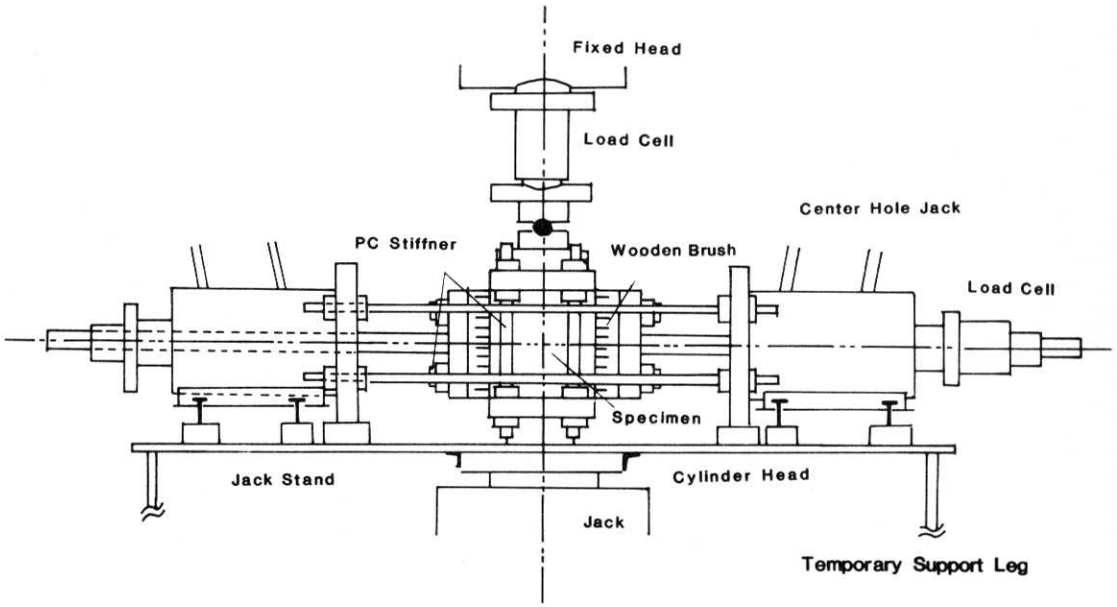

Fig.3. Biaxial loading system.

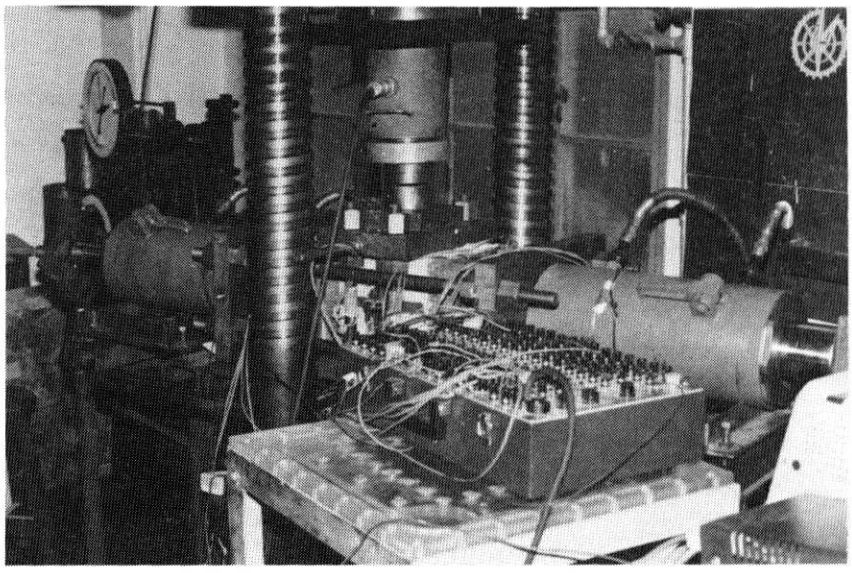

of this arrangement of jacks as shown in Fig.3 is to eliminate the eccentricity of compressive and tensile forces even when the concrete specimens were deformed during the loading. Applied forces were distributed by the bearing plates. Two compressive loading plates were connected by four prestressing bars, and two tensile loading plates were linked by two prestressing bars. These bars increase the stiffness of the total system of the biaxial loading apparatus and make it possible to get the data under the stable situation near the failure conditions of concrete.

The strains of concrete specimens and prestressing stiffners were measured by wire strain guages. The displacement-type transducers were set on the specimens to supplement the measurement of strains in the area of large deformations. Loading speed was set approximately 0.2 Mpa per second. The experimental data such as strains, stresses, loading speed were scanned with the interval of about 4 second and the real time analysis of data was carried out by an 8 bit micro-processor and the results were always displayed on console. With the updated information from the micro-processor, the operators controled the oil pumps of the jacks according to the loading programs.

2.2 Deformational characteristics of concrete under monotonic loading

2.2.1 Loading paths to get the biaxial stiffnesses and biaxial Poisson's ratios

Most of the reported biaxial loading tests concerning the concrete behavior were carried out under a special loading hystory, that is, monotonic and proportional loading where the ratio of two principal stresses was constant at any time of loading. However, from this type of loading paths, the tangential coefficients in the linear system of Eq.(1) cannot be directly obtained from the results of experiments.

$$d\varepsilon_1 = \frac{1}{E_1} d\sigma_1 - \frac{\nu_{12}}{E_2} d\sigma_2$$
$$d\varepsilon_2 = -\frac{\nu_{21}}{E_1} d\sigma_1 + \frac{1}{E_2} d\sigma_2 \qquad (1)$$

where $\varepsilon_1, \varepsilon_2$: principal strains $\varepsilon_1 > \varepsilon_2$

σ_1, σ_2: principal stresses $\sigma_1 > \sigma_2$ (tension is positive).

Even if increments of strains $d\varepsilon_1$, $d\varepsilon_2$ and stresses $d\sigma_1$, $d\sigma_2$ are measured from the proportional loading tests, that is, $d\sigma_1 / d\sigma_2 = \sigma_1 / \sigma_2 =$ constant, four unknown quantities E1, E2, ν_{12} and ν_{21} cannot be uniquely determined since the number of unknown values is larger than the number of equations. In such a

case, to get these values from experimental data, the hypothesis of isotropy and symmetry in the tangential stiffness matrix (E1=E2, $\nu_{12}=\nu_{21}$) is usually assumed. If we use this assumption, we can solve the system of Eq.(1) completely and obtain the four coefficients from experimental data. Because of simplicity, this assumption has been also used in the mathematical expressions of constitutive model of concrete. Strictly speaking, however, the applicability of the assumption of isotropy and symmetry of stiffness to the concrete mechanics has not been verified. Then author adopted two types of loading paths to get the biaxial stiffnesses and biaxial Poisson's ratios explicitly from the experiments.

(1) After uniaxial compressive stress is monotonically applied ($d\sigma_1=0, d\sigma_2\neq 0$), the tensile stress is applied in the direction normal to the principal compressive stress ($d\sigma_1\neq 0, d\sigma_2=0$). This type of loading path gives the information about the effect of the tensile principal stress on the total deformation of concrete. This type of loading path directly gives the tensile tangential stiffness and the tensile Poisson's ratio as

$$E_1=\frac{d\sigma_1}{d\varepsilon_1}, \qquad \nu_{21}=-\frac{d\varepsilon_2}{d\varepsilon_1} \tag{2}$$

where $d\sigma_2=0$, and $d\sigma_1, d\varepsilon_1, d\varepsilon_2$ were measured in experiments.

(2) After uniaxial tensile stress is monotonically applied ($d\sigma_1\neq 0$, $d\sigma_2=0$), the compressive stress is applied ($d\sigma_1=0$, $d\sigma_2\neq 0$) under the constant principal tensile stress state. The compressive stiffness and the compressive Poisson's ratio can be directly calculated by this type of loading paths as

$$E_2=\frac{d\sigma_2}{d\varepsilon_2}, \qquad \nu_{12}=-\frac{d\varepsilon_1}{d\varepsilon_2} \tag{3}$$

where $d\sigma_1=0$, and $d\sigma_2, d\varepsilon_1, d\varepsilon_2$ were measured in experiments.

2.2.2 Tension test under constant compressive stress

The stress-strain diagrams and the loading paths where the compressive principal stress was constant are shown in Fig.4. Two principal stresses are normalized by the peak stress fc under uniaxial monotonic compressive loading and uniaxial tensile strength ft. Two principal strains are also normalized by the compressive strain ε_{c0} which corresponds to the peak stress fc in uniaxial compression. Increments of strains which were newly introduced by the tensile principal stress are shown in Fig.5. The effect of the principal tensile stress on the deformation of concrete under biaxial stress state is clearly

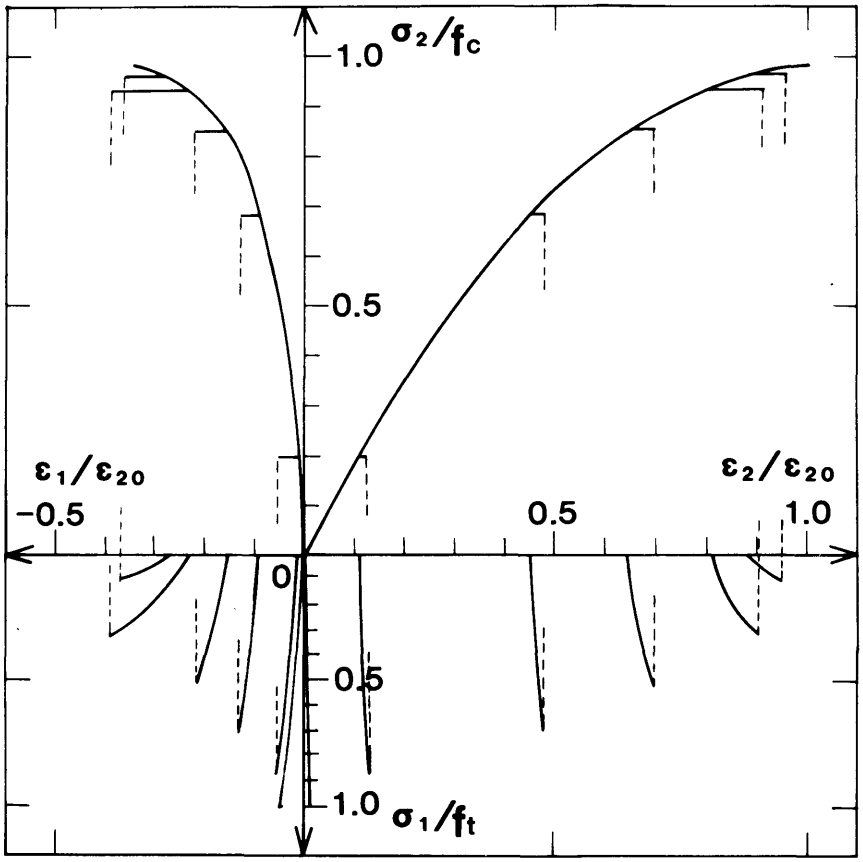

Fig.4. Stress-strain diagram when the principal compressive stress is constant.

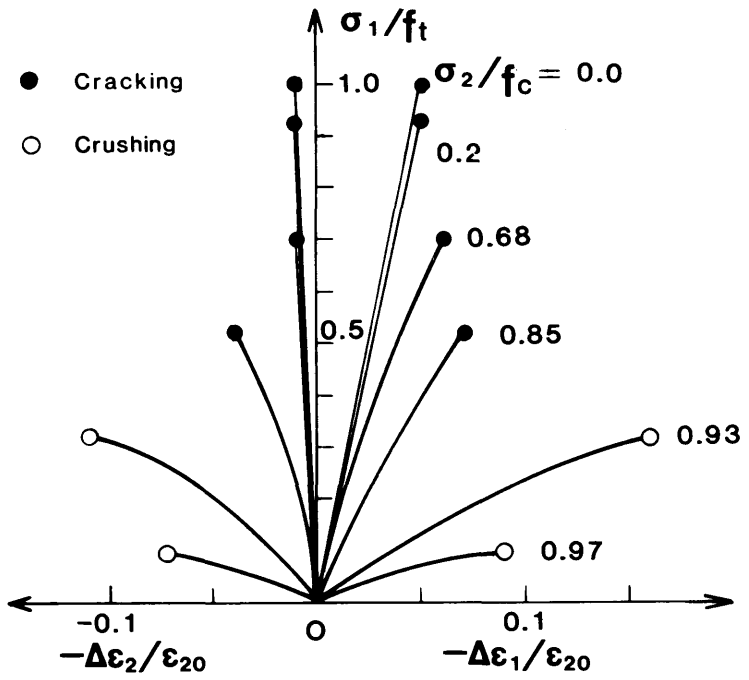

Fig.5. Principal tensile stress and incremental biaxial strains when the principal tensile stress is applied under the constant principal compressive stress.

indicated in this figure. Where the principal compressive strain is low, say $\varepsilon_2/\varepsilon_{20}<0.6$, the relationship between the principal tensile stress and corresponding increments of strains is nearly linear. But, with the increase of the level of principal compressive strain, the nonlinearity appears in these relationships. The deformation of concrete is accelerated by the increase of the tensile stress and the rate of the deformation becomes larger. This deformational characteristics of concrete can be easily expressed by the tangential tensile stiffness E1. The diagrams of the relations between the tensile stiffness and the compressive strain level are shown in Fig.6. The tensile stiffness decreases rapidly as the level of the compressive strain in the direction normal to the increment of tensile stress increases.

In the same way, the tensile Poisson's ratio ν_{21} calculated by Eq.(2) are shown in Fig.7. Where the level of compressive strain is low, the tensile Poisson's ratio is nearly equal to the initial value, but, when the level of the compressive strain $\varepsilon_2/\varepsilon_{20}$ exceeds 0.6, it becomes large rapidly. For the first time, these deformational characteristics were quantitatively measured by using this type of stress paths.

Let us now consider the equivalent uniaxial model of anisotropy (7). According to this type of constitutive model, the tangential tensile stiffness in the direction normal to the uniaxial compressive stress is evaluated as constant and is equal to the initial stiffness. This prediction contradicts with the results of this experiments. A special care should be taken in analyzing the mechanics of concrete by this modelling. In these experimental series, two types of failure modes were observed, say, cracking mode and crushing mode. The cracking mode is defined as the brittle failure mode where a crack rapidly appears in the direction normal to the principal tensile stress. This type of failure mode was observed under the stress condition where the tensile stress is relatively large. The crushing mode is defined as the ductile failure mode where the several distributed cracks appear and the two principal stresses cannot be kept constant at the peak stress condition. This type of mode was observed under high compression-low tension stress state as shown in Fig.5. It is considered that in case of the cracking mode, the failure is mainly introduced by the tensile stress, and compressive stress accelerates this type of failure. On the other side, in case of the crushing mode, the tensile principal stress is considered to help the extension of microcracking which is advanced by the compressive principal stress and at last, the strain-softening behavior starts.

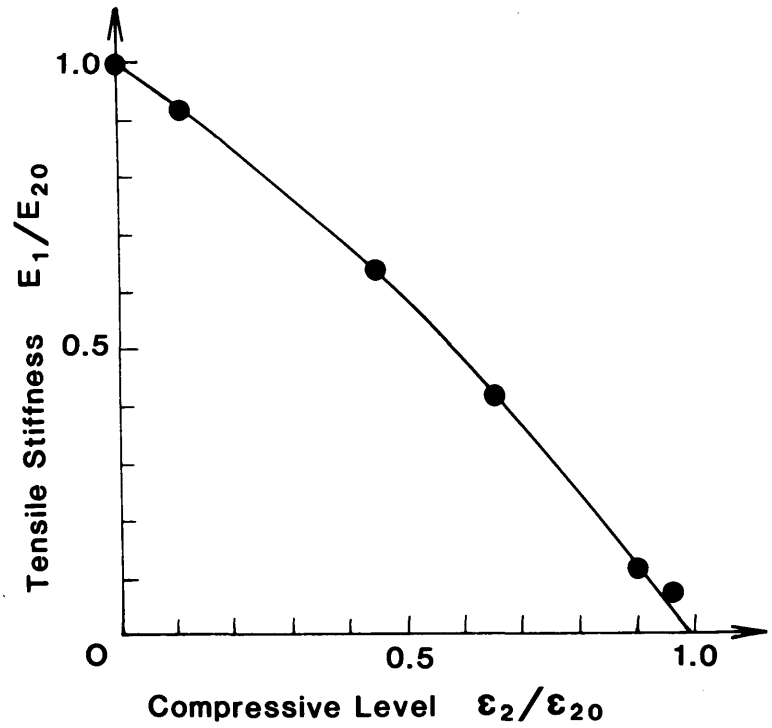

Fig.6. Relation between the tangential tensile stiffness and the compressive level.

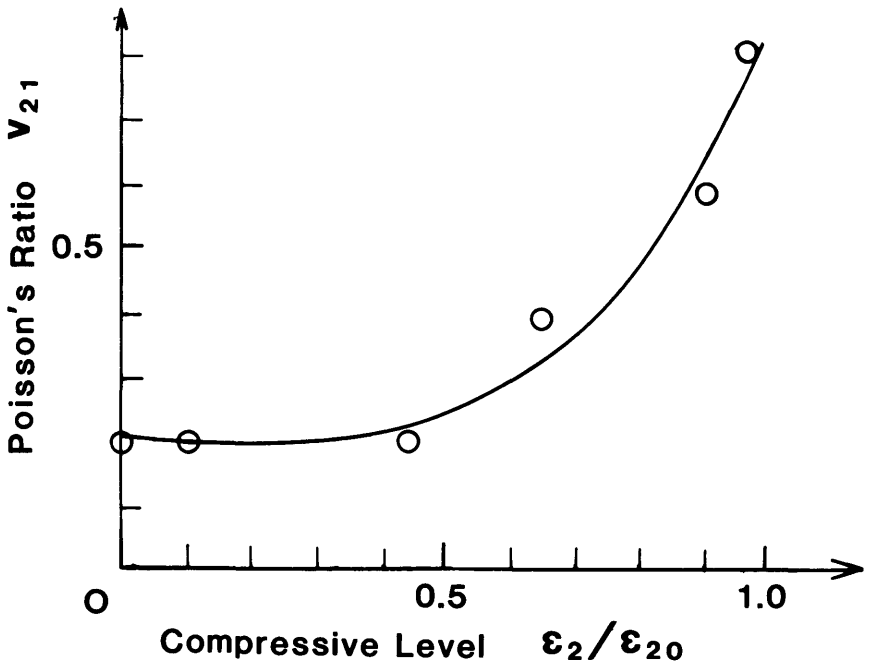

Fig.7. Relation between the tangential Poisson's ratio and the compressive level.

2.2.3 Compression test under constant tensile stress

The stress-strain diagrams and loading paths, where the principal tensile stress was constant, are shown in Fig.8. It is recognized that the tensile principal stress has little influences on the relationship between the compressive stress and strain under low compression level, but on the other hand, when the compressive strain level $\varepsilon_2 / \varepsilon_{20}$ exceeds 0.6, the total deformations are accelerated by the existence of principal tensile stress. The compressive tangential stiffness E2 calculated by Eq.(3) is shown in Fig.9, where E2 decreases as the level of compressive strain increases, and the principal tensile stress accelerates the decreasing rate of the compressive stiffness. This deformational behavior is remarkable in the high compression-tension stress state. The compressive Poisson's ratio is calculated from this experiment and shown in Fig.10. Under biaxial high stress states, the compressive Poisson's ratio increases rapidly when the compressive level $\varepsilon_2/\varepsilon_{20}$ exceeds 0.6 as in the case of the tensile Poisson's ratio. The principal tensile stress seems to advance the increase of the tensile Poisson's ratio.

2.2.4 Anisotropy under biaxial stress states

The biaxial stiffnesses and biaxial Poisson's ratios were obtained by adopting these two special types of loading paths. The biaxial stiffnesses decrease and the values of two Poisson's ratios increase as the compressive deformation level increases. These deformational characteristics are accelerated by the increment of the principal tensile stress. From the two types of loading paths, the ratio of biaxial stiffnesses E1/E2 and that of biaxial Poisson's ratios ν_{21}/ν_{12} at a certain stress or strain condition can be easily obtained. A new test which has the step-type loading paths as shown in Fig.11 was also carried out in order to get the biaxial stiffnesses and Poisson's ratios. The ratio of biaxial stiffnesses, the ratio of biaxial Poisson's ratios and the ratio of the diagonal components in the stiffness matrix, $E_1\nu_{12} / E_2\nu_{21}$, are calculated and shown in Fig.12, Fig.13 and Fig.14 respectively. If the behavior of concrete is isotropic, these ratios of biaxial stiffnesses and diagonal components in stiffness matrix must be equal to unity (E1/E2=1, ν_{12}/ν_{21} =1). According to the test results, concrete behaves isotropically when the stress level is low. But anisotropy becomes significant when the deformation level $\varepsilon_2 / \varepsilon_{20}$ exceeds 0.6 as shown in Fig.12. The decreasing rate of the tensile stiffness exceeds that of the compressive stiffness in compression-tension stress state. Significant differences between the biaxial Poisson's ratios are not observed in Fig.13. The ratio of

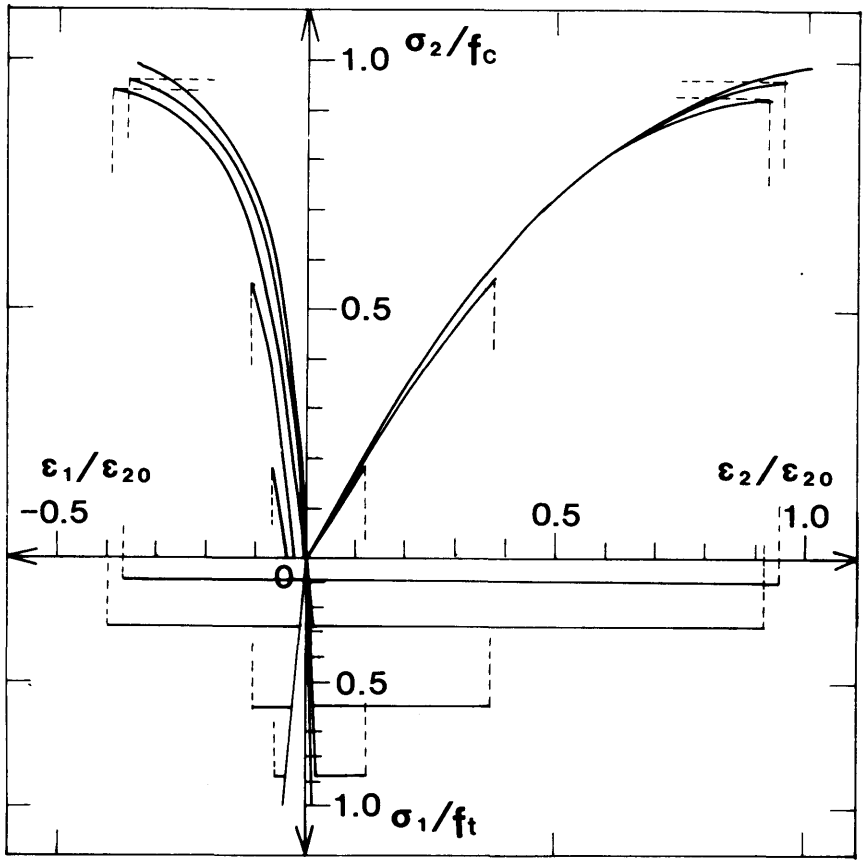

Fig.8. Stress-strain diagram when the principal tensile stress is constant.

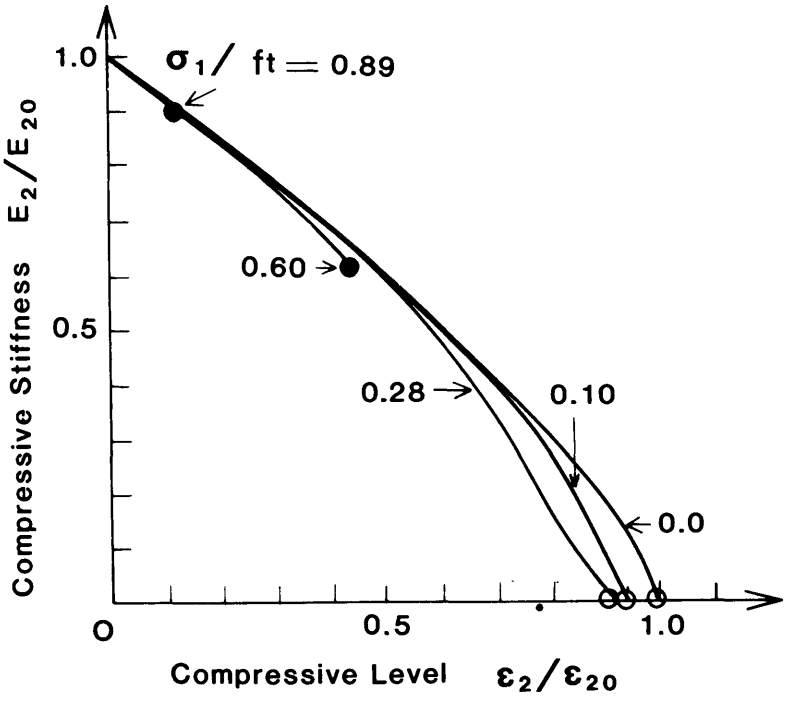

Fig.9. Relation between tangential compressive stiffness and compressive level when the principal tensile stress is constant.

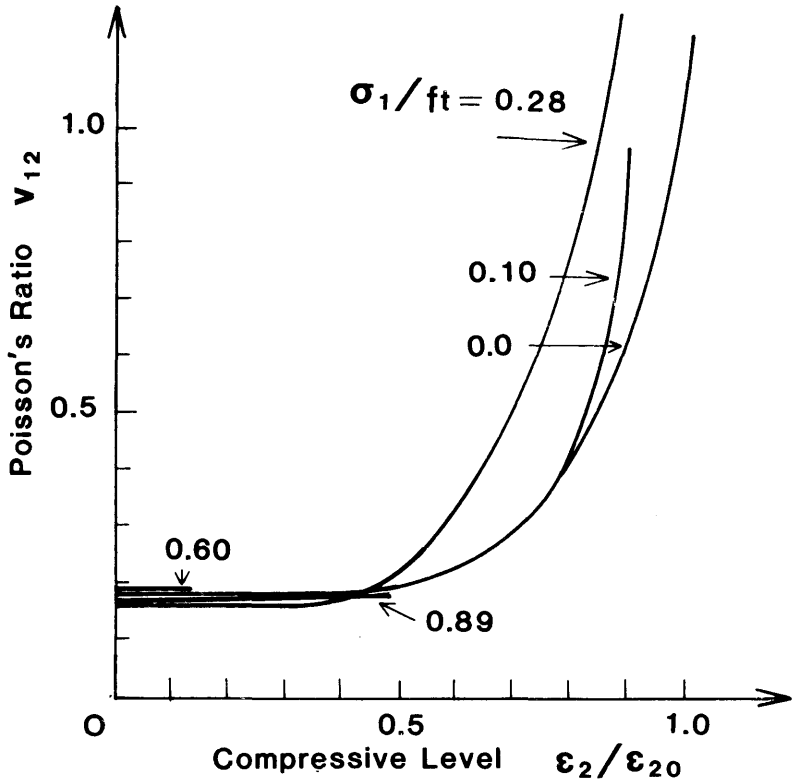

Fig.10 Relation between the tangential Poisson's ratio and the compressive level when the principal tensile stress is constant.

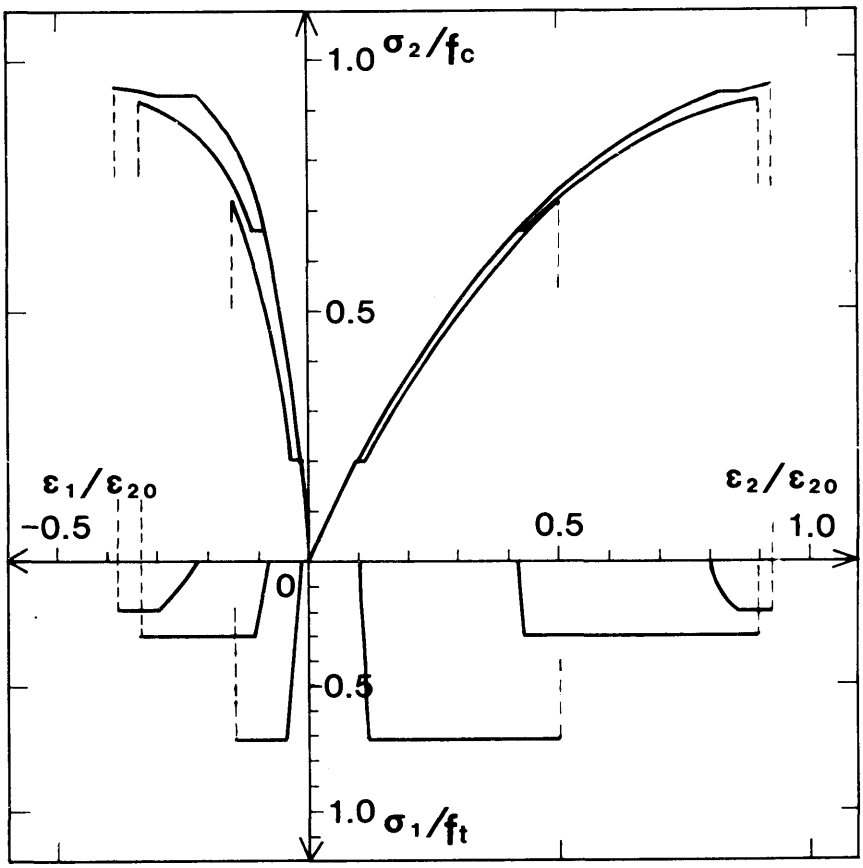

Fig.11. Stress-strain diagrams of step-type loading.

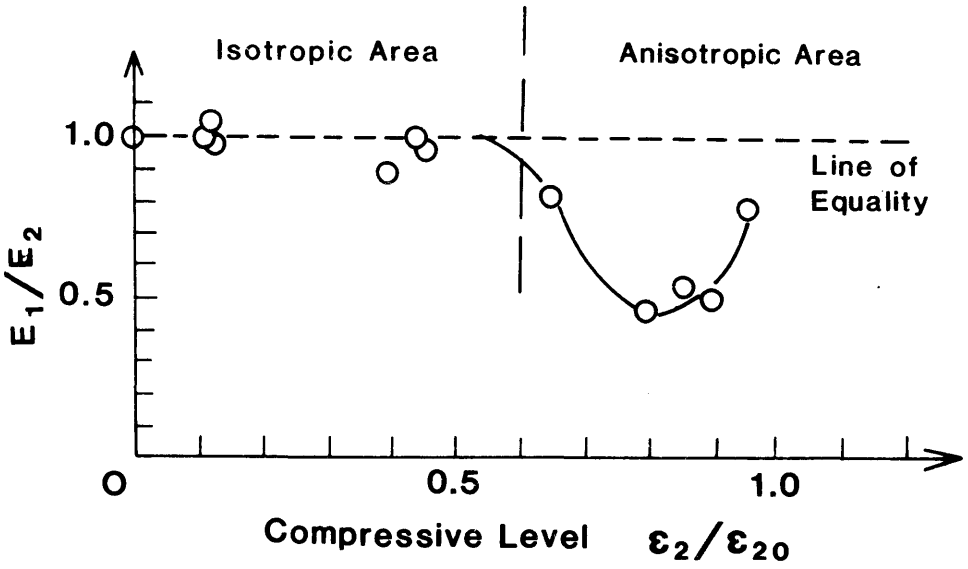

Fig.12. Ratio of the biaxial stiffnesses.

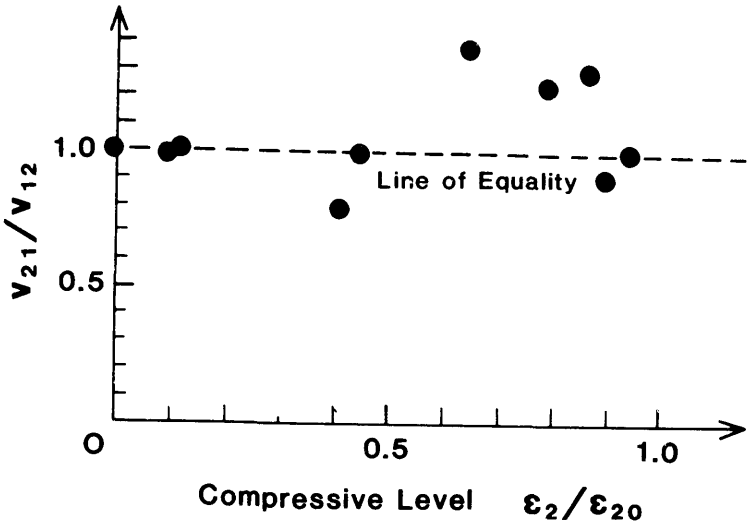

Fig.13. Ratio of the biaxial Poisson's ratios.

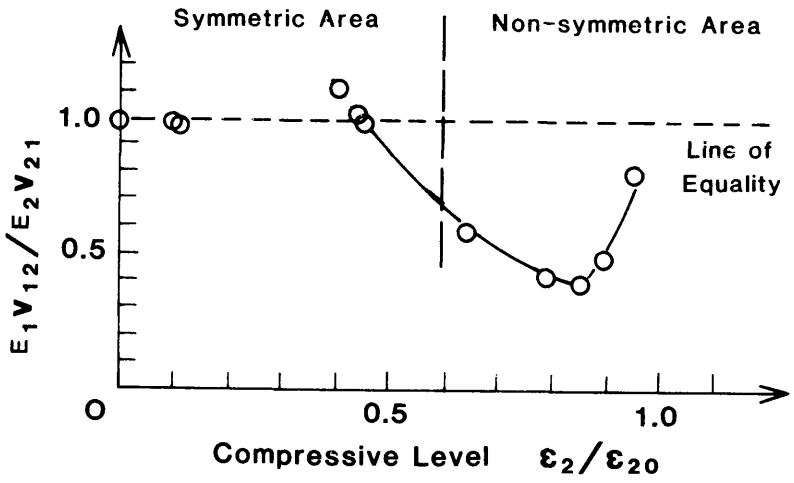

Fig.14. Evaluation of the symmetry of the tangential stiffness matrix.

diagonal components in the stiffness matrix in Eq.(1) deviates from unity under high compression-tension stress state as shown in Fig.14. This experimental result means that the tangential stiffness matrix becomes nonsymmetric under high compression-tension stress state. According to these test results, concrete behavior may be assumed isotropic within a certain compression level, that is , $\varepsilon_2/\varepsilon_{20}<0.6$ or $\sigma_2/fc<0.9$. Under high compression-low tension stress state, concrete constitutive laws should take the anisotropy and nonsymmetry of the biaxial tangential stiffness matrix into consideration. The cause of this type of anisotropy is considered to be the rapid and unstable extension of micro-cracking.

2.2.5 Failure envelope and loading paths

The main objective of the previously reported studies of multiaxial behavior of concrete was to obtain the failure envelope indicated by stresses. The obtained failure envelopes were often used for formulating the plastic potential in the theory of plasticity. The failure envelope obtained in this research is shown in Fig.15 where the data by Kupfer's experiment(2) are also included. The failure envelope on the strain space which corresponds to the envelope indicated by stresses are shown in Fig.15. According to the experimentally obtained failure envelopes and stress-strain paths to these failure envelopes in Fig.15 and Fig.16, it may be concluded that the stresses and strains at failure exist on the failure envelopes which are not dependent on the stress or strain paths under monotonic loading conditions where two principal stresses always increase or are constant in compression and tension stress state. Moreover, when the applied stress is monotonic, the relationship between stresses and strains seems to be independent of the stress paths even when the states of stress and strain are within the failure envelopes. That is, there exists unique relationship between stresses and strains under biaxial stress conditions. Accordingly, the hypo-elastic models(See Chapter 1.) and the total strain models(15) are reasonable only in the monotonic loading.

2.3 Characteristics of plastic deformation

2.3.1 Loading paths to get the plastic deformation

The plastic deformation is a very important factor of describing the mechanics of material. The plasticity is mathematically used for representing the effect of hysteresis in the constitutive laws of concrete. The classical theory of plasticity formulates the behavior of plastic deformation with the

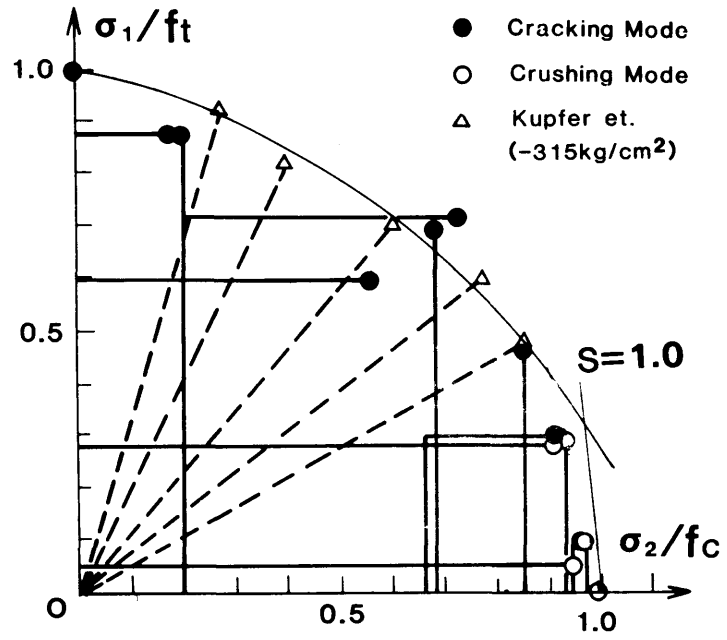

Fig.15. Stress paths and failure envelope with reported data (2).

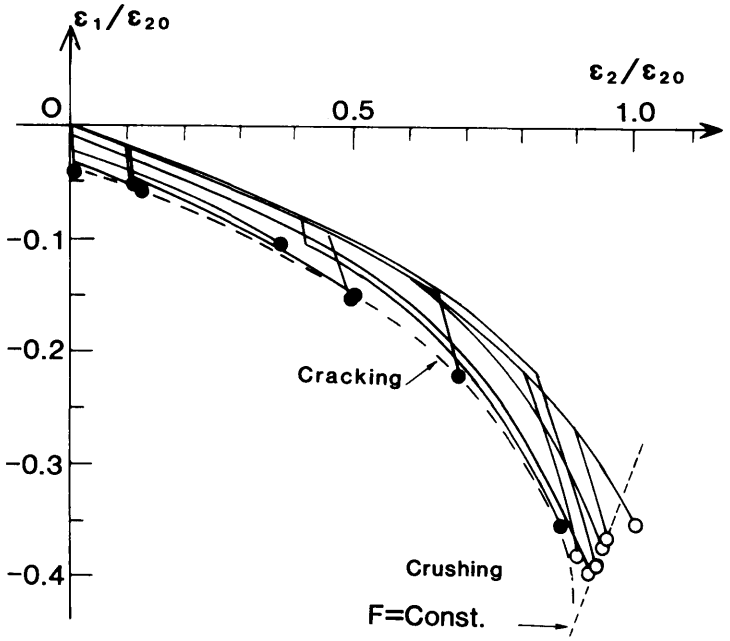

Fig.16. Strain paths and failure envelope.

strain-hardening or the work-hardening rule and the normality rule which decides the direction of the plastic flow. The theory of plasticity has been applied in the numerical analysis of concrete(17), because this theory is well established in the mathematical system and has much experiences to be applied to various nonlinear materials. Some references(9),(17) reported that the theory of plasticity has the ability to predict tne nonlinear behavior of concrete under biaxial and triaxial compression stress states. On the other hand, there is a question as to whether the theory of plasticity could express the behavior of concrete including the principal tensile stress or not(15). But unfortunately, there exist very little data discussing the concrete plasticity in the biaxial condition. Therefore, in the first place, the following type of test was carried out to get the information concerning the plastic deformation under the uniaxial stress condition. The uniaxial compressive stress was applied monotonically and unloaded completely. By this type of loading path, biaxial principal plastic strains ε_{p1} and ε_{p2} could be measured. In the second place, the following types of tests were carried out to make clear the effect of tensile principal stress on the total plastic deformation.

(1) The principal tensile stress was applied to the uniaxially compressed concrete ($d\sigma_2=0, d\sigma_1>0$) and unloaded completely.

(2) The principal compressive stress was applied to concrete specimens under uniaxial tensile stress state in the direction normal to the principal tensile stress and completely unloaded.

The plastic deformation is directly expressed by plastic strain tensors. However, the tensorial expression is not suitable for indicating the degree of total plastic deformation and the direction of the plastic flow. Accordingly, in this paper, the plastic deformation is represented by the incremental plastic strain vector d pls in the form

$$d\epsilon_{pls} = (d\varepsilon_{p1} , d\varepsilon_{p2}) \qquad (4)$$

The degree of the incremental plastic deformation represented by $d\bar{\varepsilon}_{pls}$ may be indicated by the norm of the incremental plastic strain vector, that is

$$d\bar{\varepsilon}_{pls} = |d\epsilon_{pls}| = \sqrt{(d\varepsilon_{p1})^2 + (d\varepsilon_{p2})^2} \qquad (5)$$

The integrated degree of plasticity $\bar{\varepsilon}_{pls}$ has the meaning of the accumulated damage of plastic deformation and we have

$$\bar{\varepsilon}_{pls} = \int d\bar{\varepsilon}_{pls} = \int |d\epsilon_{pls}| \qquad (6)$$

The direction of the plastic flow can be represented by

$$D = - \frac{d\varepsilon_{p1}}{d\varepsilon_{p2}} \qquad (7)$$

where D is named as direction parameter of plastic flow.

2.3.2 Characteristics of plastic deformation under uniaxial compressive stress state

The uniaxial unloading paths on the diagram of stress-strain relationship is shown in Fig.17 and strain paths are developed on the biaxial principal strain space as shown in Fig.18, where the incremental plastic strain vector $d\epsilon pls$ is illustrated as arrows. Compressive and tensile plastic strains ε_{p2}, ε_{p1} flow as the maximum deformation level $\varepsilon_{2max}/\varepsilon_{20}$ increases. As the compressive level increases, the tensile plastic strain in the direction normal to the compressive stress proceeds rapidly compared with the compressive principal plastic strain. The relationship between the calculated rate of plastic flow, $d\bar{\varepsilon}pls/d\sigma_2$, and experimental maximum principal compressive strain ε_{2max} is shown in Fig.19. The plastic deformation flows rapidly when the maximum compressive level $\varepsilon_{2max}/\varepsilon_{20}$ exceeds 0.6. There exists the correlation between the direction of incremental plastic flow and the maximum compressive level as shown in Fig.20. When the applied compressive strain is small, the value of the direction parameter of plastic flow 'D' experimentally coincides with the initial Poisson's ratio. Under the high compressive stress state, the value of D rapidly becomes larger. This means that the plastic strain in the direction normal to the uniaxial compressive stress proceeds rapidly rather than the plastic strain in the compressive direction. The direction of the incremental plastic flow is given by the normality rule in the theory of plasticity. If the isotropic plastic yield function is assumed, the unique relationship between the direction of plastic flow and the direction of stress vector is derived from the formulation of the normality rule in the theory of plasticity. According to this theory, value D must be constant, because the stress direction is uniaxial and always constant. This assumption is not applicable to express the characteristics of the direction of concrete plastic deformation.

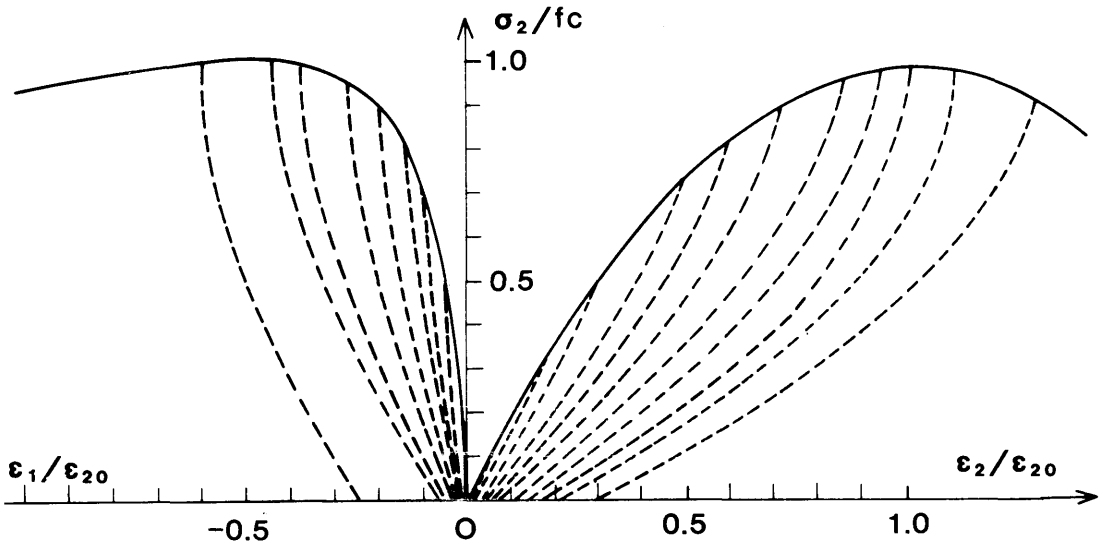

Fig.17. Uniaxial compressive stress-strain relations including the stress paths of unloading.

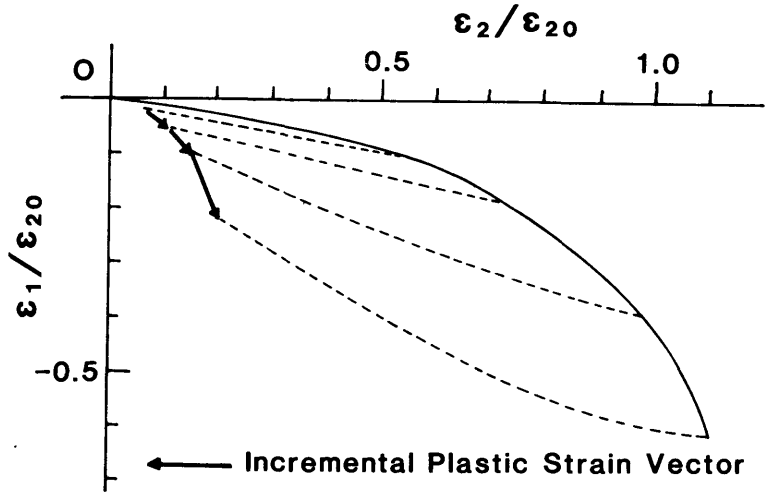

Fig.18. Strain paths under uniaxial stress state including the stress paths of unloading.

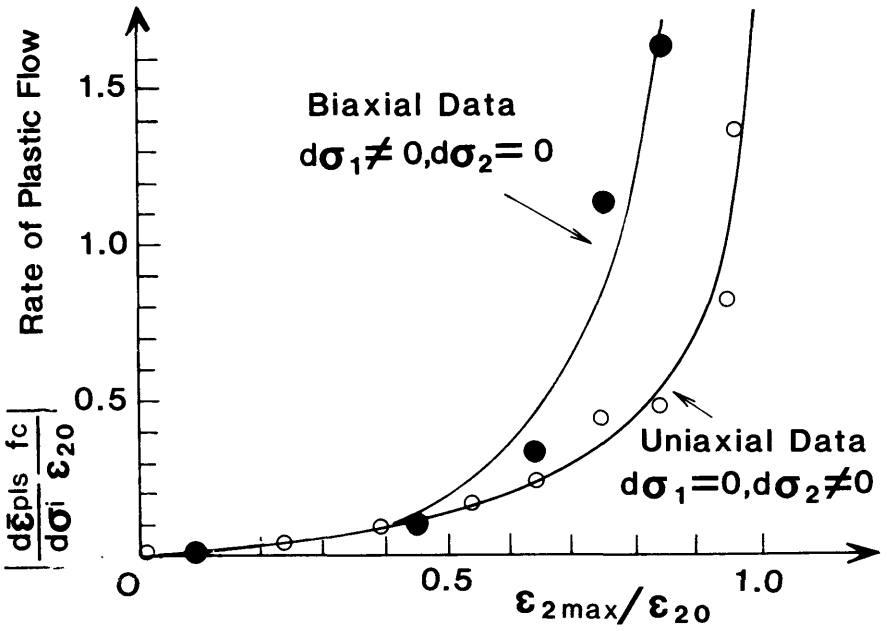

Fig.19. Plastic flow rate due to the increment of principal compressive and tensile stresses.

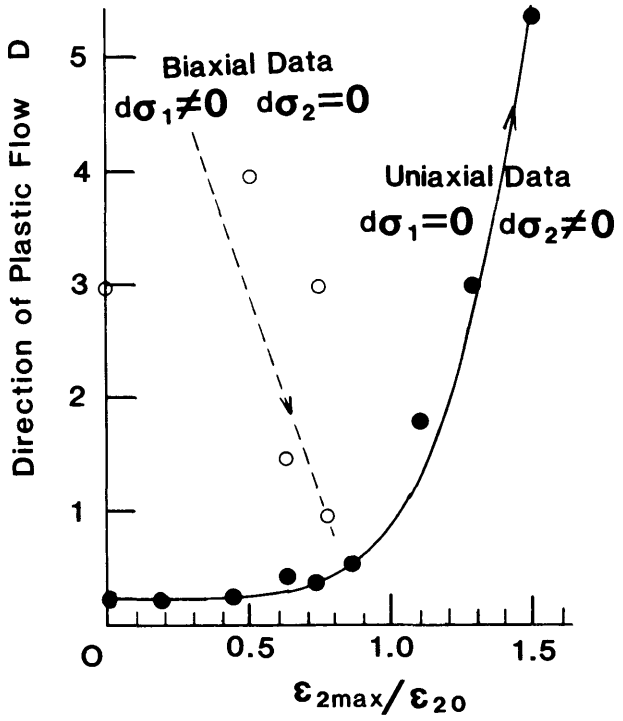

Fig.20. Direction of incremental plastic flow when the increments of the principal compressive and tensile stress are applied respectively.

2.3.3 Characteristics of plastic deformation under compression-tension stresses

The stress paths and stress-strain relationship of tensile loading test with constant principal compressive stress are shown in Fig.21. When the compressive strain level is low, the increase of tensile principal stress does not influence the plastic deformation so much. But, under the condition where the principal compressive stress is near the peak stress fc in compression, the increase of principal tensile stress normal to the principal compressive stress direction introduces the more rapid rate of the plastic deformation rather than the increase of principal compressive stress under uniaxial stress state. This deformational characteristics is mathematically and quantitatively represented by the plastic flow rate $d\bar{\varepsilon}pls/d\sigma_i$ (i=1,2) as shown in Fig.19. When the compressive level $\varepsilon_{2max}/\varepsilon_{20}$ exceeds 0.6, the increasing rate of plasticity due to the increment of principal tensile stress, $d\bar{\varepsilon}pls/d\sigma_1$, increases rapidly, and is about two times of the plastic flow rate by the increment of the principal compressive stress, $d\bar{\varepsilon}pls/d\sigma_2$. It means that under the high compression-tension stress state, the increment of the principal tensile stress accelerates the plastic deformation more rapidly than the increment of the principal compressive stress. The direction of the incremental plastic flow is shown in Fig.20. When the compressive stress is low, the direction of the plastic flow tilts in the direction normal to the principal compressive stress, therefore, the value of D becomes larger than the the value in the case of the uniaxial compressive stress state. According to the increase of the compressive strain level, the direction of the plastic flow gradually approaches the direction of compressive principal stress, and the value of D decreases. Stress paths of compression tests under constant tensile stress and stress-strain diagrams are shown in Fig.22. In this type of loading, the increment of compressive stress advances the plastic deformation when the constant tensile stress level is higher, and the rate of plastic flow by compression becomes larger.

2.4 Cracking strength of concrete

In the finite element analysis, the criterion of cracking under biaxial stress state has been often indicated by stresses. This type of criterion is useually formulated by using the biaxial data of the proportional monotonic loading tests(2),(14),(16). According to the test results in Section 2.2.5, cracking criterion can be certainly indicated by stress and is independent of the stress paths in case of the monotonic loading conditions. But, it is not reasonable to use the cracking criterion which was derived from the data of

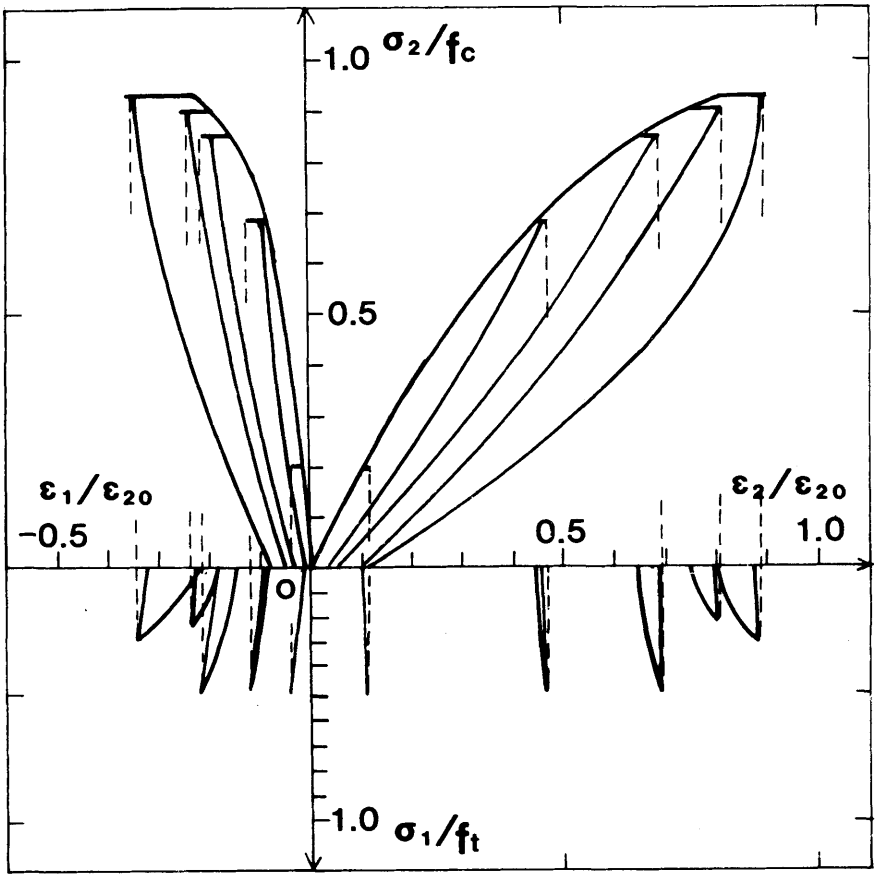

Fig.21. Stress-strain diagram including biaxial unloading paths.

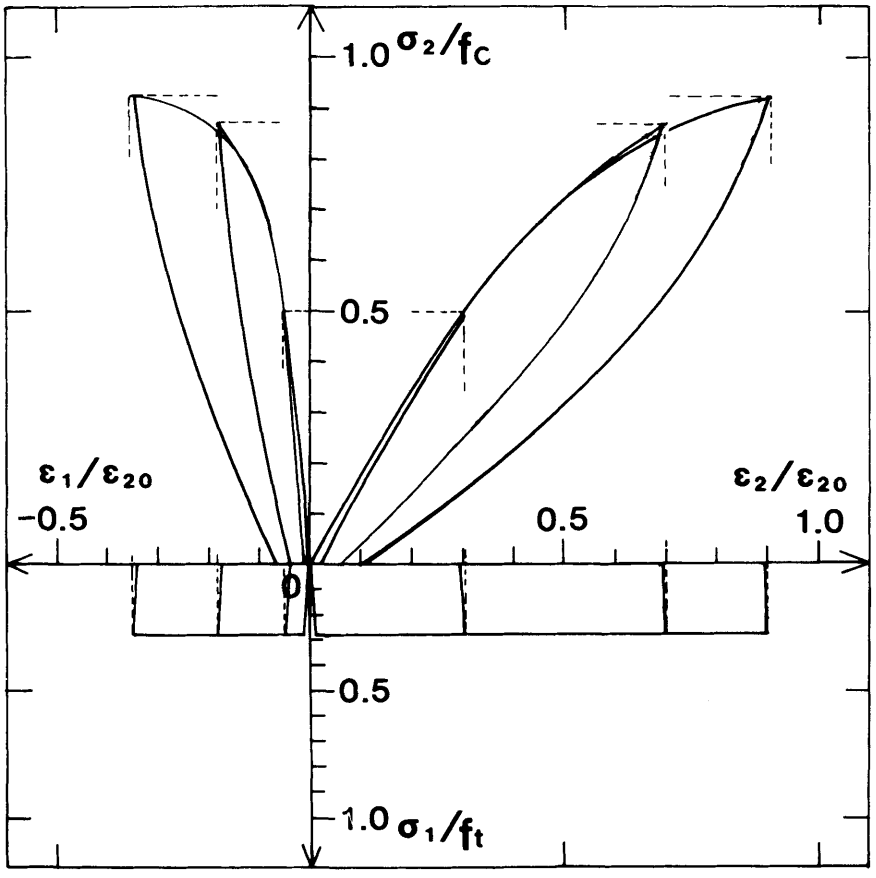

Fig.22. Stress-strain diagram including biaxial unloading paths.

monotonic loading condition for analyses including the stress hysteresis such as unloading and cyclic loading. Actually, it is easily imagined that the tensile strength of concrete which has been compressed to the strain softening level is nearly zero. In order to investigate the effect of the stress hysteresis on the tensile strength and the stiffness, a uniaxial tensile stress was applied to the concrete specimens which have the experiences of being compressed in the direction normal to the uniaxial tensile stress, and strains were measured and shown in Fig.23. The uniaxial tensile stiffness E1 decreases as the maximum compressive strain increases. The stress points when the crack forms are plotted on the stress space as shown in Fig.24. The uniaxial tensile strength of concrete with the compression hystory exists not on the cracking failure envelope of monotonic loading but within this envelope. The cracking criterion indicated by stress is not enough to take the effect of the stress hystory into account. Accordingly, failure criterion of cracking mode must include a parameter which represents the effect of stress paths or strain ones. The relationship between the principal tensile stress at cracking and the maximum value of the principal compressive strain at cracking under the compression-tension stress state is shown in Fig.25. In case of the monotonic loading condition, the maximum value of the principal compressive strain, ε_{2max}, is equal to the total compressive strain, ε_2 , at cracking. At the cracking failure exists unique relationship between the principal tensile stress and maximum level of principal compressive strain which represents the deformational hystory of concrete. This experimental results suggests the possibility to get the cracking criterion applicable to all the case of stress or strain hysteresis.

2.5 Concluding remarks

As the biaxial strains were precisely measured under various types of biaxial loadings with unloading paths, it became possible to obtain the following characteristics of concrete directly from experimental data.

(1) Biaxial stiffnesses and Poisson's ratios

As the previously reported biaxial loading tests were mainly carried out under monotonic proportional loading hysteresis, we could not determine the biaxial stiffness matrix quantitatively.

However, by adopting non-proportional stress paths reported in this chapter, the components of tangential stiffness matrix, say biaxial stiffnesses E1 ,E2 and corresponding Poisson's ratios ν_{12} , ν_{21} could be quantitatively obtained.

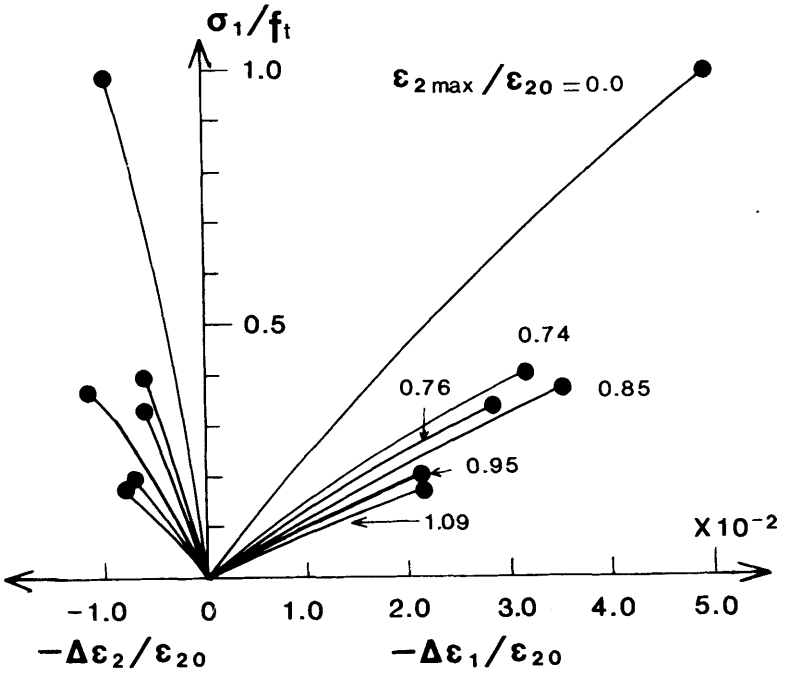

Fig.23. Relations between uniaxial tensile stress and incremental biaxial strains of pre-compressed concrete.

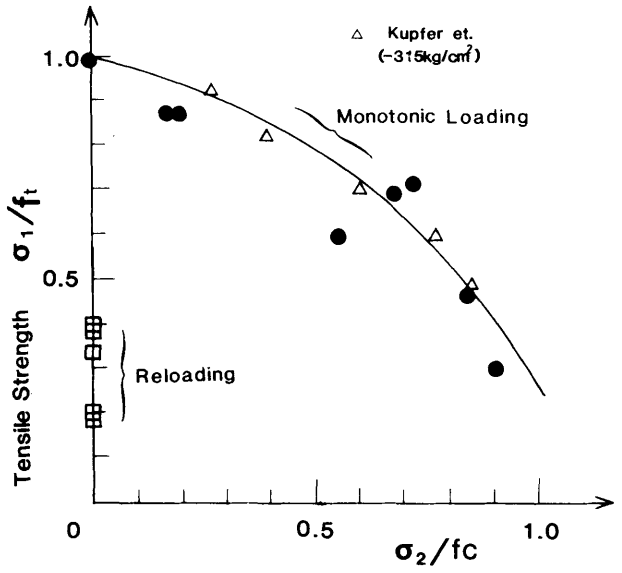

Fig.24. Cracking failure points on the biaxial stress space.

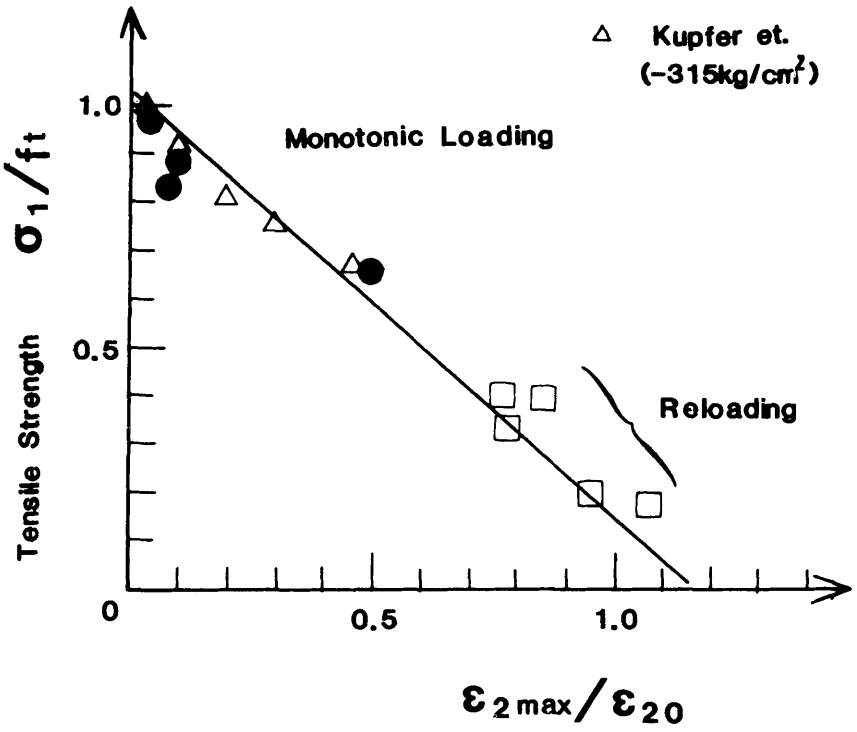

Fig.25. Relation between the cracking strength and the strain history.

(2) Anisotropy of concrete

Since an early age, the anisotropic behavior of concrete has been discussed and idealized in using some simple assumptions. However, this anisotropy has not been experimentally investigated, therefore, we had no data to verify the constitutive models concerning anisotropy of concrete.

But, as the biaxial stiffness matrix could be quantitatively investigated, the degrees of anisotropy and non-symmetry of stiffness could be indicated by the ratio of these stiffnesses and the ratio of diagonal components of stiffness matrix.

(3) Plasticity of concrete

In order to formulate the effect of strain hysteresis on the stress-strain relationship, it is important to follow the plastic deformation in biaxial stress conditions. But, in spite of the wide applications of the theory of plasticity to the engineering problems, the plastic flow rate and its direction under biaxial stress states have not been investigated at all. Then, unloading stress paths under biaxial stress states were chosen in this experimental program, and biaxial plastic strains were for the first time measured. Using biaxial plastic strains, we can express the plastic deformations.

These deformational behaviors of concrete above have been qualitatively supposed and discussed by researchers of concrete engineering but, for the first time quantitatively made clear by using the stress paths. Moreover, the following new results were quantitatively obtained in this research.

(4) Under the compression-tension stress state, the behavior of concrete is isotropic and independent of the stress paths when the deformational level is low. As the level of deformation increases, the tensile stiffness in the direction of the tensile principal stress becomes smaller than the compressive stiffness in the direction normal to the principal tensile stress, and the tangential stiffness matrix gradually becomes non-symmetric and anisotropic.

(5) In the monotonic loading condition under the compression-tension stress state, there exists unique relationship between the biaxial stresses and strains. Both the failure envelopes indicated by stresses and the failure one indicated by strains are not also influenced by the stress paths.

(6) Under high compression-tension stress state, the increment of principal tensile stress accelerates the plastic deformation more effectively than that of principal compressive stress, and the plastic strain in the direction of principal tensile stress more rapidly flows than that in the direction of principal compressive stress.

(7) The failure mode in the compression-tension stress states can be categorized into the cracking mode and the crushing mode. In the cracking

mode, a few brittle cracking appeared and the tensile stress could not be sustained. In the crushing mode, the strain-softening behavior was observed and both the principal stresses could not be kept constant. The mode of failure is not also influenced by the stress paths in the monotonic loading condition.

(8) The uniaxial tensile strength is influenced by the loading hysteresis. The strength and the tensile stiffness decrease rapidly when a large compressive stress was applied to the concrete.

The formulations of these caracteristics of concrete and derivation of concstitutive laws are discussed in the next chapters.

3. Formulation of Constitutive Equation based on the Elasto-Plastic and Fracture Model

In Chapter 2, the complicated nonlinear behaviors of concrete were quantitatively investigated by the newly adopted experimental approach. From an engineering point of view, the constitutive equations which predict the stress vector (σ_{ij}) under arbitrary strain paths must be formulated for the nonlinear finite element analysis. In order to formulate the stress vector, the author proposes the following two types of constitutive equations based on the investigated nonlinear behaviors of concrete, the elasto-plastic and fracture constitutive equation which describes the degree of the stress vector and the flow rules which predict the direction of the stress vector (Section 4) under arbitrary strain hysteresis.

In this chapter, the constitutive equation to predict the invariant of the stress vector ("length" of the vector) is proposd. In formulating this type of equation, the macroscopic deformational characteristics, such as the difference of stress-strain curves between the monotonic loading and unloading stress paths, the progress of the plastic deformation, strain hardening and softening behaviors and the change of stiffness in unloading and reloading (effect of the fracture defined later) are taken into account.

3.1 The concepts of plasticity and fracture, and the definition of reversible and irreversible process

As shown in Fig.17, the relationship between the uniaxial compressive stress and strain is nonlinear, even in the low compressive stress state. When the applied compressive stress is unloaded, the incremental stress-strain relationship becomes practically linear and average stiffness (or secant stiffness) gradually decreases as the maximum value of compressive strain becomes large. These nonlinearities are considered to appear because a part of the strain energy given by the external load may be consumed. In this report, authors define the plasticity as the change of the plastic strain. The plastic strain is the total strain which corresponds to the zero stress state. The plasticity can be taken up first as an index which represents the "degree" of the accumulated damage in concrte. It is imagined that the plasticity originates from the collapse of fine voids of concrete, dislocation of the cement paste, the mechanical slip between coase aggregates and mortar.

If the concrete nonlinearity is explained only by theplasticity, the stiffness must be constant and equal to the initial stiffness when the plastic

strains do not change, such as, in the unloading process. This model is successful in expressing the macroscopic deformational behaviors of metals. This classical theory of plasticity explains the degree of plasticity with a "state value" named the effective or equivalent plastic strain and introduces the nonlinearity in the constitutive laws by giving the nonlinear relationship between the effective plastic strain and the degree of externally applied stress named the effective stress(18),(19) (plastic hardening rule). This process is illustrated in Fig.26.

However, in the case of concrete, the unloading stiffness is not constant. Accordingly, above and beyond the plasticity, it is necessary to take another factor which represents the concrete nonlinearity and the degree of the accumulated mechanical damage into consideration. There must exists another factor which represents the damage of concrete such as the appearance of microcracking, microscopic buckling and collapse of mortar and aggregates. These phenomena are characteristic of concrete as the composite material.

It is considered that these nonlinear factors can be mechanically explained with the concept of the disappearances of a volume of the constituent material of concrete which has the ability to reserve the elastic strain energy. In this paper, this type of damage in concrete is defined as "fracture". Authors consider that the nonlinearity of concrete can be macroscopically explained with the concept of the plasticity and the fracture.

In the following sections, symbol d and Δ. mean the differentiation (infinite value) and difference (finite value) respectively. Index T means the transformation of matrix.

3.2 Basic model of deformation for concrete

In this report, the author adopts the approach of formulation which connects the concepts of the plasticity and the fracture quantitatively with the relationship between biaxial stresses and strains. The following basic models (conceptual models) concerning the stress-strain relationship are assumed.

(1) Concrete is modelled to be constructed by some constituent elements as shown in Fig.27. Symbols Eo, Ep, Ee, E, S ,Se indicate the idealized values which represent the degrees of the elastic stiffness of each constituent element, plastic strain, elastic strain, total strain , total stress and element stress respectively. These elements behave as the strain-hardening material as shown in Fig.26 and are located in parallel. Therefore, the plastic strain level Ep is uniquely determined by the maximum stress level of

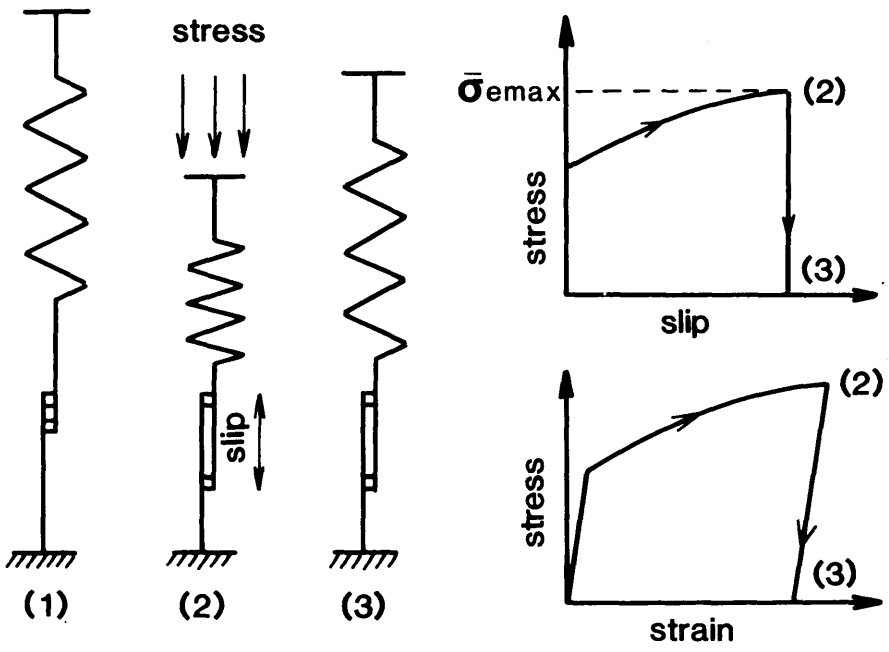

Fig.26. Modelling of strain-hardening plasticity

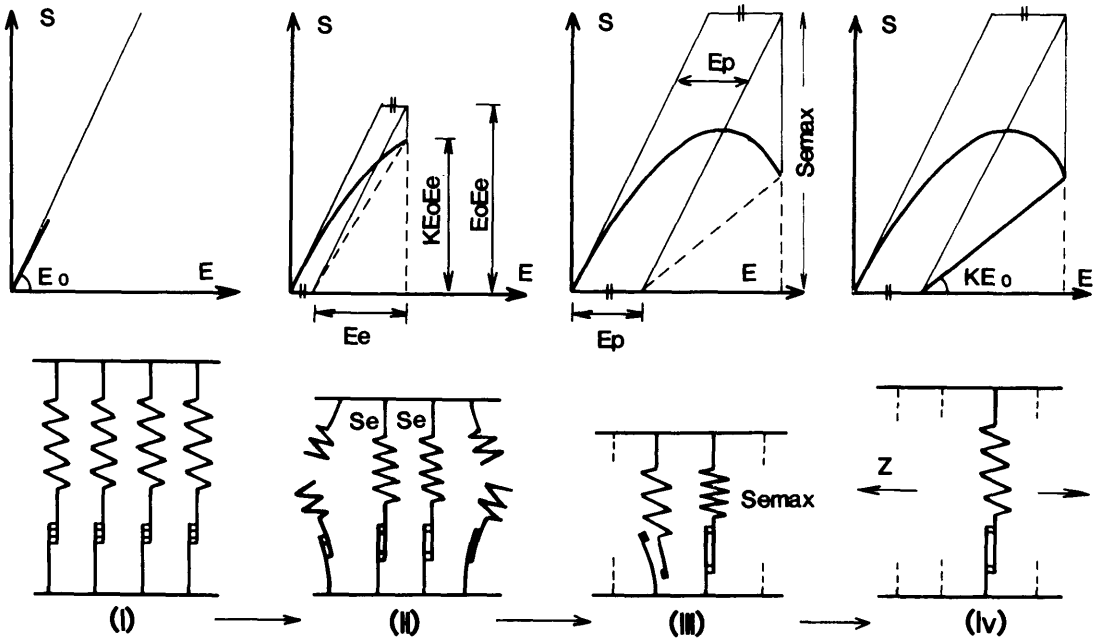

Fig.27. Elasto-plastic and fracture model for concrete.

each element 'Semax'. The elastic spring of each constituent element represents the area which reserves the strain energy reversibly. The Z-direction in Fig.27 corresponds to the direction normal to the biaxial plane stresses.

(2) Each constituent element loses its ability to support stress when the applied stress level of each element Se in Fig.27 reaches its fracture strength. This assumption represents the appearance of microcracking and local buckling. Accordingly, the fractured elements do not reserve the strain energy at all. This process is the irreversible one.

(3) The fracture strength of constituent elements 'f' is not constant but has a strength distribution P as shown in Fig.28. Pdf indicates the ratio of elements whose fracture strengths exist between f and f+df. This assumption represents the distribution of material quality in concrete.

The deformational behaviors of concrete are derived from the above assumptions as follows and illustrated in Fig.27 (I)-(IV).

(I) When the deformation level is low, the element stress level is small. Accordingly, the plasticity and the fracture proceed very little. As a result, the stress-strain relationship becomes almost linear.

(II) In this model, the stress-strain relationship is generally explained as follows. According to the assumption (1), element stress level is

$$Se = Eo\ (E - Ep) = Eo\ Ee \qquad (8)$$

where $E = Ee + Ep$

From the assumption, the ratio of fractured constituent elements is

$$n = \int_0^{Se\ max} P(f)df, \quad Semax = Eo\ (Emax - Ep) = Eo\ Eemax \qquad (9)$$

where Semax, Emax, Eemax: maximum values of element stress, total strain and elastic strain level in the stress and strain hysteresis of deformed concrete.

According to the assumption (1), the total stress level of concrete as a concrete composite is

$$S = (1-n)S_e = (1-\int_0^{Se\ max} P(f)df)E_0(E-E_p)$$

$$= KE_0(E-E_p) \qquad (10\text{-}1)$$

$$K = 1-\int_0^{Se\ max} P(f)df \qquad (10\text{-}2)$$

From the definition, the value of K means the ratio of constituent elements which maintain the abilities to support stress. At an initial condition, the value of K is equal to unity.

(III) In this model, the strain-softening behavior is unifiedly explained as follows. Under the high deformation level, as the plastic strain proceeds, the element stress level becomes large due to the strain-hardening as shown in Fig.26. As a result, the fracture proceeds rapidly. The reduction of the total stress due to the fracture exceeds the increase of the element stress due to the plastic strain-hardening, therefore, the total stress level as a composite gradually decreases in appearance.

(IV) The unloading process is systematically modeled as follows. If the applied stresses are unloaded, element stress level decreases and the plasticity and fracture does not proceed according to the assumptions (1) and (3). The stress-strain relationship has the same mathematical form as Eq.(10), but in this case, the maximum elastic strain level Eemax is larger than the elastic strain level Ee. Therefore, the idealized stress-strain relation in Eq.(10) becomes linear and its stiffness Eo K is constant. In other words, value of K indicates the ratio of the unloading linear stiffness to the initial one. The effect of the fracture appears directly in the decrease of the unloading stiffness, accordingly, K is the parameter to represent the degree of the fracture and defined as "fracture parameter".

From a macroscopic point of view, these idealized relationship can describe the behavior of concrete qualitatively with the unified philosophy. Therefore, laws derived from the concepts of the fracture and the plasticity are considered to be effective for constitutive model of concrete. It is implicitly assumed that the degree of the plasticity and the fracture has one-to-one relationship because the plastic strain level and fracture parameter are uniquely determined by the element stress level.

In this modelling, the stress-strain relationship of unloadng process is idealized as linear in spite of the nonlinearity of actual behavior under high strain levels. This nonlinearity of concrete is an important factor in analyzing rainforced concrete structures under large and cyclic deformations. However, in this type of analysis, the modelling of time-dependent deformational behaviors of concrete and the effect of cyclic loading hysteresis is also important. Therefore, authors discuss the unloading nonlinearity of concrete with the time-dependent problems in another papers. In this paper, the process where the plasticity and the fracture do not proceed is defined as reversible process, and the process where the plastic strain changes and the fracture proceeds and damage is accumulated in concrete as irreversible process.

3.3 State values to indicate the damage in concrete mechanics

The author considered that equivalent plastic strain Ep and fracture parameter K are quantitatively introduced in the constitutive model as state values for the plasticity and the fracture. As these parameters represent the state of damage in concrete, they must be defined as scalar values which are independent of the transformation of coordinate system, and which take the effect of strain paths into account.

The stress paths in the stress space and corresponding strain paths in the strain space in case of the plane stress condition are demonstrated in Fig.29. The stress point moves on the limited plane in 6D (six dimensional) stress tensorial space where the stress components σ_{zi} are all equal to zero (i=x,y,z), and the corresponding strain point (state) moves generally in 6D total strain tensorial space. But, in the plane stress constitutive equations, the strain components ε_{zz}, ε_{zx} and ε_{zy} do not explicitly appear. In other words, the plane stress constitutive equation is the mathematical expression which describes the relations between the position of stress point in the stress tensorial space and the projecting position of strain point on the plane where strain components ε_{zi} are equal to zero. Considering the lack of stresses and strains' data under 3D condition, constitutive equations in this paper expresses the strain state with strain tensors ε_{xx}, ε_{yy} and ε_{xy} as illustrated in Fig.29.

3.3.1 Equivalent stress

The equivalent stress S, which indicates the level of applied stress under plane stress conditions, is introduced. The mean stress $\bar{\sigma}_0$ and the deviatoric stress $\bar{\tau}_0$ can be defined as stress invariants which are independent of the coordinate transformation.

$$\bar{\sigma}_0 = \sqrt{2}\frac{\sigma_1+\sigma_2}{2} = \sqrt{2}\frac{\sigma_{xx}+\sigma_{yy}}{2} \tag{11}$$

$$\bar{\tau}_0 = \sqrt{2\left(\frac{\sigma_1-\sigma_2}{2}\right)^2} = \sqrt{2}\sqrt{\tau_{xy}^2+\left(\frac{\sigma_{xx}-\sigma_{yy}}{2}\right)^2} \tag{12}$$

The geometrical relationship between the stress invariant space($\bar{\sigma}_0$, $\bar{\tau}_0$) and principal stress space(σ_1, σ_2) is illustrated in Fig.30. The mean stress

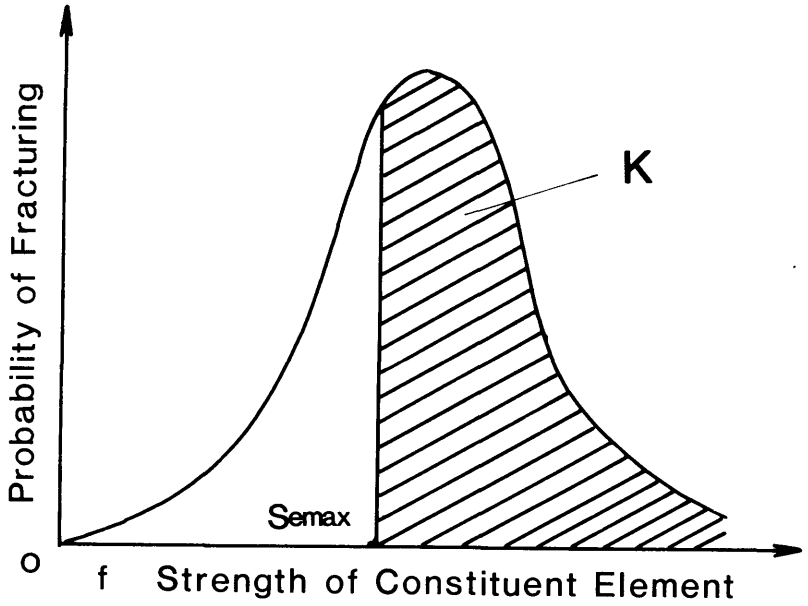

Fig.28. Fracture strength distribution of constituent elements.

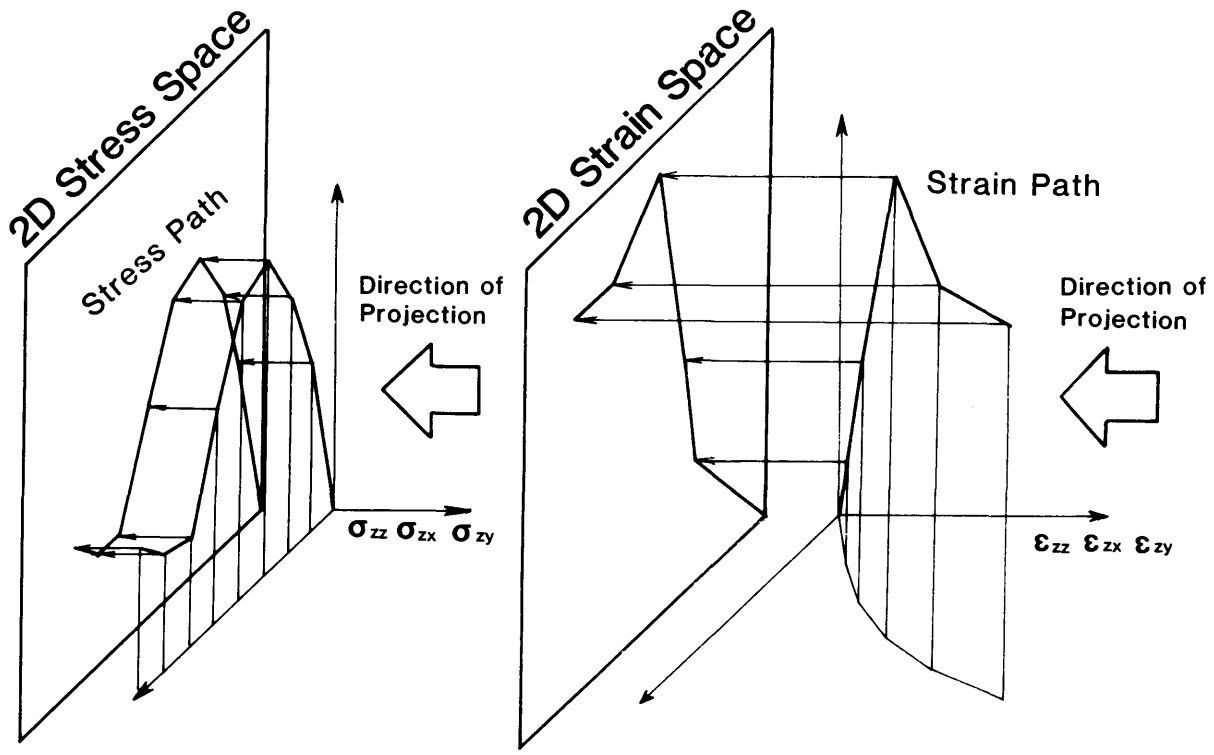

Fig.29. Stress and strain paths under the plane stress condition.

represents the average stress level in the plane stress condition and has an effect to introduce the fracture normal to the principal stress directions, and the deviatoric stress has an effect to introduce the in-plane fracture as shown in Fig.31.

Let us now consider the isotropic stress state where the deviatoric stress is zero. In this condition, shear stress component τ_{xy} is equal to zero and in-plane normal stress components σ_{xx} and σ_{yy} are equal to $\bar{\sigma}_0/\sqrt{2}$ in any coordinate system. It may be reasonable that the equivalent stress be in proportion to the mean stress.

In the pure shear stress condition, that is, the mean stress is zero where the normal stress components σ_{xx} and σ_{yy} are all equal to zero and the shear stress component $|\tau_{xy}|$ is equal to $\bar{\tau}_0/\sqrt{2}$ at a certain coordinate system, it will be also reasonable to define the equivalent stress as proportional to the deviatoric stress.

In the general case where $\bar{\sigma}_0 \neq 0$, $\bar{\tau}_0 \neq 0$, the equivalent stress should be evaluated to be larger than the stress states $(\bar{\sigma}_0, 0)$ and $(0, \bar{\tau}_0)$. From these considertions, the equivalent stress S was defined in the form

$$S = \sqrt{(a\,\bar{\sigma}_0)^2 + (b\,\bar{\tau}_0)^2} \qquad (13)$$

where coefficients a and b indicate the contribution level of the mean stress and the deviatoric stress to the value of S.

According to Eq.(13), the equivalent stress has the conceptual "length" of stress vector (σ_{ij}) or distance between the origin and the stress point in the stress space (See Fig.30.). The envelope which corresponds to the set of constant equivalent stress points on $\bar{\sigma}_0 - \bar{\tau}_0$ space has an elliptical shape. The stress states at the peak conditions with the crusing mode (See Section 2.2.5.) may be considered to have the same stress level respectively. Because, these peak stress points are considered to be in the common condition, where the effect of plastic strain-hardening balances the effect of the fracture so that the apparent tangent stiffness becomes zero (See Section 3.2). Moreover in the monotonic loading condition, the failure envelope indicated by stresses is little influenced by the stress paths (See Section 2.2.5.).

The data of peak stresses failed in crushing and strain-softening mode on $\bar{\sigma}_0 - \bar{\tau}_0$ space are shown in Fig.15 and Fig.32. Coefficients a and b were determined so that the envelope where the values of the equivalent stress are constant may envelope those peak data with acceptable accuracy as shown in Fig.32, where

$$a = 0.60 / fc \qquad b = 1.30 / fc \qquad (14)$$

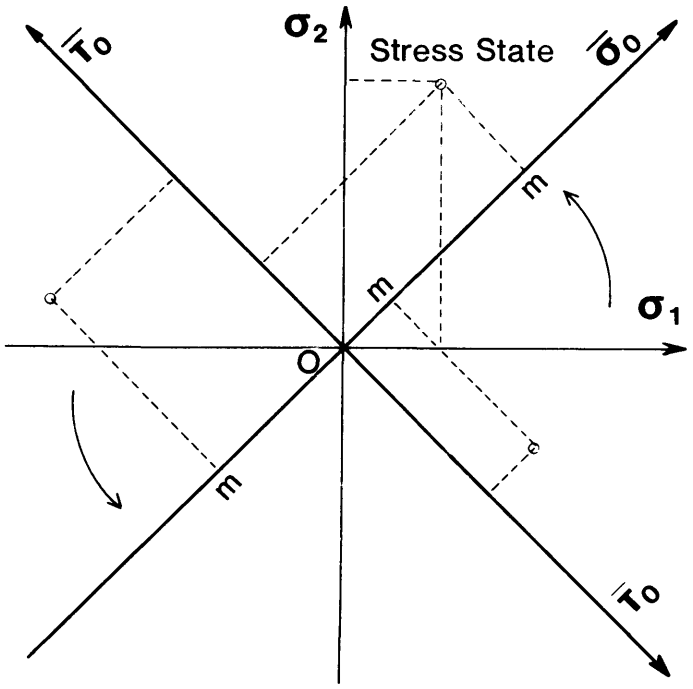

Fig.30. Mean and deviatoric stress coordinates.

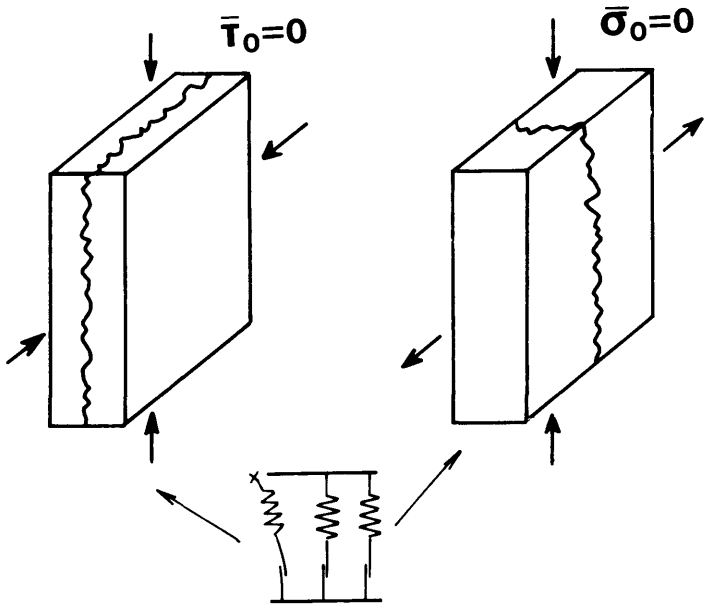

Fig.31. Direction of fracture and stress components.

Using Eq.(13) with Eq.(14), the stress level can be evaluated in all the biaxial stress states.

3.3.2 Strain measure function

The total strain vector (ε_{ij}) is divided into the elastic and plastic strain vectors in the form

$$\{\varepsilon_{ij}\} = \{\varepsilon_{eij}\} + \{\varepsilon_{pij}\} \tag{15}$$

where ε_{eij}: elastic strain tensor ε_{pij}: plastic strain tensor.
(Green's tensorial expression is adopted for the strain tensors.)

This research deals with the short-time strains and the time dependent deformations are ignored. Accordingly, delayed elastic and delayed plastic strains in the short-time loading are included in elastic and plastic strains in Eq.(15).

In order to formulate the degrees of elastic, plastic and total strain vectors, the author defines the strain measure function with the same procedure as the equivalent stress by

$$F = F(\delta_{ij}) = \sqrt{(c\bar{\varepsilon}_0)^2 + (d\bar{\gamma}_0)^2} \tag{16}$$

$$\bar{\varepsilon}_0 = \sqrt{2}\frac{\delta_{xx} + \delta_{yy}}{2}, \qquad \bar{\gamma}_0 = \sqrt{2}\sqrt{\left(\frac{\delta_{xx} - \delta_{yy}}{2}\right)^2 + \delta_{xy}^2}$$

where δ_{ij} : 2D tensor, $\bar{\varepsilon}_0$, $\bar{\gamma}_0$: the mean and deviatoric components of tensor δ_{ij}

The coefficients c and d in Eq.(16) can be determined as

$$c = 0.62 / \varepsilon_{20} \qquad d = 0.98 / \varepsilon_{20} \tag{17}$$

by the same method as in the case of coefficients a and b, because the failure envelope representing the crushing or strain softening mode on the total strain space as shown in Figs.16 and 33 seems not to be influenced by the strain paths under monotonic loading (See Section 2.2.5.).

3.3.3 Equivalent elastic strain

When the deformation is limited only in the reversible process where the plastic strain is idealized to be constant, the stress and elastic strain

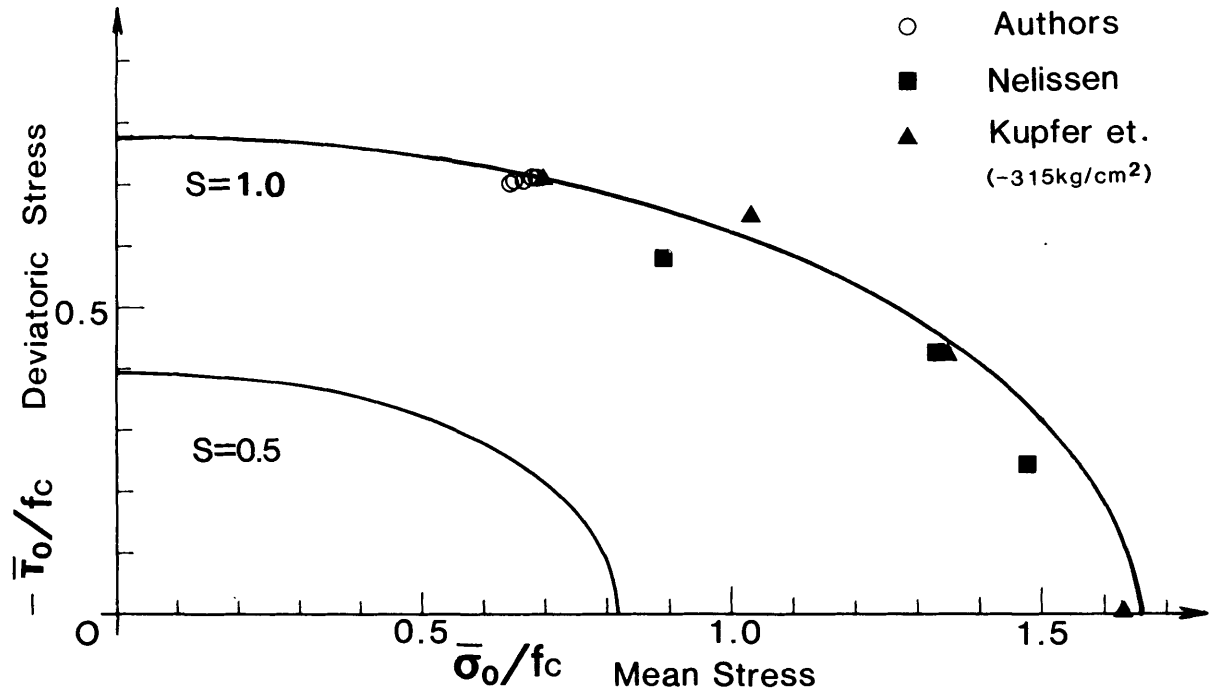

Fig.32. Failure envelope and the equivalent stress with reported data (2),(16).

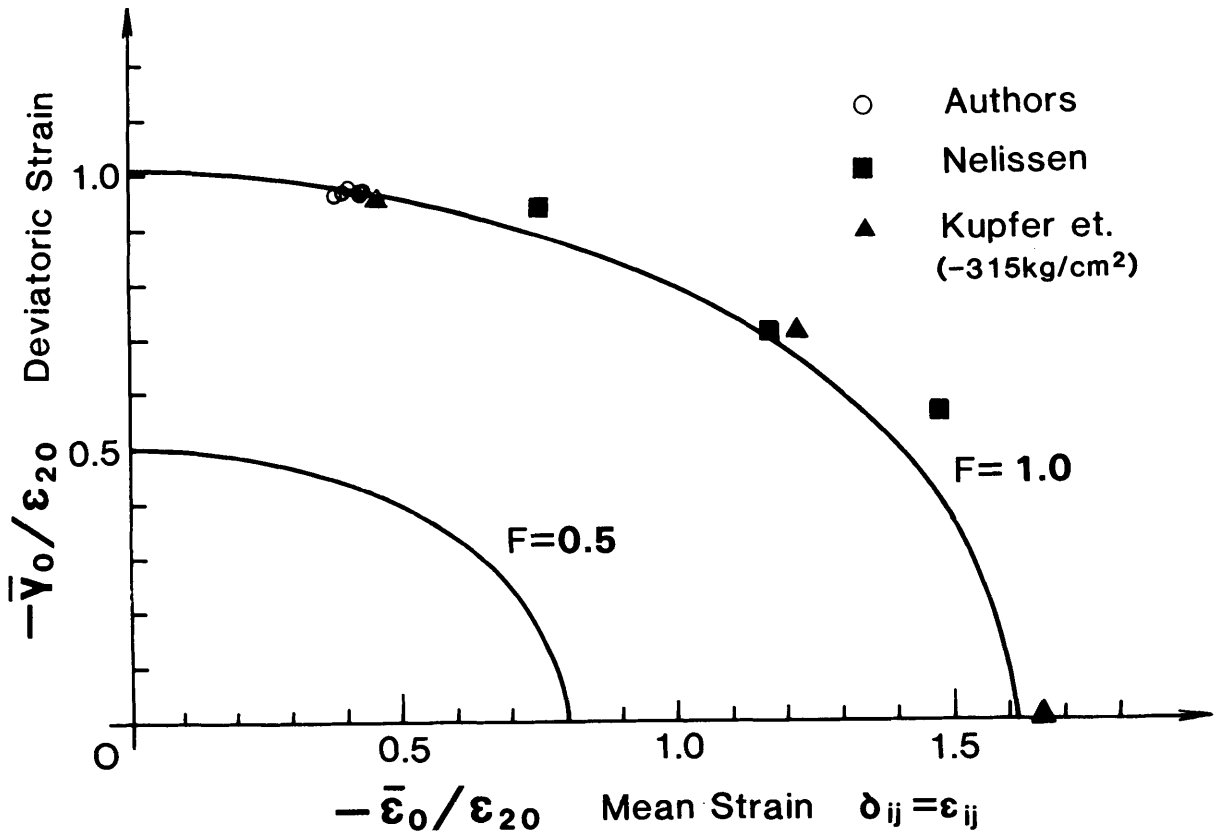

Fig.33. Failure envelope and strain measure function with reported data (2),(16).

relationship is likely to be linear. Accordingly, the biaxial stiffnesses and Poisson's ratios in the reversible process can be calculated by Eq.(2) and Eq.(3) with the experimental data in Section 2.3.

The ratio of the biaxial stiffnesses under the uniaxial stress conditions is approximately equal to unity as shown in Fig.34, therefore, the isotropic stiffness in the reversible process can be assumed within acceptable accuracy. The ratio of the diagonal components in the stiffness matrix $E1\nu_{12}/E2\nu_{21}$ (See Section 2.2), is approximately equal to unity at any strain level as shown in Fig.35.

These results as shown in Fig.34 and Fig. 35 indicate that the stiffness matrix in the reversible process, in other word, the secant stiffness matrix between total stresses and elastic strains is symmetric and isotropic, and that the relationship between stresses and elastic strains do not depend on the coordinate transformation. Then, as the relatioship between stress and elastic strain is not influenced by the strain paths, the equivalent elastic strain Ee which represents the degree of elastic deformation can be described by the integrated form including the strain invariant parameters as in case of the equivalent stress. Therefore, the definition of equivalent elastic strain is

$$Ee = F(\delta_{ij} = \varepsilon_{eij}) = F(\delta_{ij}, \delta_{ij} = \varepsilon_{ij} - \varepsilon_{pij}) \qquad (18)$$

The value of the formulated equivalent elastic strain in Eq.(18) is not dependent on the effects of strain paths but uniquely determined by the update elastic strains.

Let us now consider the criterion of reversible and irreversble processes. According to the basic model of deformation, the yield criterion of concrete as the composite material is equivalent to the yield criterion of each constituent element. From the theory of plasticity, the yield criterion, in other words, the irreversible criterion should be formulated as Eq.(19) with the element stress $\bar{\sigma}_{eij}$ and the loading (or yield) function of each constituent element Q in the form

$$Q(\bar{\sigma}_{eij}) = \bar{\sigma}_{e\max}(E_p) \qquad (19)$$

and

$$\frac{\partial Q}{\partial \bar{\sigma}_{eij}} d\bar{\sigma}_{eij} > 0$$

The maximum stress level of constituent element, $\bar{\sigma}_{emax}$, has a meaning of the plastic potential which is determined by the effective plastic strain in the theory of plasticity. $\bar{\sigma}_{eij}$ and Q are the imaginary values and cannot be

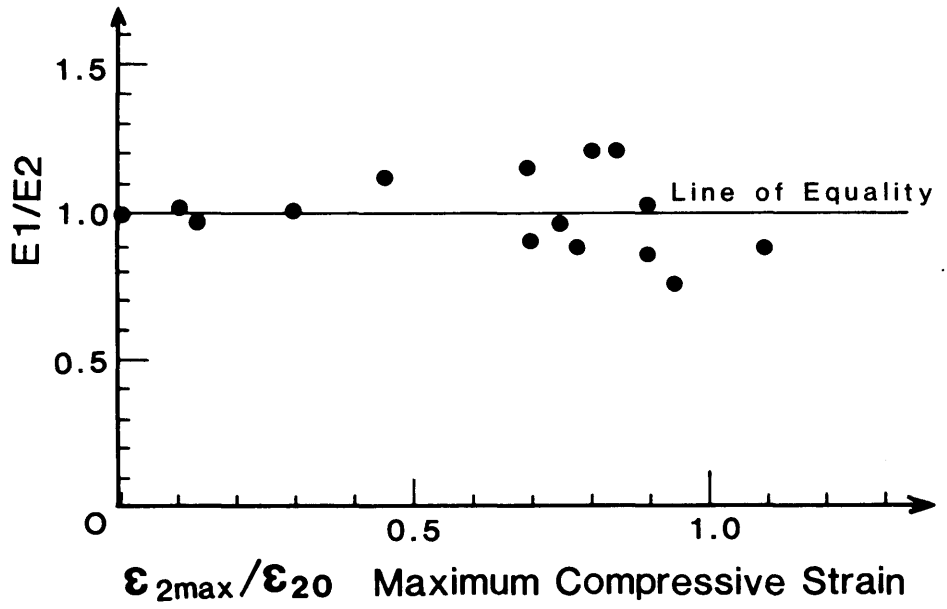

Fig.34. Ratio of the biaxial stiffnesses in reversible process.

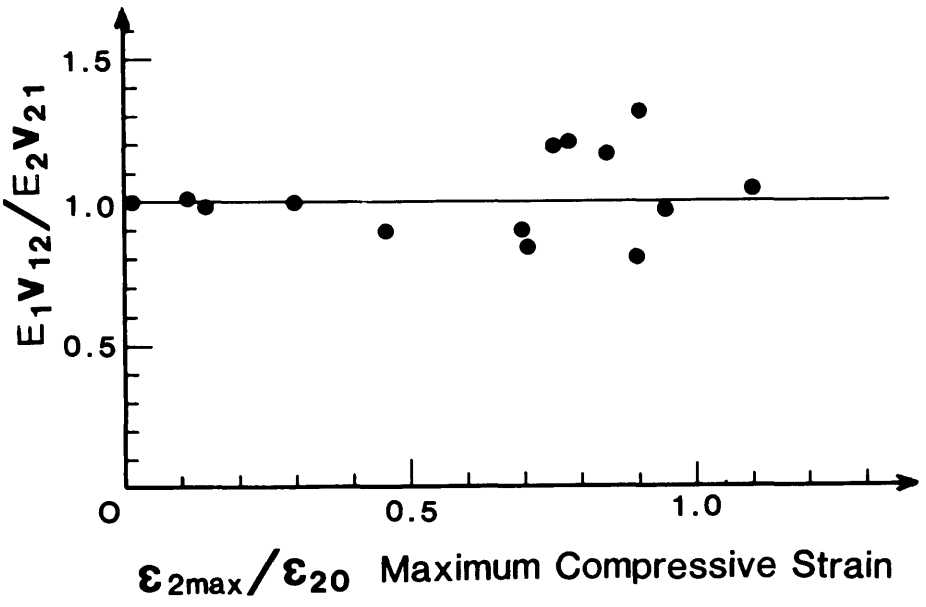

Fig.35. Symmetry of stiffness matrix in reversible process.

measured directly from experiments. However, the value of the plastic potential of each constituent element is equivalent to the maximum value of element stress level in this elasto-plastic and fracture model, therefore, using Eq.(9) we find

$$\bar{\sigma}_{emax} = Semax = Eo\ Eemax \tag{20}$$

Similarly, loading function Q is theoretically indicated by the function which formulates the value of element stress level Se, where

$$Q(\bar{\sigma}_{eij}) = Se = Eo\ Ee(\varepsilon_{eij}) \tag{21}$$

Substituting Eqs.(20) and (21) into Eq.(19), as the irreversible criterion of elasto-plastic and fracture model, we have

$$Ee(\delta_{ij} = \varepsilon_{eij}) = Eemax \tag{22-1}$$

$$dE_e = \frac{\partial E_e}{\partial \delta_{ij}}\Big|_{\delta_{ij} = \varepsilon_{eij}} d\varepsilon_{eij} > 0 \tag{22-2}$$

The definition of irreversible process in Eq.(22) gives the envelope on the strain space mathematically as the boundary of reversible area (Reversible area is defined as the elastic area on the strain space where the plasticity and the fracture does not proceed.). This boundary expands and kinematically shifts due to the strain-hardening in the strain space as illustrated in Fig.36.

In order to confirm the applicability of irreversible criterion by Eq.(22), three types of stress paths as shown in Fig.37-Fig.39 were applied to concrete. Stress and strain paths under uniaxial compressive stress condition are shown in Fig.37. The stress and strain paths when the tensile principal stress was applied under constant principal compressive stress are shown in Fig.38. In Fig.39 are shown the strain path corresponding to the stress path including the rotation of the direction of the maximum principal stress.

The incremental stress-strain relationships in the reversible area ($Ee < \varepsilon emax$) are practically linear and, when the strain state reaches and pass the reversible boundary Ee=Eemax (in the irreversible process), the nonlinearities in stress-strain relationship appear, and the plastic strains flow and the plastic potential expands and shifts as shown in Fig.37-Fig.39. These experimental results verify that the definition of the equivalent elastic

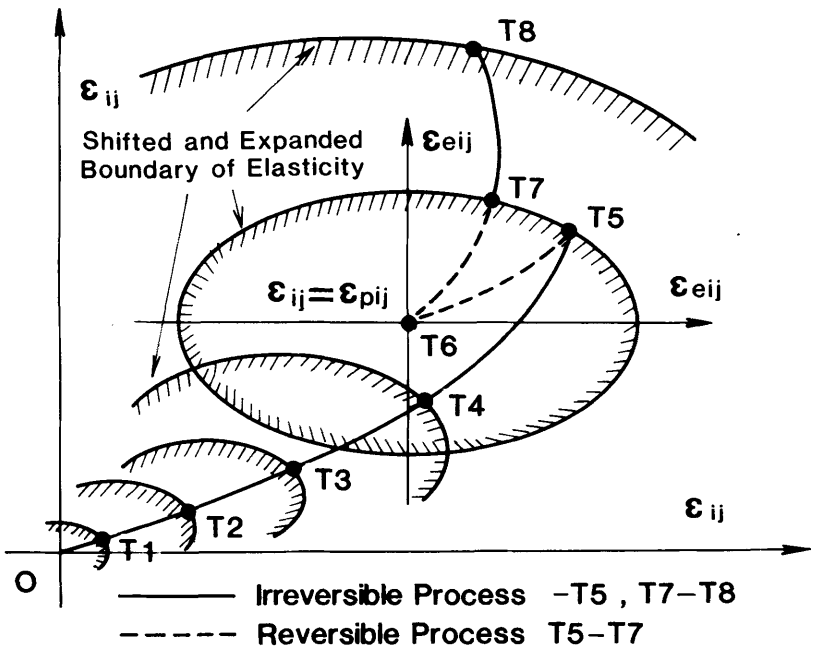

Fig.36. Kinematic shift and expansion of boundary of reversible area. (elasticity boundary)

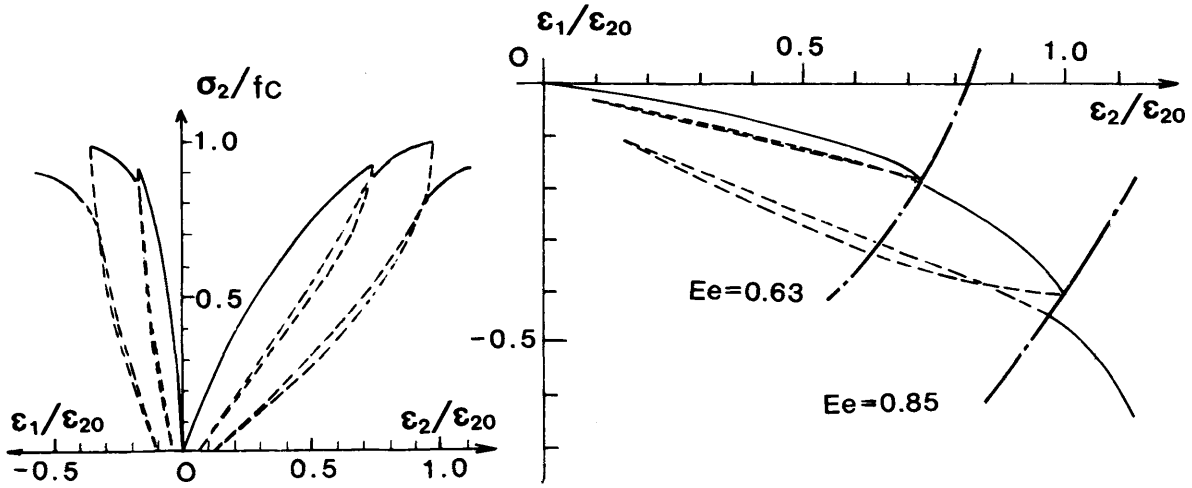

Fig.37. Biaxial strain path under uniaxial cyclic compressive loading.

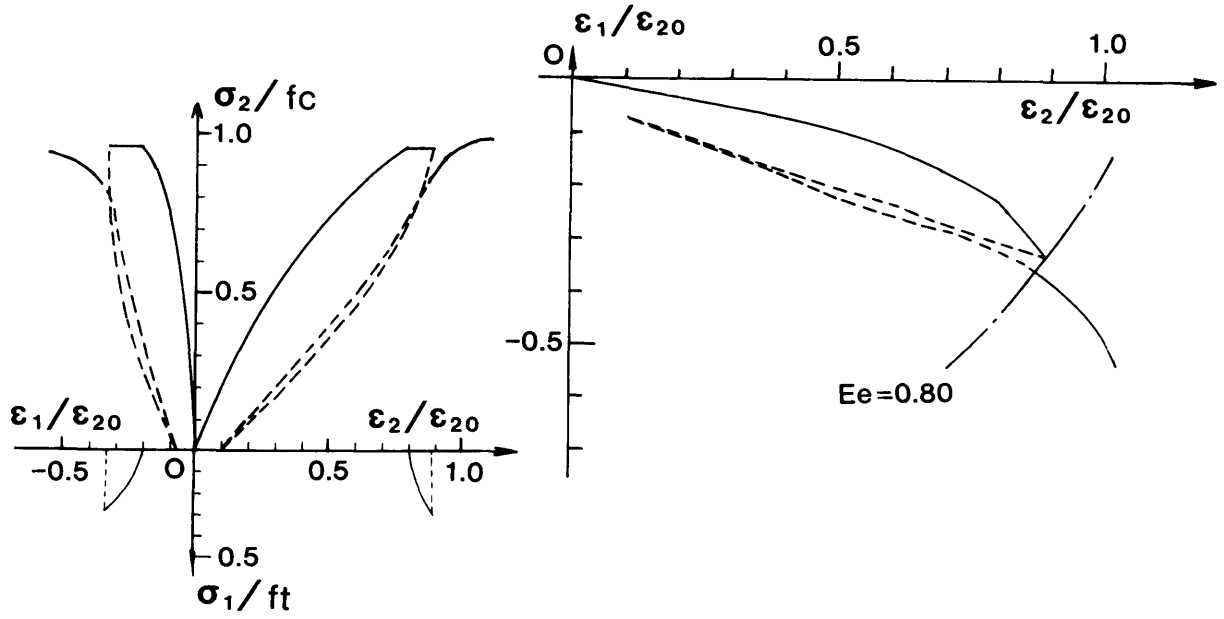

Fig.38. Biaxial strain path under compression-tension stress states.

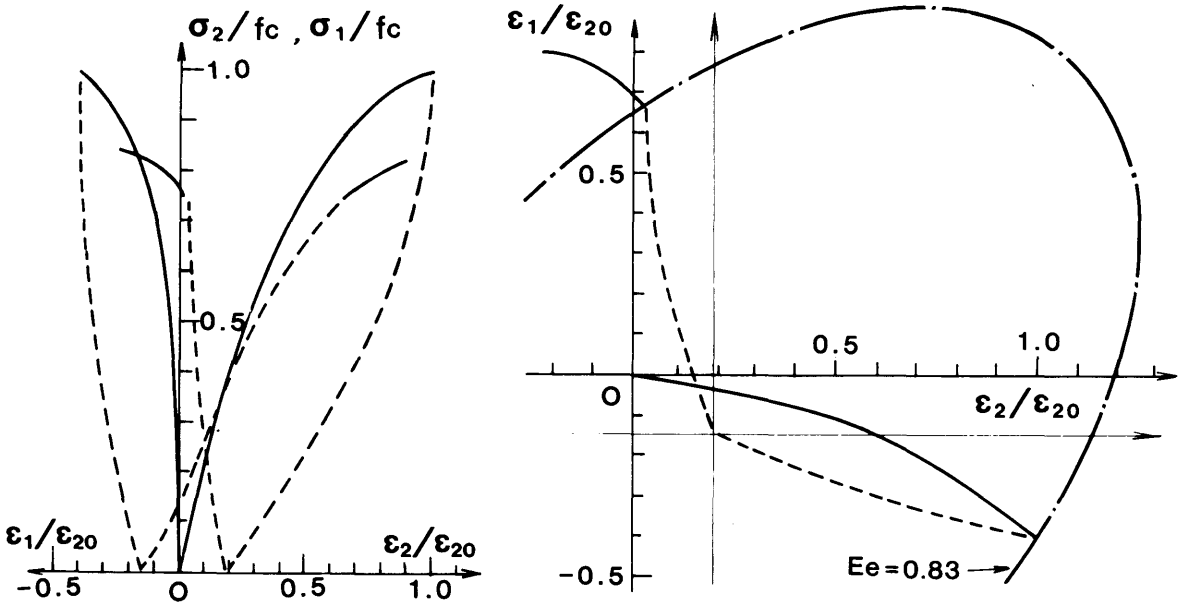

Fig.39. Biaxial strain path under bi-directional cyclic loading.

strain is a reasonable one for the index of elastic deformation.

3.3.4 Equivalent plastic strain

The equivalent plastic strain Ep should be given so as to represent the level of plastic deformation with mechanically reasonable definition. The plastic strains are influenced by the stress and strain paths, therefore, the equivalent plastic strain cannot be defined only by the integrated plastic strain ε_{pij} in the total format. The effect of the strain paths must be taken into consideration in the definition of the equivalent plastic strain. From the basic model in Fig.27, the plastic deformation of concrete composite is equal to the plastic one of each constituent element. In the classical theory of plasticity, there are two types of definitions to evaluate the degree of plasticity.

In strain hardening rule,

$$\bar{\varepsilon}_{pls} = \int d\bar{\varepsilon}_{pls} , \qquad d\bar{\varepsilon}_{pls} = \sqrt{d\varepsilon_{pij} \cdot d\varepsilon_{pij}} \qquad (23)$$

In work hardening rule,

$$\bar{\varepsilon}_{plw} = \int d\bar{\varepsilon}_{plw} , \qquad d\bar{\varepsilon}_{plw} = \frac{\bar{\sigma}_{eij}}{S_e} d\varepsilon_{pij} \qquad (24)$$

where $\bar{\varepsilon}_{plw}$, $\bar{\varepsilon}_{pls}$: equivalent or effective strains.

At first, let us now consider the strain hardening formulation. The effective plastic strain of the strain hardening rule indicates the total tracing length of the plastic strains on the strain space. The values of $\bar{\varepsilon}_{pls}$ calculated by Eq.(23) in the plane stress condition are shown in Fig.19, where the increasing rate of $\bar{\varepsilon}_{pls}$ to the increment of uniaxial compressive stress and that of $\bar{\varepsilon}_{pls}$ to the increment of the tensile principal stress which was applied in the direction normal to the uniaxial compressive stress are given.

The strain hardening rule in the theory of plasticity requires the one-to-one relationship between the effective plastic strain and element stress level Semax (or maximum value of the equivalent elastic strain Eemax, because Eemax is in proportion to Semax.) in all the cases of stress and strain paths. The calculated values of plastic flow rate in terms of Ee using data in Fig.19 are shown in Fig.40. There exists large difference of the plastic flow rate between the uniaxial stress and compression-tension stress states. Therefore, when the effective plastic strain $\bar{\varepsilon}_{pls}$ is used for the index of plasticity, it is difficult to formulate this characteristics of plastic deformation with the

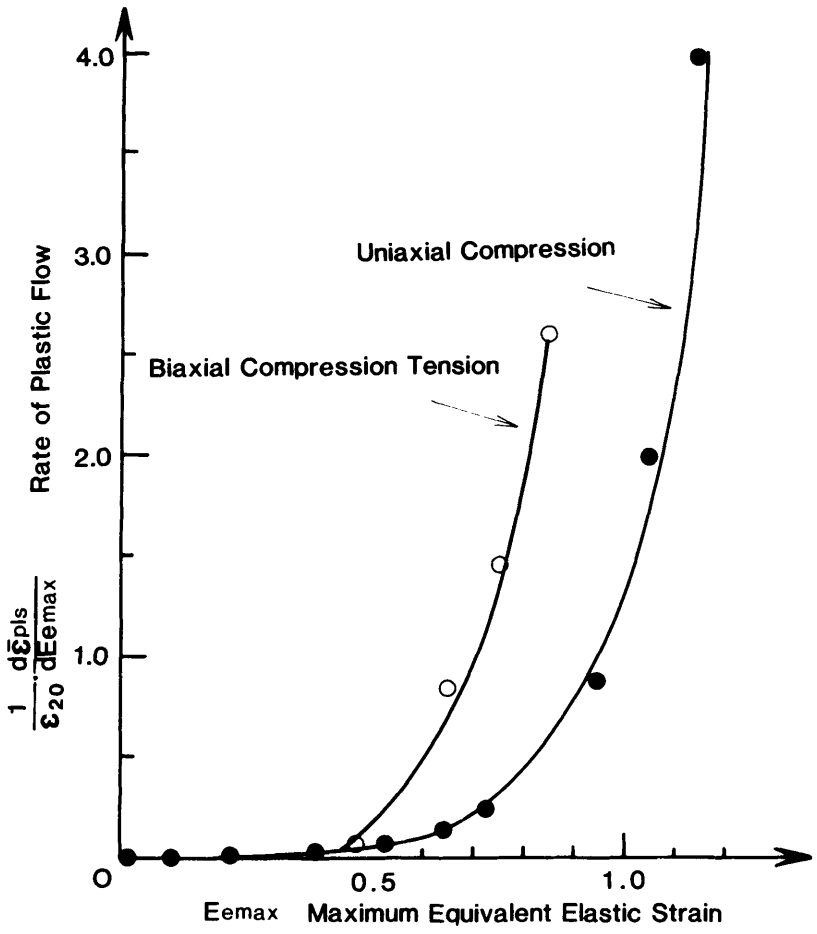

Fig.40. Difference of strain-hardening characteristics between uniaxial compressinn and biaxial compression-tension stress state.

unified approach such as the strain-hardening rule.

This rapid plastic flow advanced by the increment of the tensile stress (See Section 2.3.3) is characteristic of concrete and is considered to be introduced by the fracture due to the extension of microcrackings in the direction normal to the tensile stress. Therefore, it is not physically reasonable to expect that the fracture due to the extension of microcrackings introduces the strain-hardening.

Let us now consider the case of the work hardening formulation. The definition of the effective plastic strain $\bar{\varepsilon}_{plw}$ in Eq.(24) evaluates the value of the plastic index as smaller in case of the high compression-low tension stress state. Because, if the applied stress is low, the plastic strain work is small even when the larger plastic deformation proceeds. Accordingly, this work-hardening rule does not evaluate the effect of the plastic deformation which is introduced by the fracture as by-product and is considered to be reasonable in this deformational basic model. However, stress of each constituent element $\bar{\sigma}_{eij}$ is the theoretical values and is not directly measured by experiments.

The formulation of the work hardening plasticity cannot be directly applied to the concrete including the nonlinear factor of the fracture. Accordingly, a new definition which evaluates the plasticity must be introduced for the elasto-plastic and fracture model. Defining the increment of the equivalent plastic strain by the inner product of incremental plastic strain vector and the strain measure vector defined as $\left\{\frac{\partial F}{\partial \delta_{ij}}\middle|\delta_{ij} = \varepsilon_{eij}\right\}$ which is normal to the boundary of the reversible area, we have

$$E_p = \int dE_p, \quad dE_p = \frac{\partial F}{\partial \delta_{ij}}\bigg|_{\delta_{ij}=\varepsilon_{eij}} \cdot d\varepsilon_{pij}, \quad F\big|_{\delta_{ij}=\varepsilon_{eij}} = E_e$$

$$\frac{\partial F}{\partial \delta_{ij}}\bigg|_{\delta_{ij}=\varepsilon_{eij}} = \frac{c\bar{\varepsilon}_0 \dfrac{\partial \bar{\varepsilon}_0}{\partial \delta_{ij}} + d\bar{\gamma}_0 \dfrac{\partial \bar{\gamma}_0}{\partial \delta_{ij}}}{F}\bigg|_{\delta_{ij}=\varepsilon_{eij}} = \frac{E_0\left(c\bar{\varepsilon}_0 \dfrac{\partial \bar{\varepsilon}_0}{\partial \delta_{ij}} + d\bar{\gamma}_0 \dfrac{\partial \bar{\gamma}_0}{\partial \delta_{ij}}\right)}{E_0 E_e}\bigg|_{\delta_{ij}=\varepsilon_{eij}}$$

$$(E_0 E_e)dE_p = E_0\left(c\bar{\varepsilon}_0 \frac{\partial \bar{\varepsilon}_0}{\partial \delta_{ij}} + d\bar{\gamma}_0 \frac{\partial \bar{\gamma}_0}{\partial \delta_{ij}}\right)\bigg|_{\delta_{ij}=\varepsilon_{eij}} \cdot d\varepsilon_{pij} \tag{25}$$

Compared with Eq.(24), the first term of the right hand side of Eq.(25) corresponds to the constituent elements' stresses $\bar{\sigma}_{eij}$.

In another form, the increment of equivalent plastic strain is

$$dE_p = \left\|\frac{\partial F}{\partial \delta_{ij}}\bigg|_{\delta_{ij}=\varepsilon_{eij}}\right\| \cdot \left\|d\varepsilon_{pij}\right\| \cos\theta_0 = \left\|\frac{\partial F}{\partial \delta_{ij}}\bigg|_{\delta_{ij}=\varepsilon_{eij}}\right\| \cdot d\bar{\varepsilon}_{pls} \cdot \cos\theta_0 \tag{26}$$

where, θ_0 represents the angle between strain measure vector and incremental plastic strain vector. The equivalent plastic strain can be also understood to be the modification of the effective plastic strain in the strain hardening rule.

3.3.5 Equivalent total strain

Equivalent total strain E, which represents the degree of the total strain vector (ε_{ij}), should be given by the summation of the equivalent elastic and plastic strains from the basic model of deformation as follows.

$$E = Ee + Ep \tag{27}$$

By substituting Eqs.(22) and (25) into Eq.(27), the following incremental equations concerning the equivalent total strain are obtained.

In the reversible process, $d\varepsilon_{pij}=0$, then

$$dE = dEe + dEp$$

$$= \left.\frac{\partial F}{\partial \delta_{ij}}\right|_{\delta_{ij}=\varepsilon_{eij}} \cdot (d\varepsilon_{ij} - d\varepsilon_{pij}) = \left.\frac{\partial F}{\partial \delta_{ij}}\right|_{\delta_{ij}=\varepsilon_{eij}} \cdot d\varepsilon_{ij} \tag{28}$$

where $E = Ee + Ep \leqq Eemax + Ep = Emax$ (reversible criterion)

In irreversible process, $d\varepsilon_{pij} \neq 0$, then

$$dE = dE_e + dE_p = \left.\frac{\partial F}{\partial \delta_{ij}}\right|_{\delta_{ij}=\varepsilon_{eij}} (d\varepsilon_{ij} - d\varepsilon_{pij}) + \left.\frac{\partial F}{\partial \delta_{ij}}\right|_{\delta_{ij}=\varepsilon_{eij}} d\varepsilon_{pij}$$

$$= \left.\frac{\partial F}{\partial \delta_{ij}}\right|_{\delta_{ij}=\varepsilon_{eij}} \cdot d\varepsilon_{ij} \tag{29}$$

where $dE = dEe + dEp > 0$ (30)

and $E = Ee + Ep = Eemax + Ep = Emax$ (irreversible criterion).

The equivalent total strain is calculated by the unique equation without classification between the reversible and irreversible processes. The criteria of reversible and irreversible processes are also formulated by the equivalent total strain with simple forms as Eq.(29) and Eq.(30). This equivalent total strain is formulated by the total strain tensors, therefore, these criteria can be also used in the strain softening area, where the classical theory of

plasticity cannot be applied. It is very useful in the nonlinear finite element procedure.

The equivalent total strain is experimentally calculated by

$$E = \Sigma \Delta E \tag{31}$$

$$\Delta E \fallingdotseq \frac{\partial F}{\partial \delta_{ij}} \Delta \varepsilon_{ij} = F(\delta_{ij} | \delta_{ij} = \varepsilon_{ij} + \Delta \varepsilon_{ij} - \varepsilon_{pij}) - F(\delta_{ij} | \delta_{ij} = \varepsilon_{ij} - \varepsilon_{pij})$$

3.4 Rate of the plasticity

The state values of Ep, Ee and E can be calculated from the uniaxial and biaxial tests by Eqs.(18),(27) and (31). The relation between the equivalent plastic strain Ep and the maximum value of the equivalent total strain 'Emax' is shown in Fig.41. The equivalent plastic strain is considered to be uniquely determined by the maximum value of the equivalent total strain under arbitrary strain paths including uniaxial and biaxial stress states. The relationship between the equivalent plastic strain and the maximum level of the equivalent elastic strain 'Eemax' are shown in Fig.42. There exists unique correlation between Ep and Eemax from experiments and Eemax is proportional to the element stress level Semax from Eq.(9) in arbitrary loading paths. Therefore, there exists unique relation between the equivalent plastic strain and the element stress level. This means that the equivalent plastic strain is suitable for plastic index of the elasto-plastic and fracture model. In taking the numerical merits of FEM analysis into account, the equivalent plastic strain is indicated by

$$Ep = Ep(Emax) = Emax - \frac{20}{7}(1 - \exp(-0.35\ Emax)) \tag{32}$$

3.5 Rate of the fracture

From the definition, the fracture parameter K is directly measured from experiments as the ratio of the secant stiffness in the reversible process to the initial stiffness in the concept of the elasto plastic and fracture model. The reversible stiffness is verified to be isotropic in Section 3.3.3,

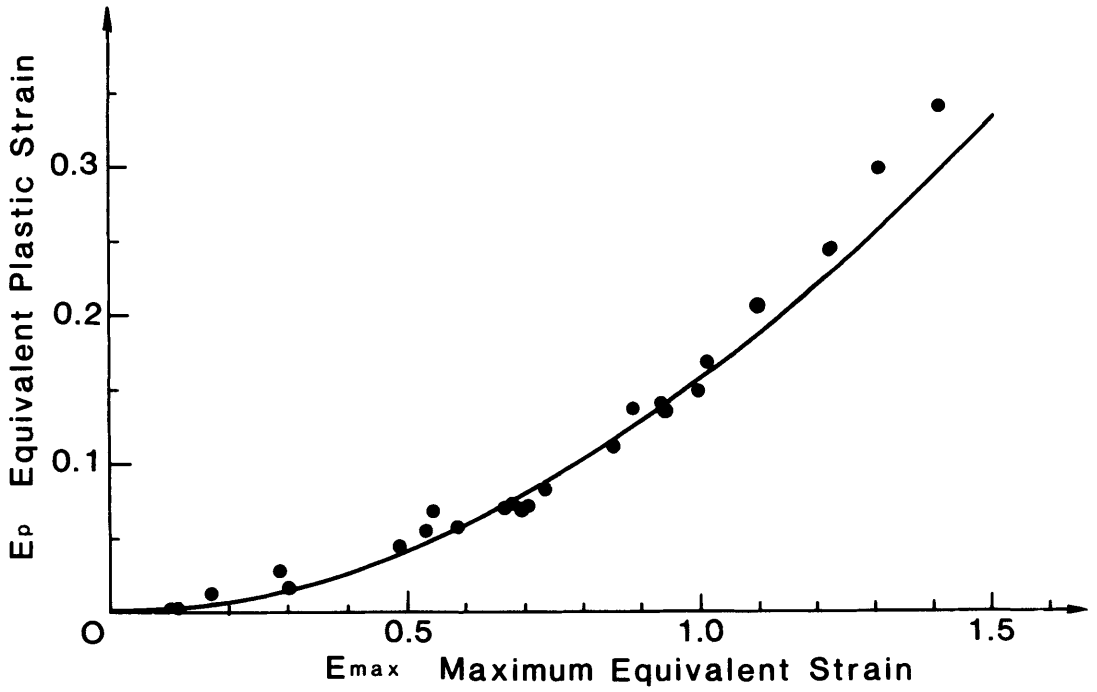

Fig.41. Progress of plastic deformation under biaxial stress states.

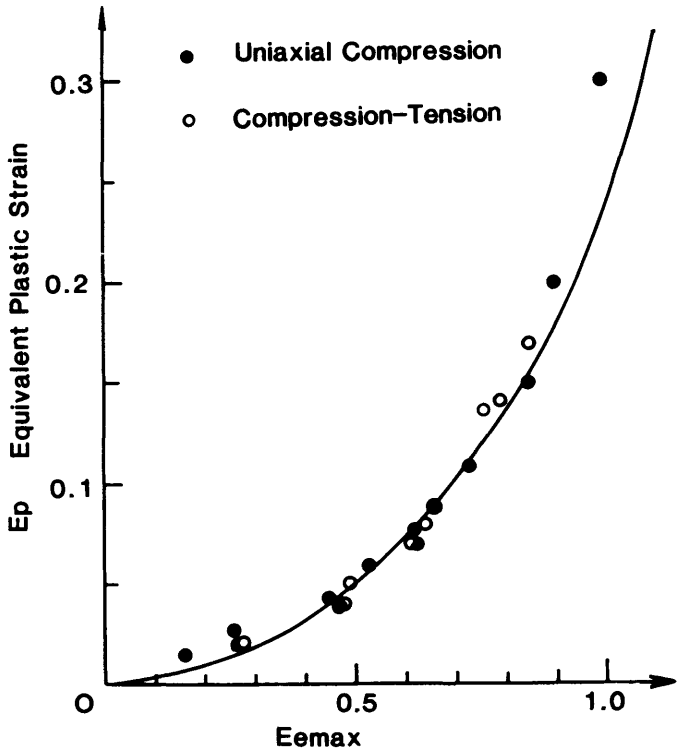

Fig.42. Relation between equivalent elastic and plastic strains.

therefore, the fracture parameter is suitable for the state value of concrete.

The secant stiffness Eo K is calculated by Eq.(10) and uniquely determined by the maximum stress level of each constituent element(See Eq.(10)), therefore, the value of Eo K must be expressed by the function of Eemax or Emax such as the definition of the equivalent plastic strain. The relationship between the fracture parameter K and maximum equivalent total strain Emax which were calculated from the biaxial experimental data is shown in Fig.43, where exists a unique correlation between K and Emax. The mathematical indication of the fracture parameter is

$$K = \exp(-0.73 \, Emax \, (1 - \exp(-1.25Emax))) \qquad (33)$$

The existence of the unique relation means the practical applicability of the concepts of the plasticity and the fracture to the model of concrete under biaxial stress states. The strength distribution P can be inversely calculated by solving the definition of the fracture parameter as

$$P \, (Eo \, (Emax - Ep)) = - \, (dK/dEmax)/ \, (Eo \, (1 - dEp/dEmax)) \qquad (34)$$

Strength distribution P is numerically obtained from Eq.(34) as shown in Fig.44. Then, coefficient Eo is set to be 2.0 so as to make the value of K at Emax=0 equal to unity.

3.6 Relations of the equivalent stress and the equivalent strain

From the basic modellings of deformation, the equivalent stress is

$$S = Eo \, K \, (E - Ep) \qquad (35)$$

where K and Ep are the functions of Emax.

The calculated values of S and E from the experiments are plotted with the analytical prediction by Eq.(35) in Fig.45. Eq.(35), which is defined as the elasto-plastic and fracture constitutive equation, can predict the macroscopic stress-strain relations with reasonable accuracy. The elasto-plastic and fracture constitutive equation can be applied to the reversible and irreversible processes with the same mathematical format, accordingly, it is very convenient to be used in the cyclic loading analysis.

Let us consider the case of biaxial and proportional loading(2). In the monotonic loading condition where the increment of the equivalent total strain

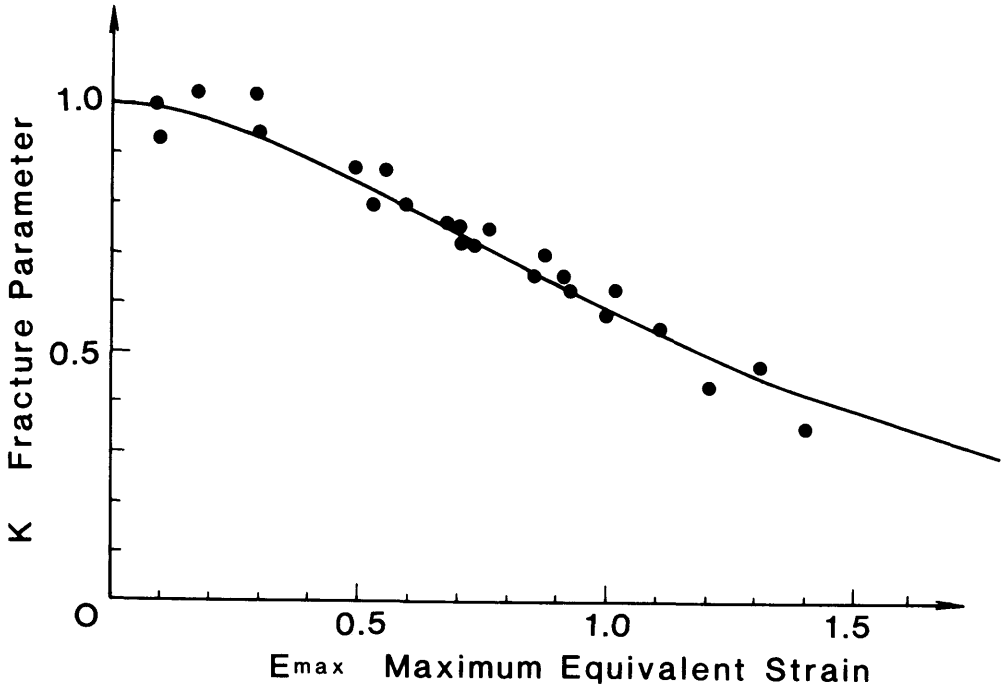

Fig.43. Progress of fracture under biaxial stress states.

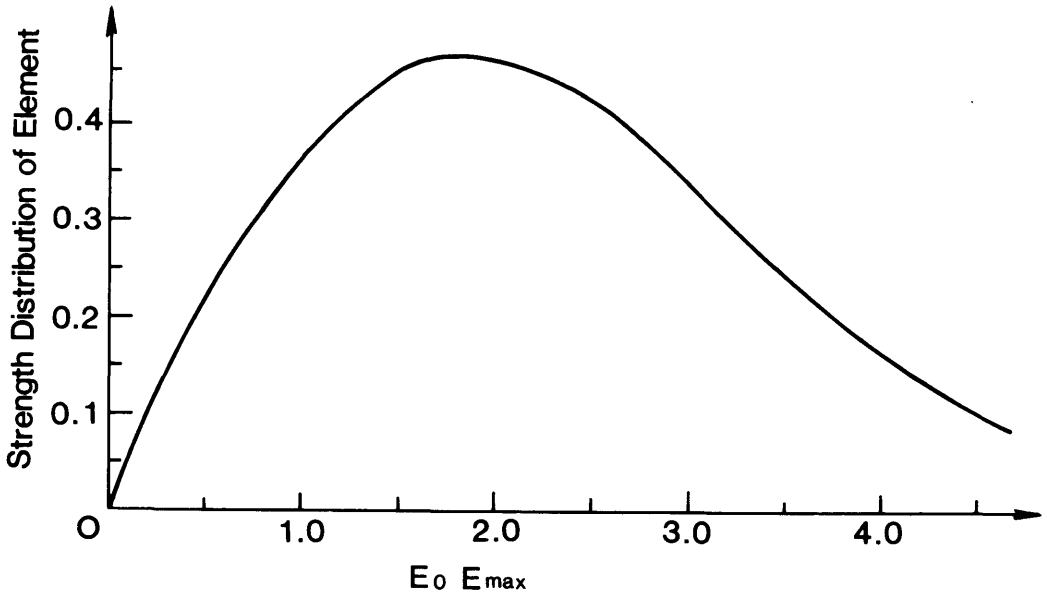

Fig.44. Calculated fracture strength distribution of constituent elements.

is always positive, the equivalent total strain is practically given in the form

$$E = \int \left.\frac{\partial F}{\partial \delta_{ij}}\right|_{\delta_{ij}=\varepsilon_{ij}} \cdot d\varepsilon_{ij} \fallingdotseq F(\varepsilon_{ij}) \qquad (36)$$

The derivation of Eq.(36) is explained in Appendix (I).

The experimental relations between the equivalent stress and equivalent strain in biaxial compressions and the predicted relations by Eq.(35) are shown in Fig.46. The monotonic equivalent stress-strain relations can be easily obtained by substituting E into Emax in Eq.(35), because the maximum level of the equivalent total strain Emax in the monotonic loading condition is always equal to the update equivalent total strain E. The integrated form of equivalent total strain in Eq.(36) corresponds to experimental fact of the path-independency discussed in Section 2.2.5.

3.7 Concluding remarks

From the analysis of the experimental data in Chapter 2, it was made clear that the relationship between biaxial stresses and strains (including elastic and plastic strains) can not be unifiedly explained by the classical theory of plasticity in compression-tension stress states.

Then, in order to express the investigated deformational behaviors of concrete mathematically, the concepts of equivalent elastic, plastic and total strains were introduced for representing the levels of elastic, plastic and total deformations. Moreover, the concept of "fracture" was newly introduced for indicating the irreversible nonlinear factor and formulated by fracture parameter.

Organizing these scalar values in unsing elasto-plastic and fracture law, authors succeeded in deriving a simple formed constitutive equation as follows.

(1) Elasticty of concrete

Previously reported constitutive laws often adopt the assumption that the relationship between stress and elastic strain is described by the isotropic and symmetric stiffness matrix. But this assumption has not been confirmed by experimental data in biaxial stress states.

Then, from experimental results under unloading paths, it was for the first time verified that the behavior of concrete in unloading condition and relationship between stress and elastic strain can be expressed by the isotropic and symmetric secant stiffness matrix in compression-tension stress states. Based on this experimentaal result, the equivalent elastic strain was

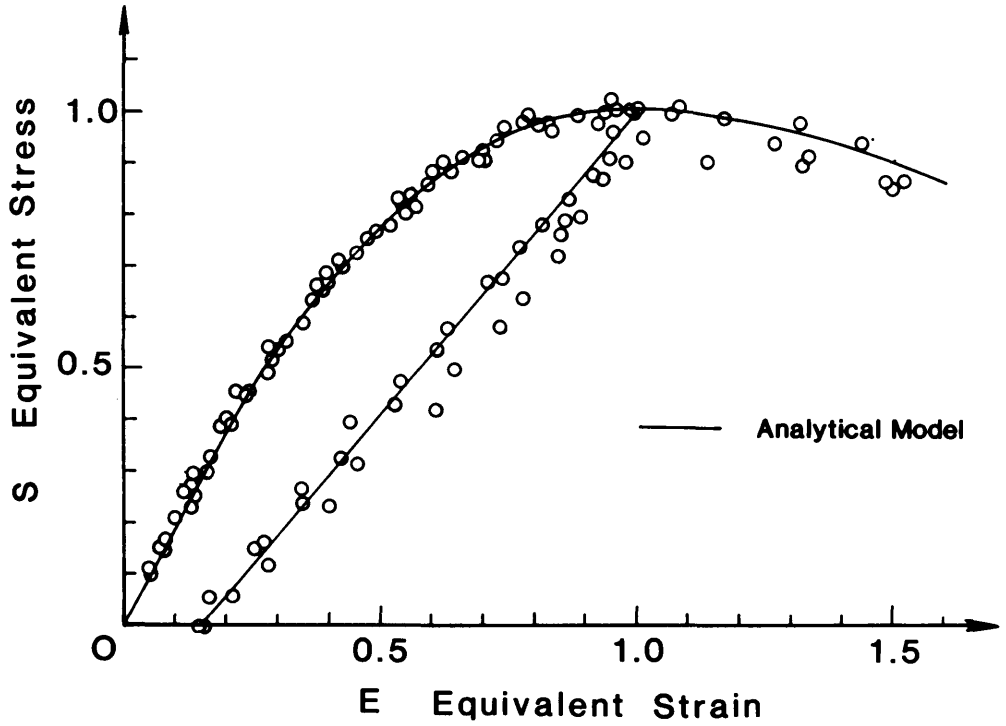

Fig.45. Equivalent stress-strain relationship under compression-tension stress states.

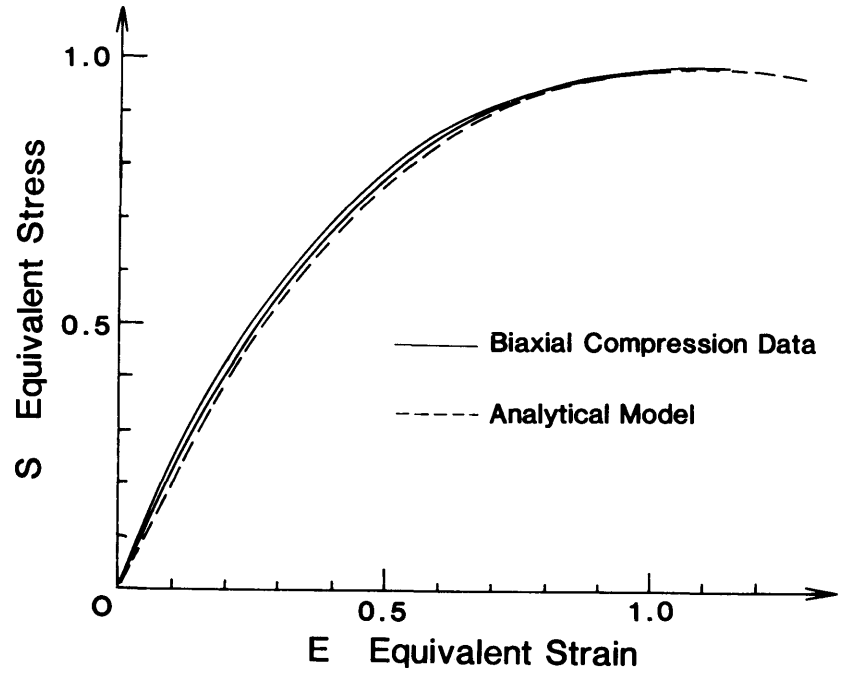

Fig.46. Equivalent stress-strain relationship under biaxial compression stress states with reported data (2).

introduced for representing the "length" of the elastic strain vector. By using this equivalent elastic strain, the elasticity criterion under biaxial stress states could be derived, and its applicability was checked by the various types of stress paths. With acceptable accuracy, this criterion can be used in any deformational process even in the strain-softening area, where the theory of plasticty can not be applied theoretically.

(2) Plasticity of concrete

It was made clear from experimental approach that the behavior of concrete as to the plastic deformations, say, plastic flow rate and its direction, is difficult to be unifiedly explained by the classical theory of plasticity in compression-tension stress states. Then, the equivalent plastic strain, which is the path-dependent scalar invariants, was newly introduced by modifining the theory of plasticity. With this definition of equivalent plastic strain, the progress of biaxial plastic strains could be unifiedly described.

(3) Fracture of concrete

The nonlinearlities of concrete could not be explained only with the theory of plasticity. Accordingly, the concept of fracture was introduced in this research. It is idealized as the dissipation of elastic strain energy due to the disappearances of a part of volume which constitutes concrete, such as the local buckling in concrete. In order to formulate the fracture of concrete, fracture parameter was defined as a state value to represent the degree of accumulated damage in concrete.

The fracture parameter is successful in expressing the decrease of unloading stiffness of concrete.

(4) Elasto-plastic and fracture constitutive law

Organizing the concepts of elasticity, plasticity and fracture, authors succeeded in deriving the elasto-plastic and fracture constitutive equation which gives the invariant of stress vector under arbitrary strain paths. The mathematical form of the derived constitutive equation is very simple and easy to be used in the numerical analysis, because it was formulated by the unified philosopy to concrete mechanics.

4. Formulation of Flow Rule

In Chapter 3, the relation between the degree of the stress vector (equivalent stress) and the level of the strain vector (equivalent strain) was derived by the unified concept, named the elasto-plastic and fracture constitutive law. However, if there is no constitutive law other than the elasto-plastic and fracture law, the stress vector under an arbitrary strain path can not be determined, because the numbers of the unknown values are more than those of the constitutive equations which are independent of each other. Therefore, other constitutive law which formulates the directional correlation between the stress vector and the strain vector is necessary for deriving the complete plane stress constitutive equations. (In this paper, this type of constitutive law is named as "flow rule".)

There exist some flow rules for concrete, such as, normality rule in the theory of plasticity(10), compression field theory(20), hypo-elasticity model(See Section 1) and so on. However, these modellings are not careful for the anisotropy of concrete under compression-tension stress state.

The main objective of this section is to formulate the flow rule in taking the anisotropy of concrete into account.

4.1 New system of flow rule

Differentiation terms of higher orders are disregarded in formulating flow rule equations, therefore, formulated differential equations in this paper are first linear differential ones. Three dimensional plane stress vector (σ_{ij}) can be expressed by two dimensional stress invariant vector ($\bar{\sigma}_0$, $\bar{\tau}_0$)^T and the principal stress direction "θ" which indicates the direction of the maximum principal stress to the X-coordinate in the form

$$\{\sigma_{ij}\} = [c(\theta)]\begin{bmatrix}\bar{\sigma}_0\\ \bar{\tau}_0\end{bmatrix}, \qquad [c(\theta)] = \frac{1}{\sqrt{2}}\begin{bmatrix}1, & \cos 2\theta\\ 1, & -\cos 2\theta\\ 0, & \sin 2\theta\end{bmatrix}$$

$$\{\sigma_{ij}\} = (\sigma_{xx},\ \sigma_{yy},\ \sigma_{xy})^T$$

$$\theta = T(\delta_{ij} = \sigma_{ij})$$

$$T(\delta_{ij}) = \frac{\pi}{2} - \mathrm{sig}\,n(\delta_{xy})\tan^{-1}\sqrt{\left|\frac{2\sqrt{\left(\frac{\delta_{xx}-\delta_{yy}}{2}\right)^2+\delta_{xy}^2}+\delta_{xx}-\delta_{yy}}{2\sqrt{\left(\frac{\delta_{xx}-\delta_{yy}}{2}\right)^2+\delta_{xy}^2}+\delta_{yy}-\delta_{xx}}\right|} \tag{37}$$

where, counterclockwise direction is defined positive.

The differentiation of Eq.(37) takes the form

$$\{d\sigma_{ij}\} = [C(\theta)]\begin{bmatrix} d\bar{\sigma}_0 \\ d\bar{\tau}_0 \end{bmatrix} + \frac{d}{d\theta}[C(\theta)]\begin{bmatrix} \bar{\sigma}_0 \\ \bar{\tau}_0 \end{bmatrix} d\theta \tag{38}$$

where, the first term of the right side of Eq.(38) represents the increment of the stress vector caused by the increment of the stress invariant vector under the condition where the principal stress direction is fixed, say $d\theta=0$, and the second term corresponds to the component of the increment of the stress vector due to the rotation of the principal stress axis under the constant stress invariants.

In this paper, the system of the flow rule is compcsed of equations to determine the direction of the stress invariant vector and a equation to determine the principal stress direction under arbitrary strain paths. When this mathematical approach is adopted, the direction of two dimensional stress invariant vector can be formulated in using the biaxial loading tests with the loading paths of the fixed principal stress direction.

The principal stress direction can be formulated by using the experimental data which were carried out under the stress conditions with the rotation hysteresis of principal axis reported in Section 4.3. This approach can make the experimental loading paths coincide with the loading hysteresis used in deriving the constitutive equations. Moreover, experimental data are not used only for determining the material coefficients in the already constructed constitutive equations, but can be directly used for deriving the flow rule.

The previously reported theories as to the flow rules (5),(7),(8),(11),(12),(20) were in general formulated in considering the simplicity of mathematical treatment and were difficult to be checked whether these models could describe the behaviors of concrete or not, because plane stress state is described by three or six dimensional vector. Taking these problems into account, the author took up this mathematical approach of deriving the constitutive flow laws, where the plane stress state is described by the two dimensional invariant vector and one dimensional stress direction.

In the first place, the direction of stress invariant vector is formulated under the loading paths where the principal stress direction remains constant, say $d\theta=0$.

In the second place, applicability of flow rule equations in the first place in case of the loading paths with the principal axis rotation are verified by a series of principal stress rotation tests reported in Section 4.3.

In the third place, the flow rule equation which predicts the principal

stress direction "θ" is derived from the principal stress rotation tests.

In the forth place, the applicability of the proposed flow rules are checked by experimental data obtained under another type of stress paths which are actually produced in RC structures in Chapter 7.

4.2 Direction of stress invariant vector

The objective of this section is to formulate the directional correlation between the the direction of the stress invariant vector $(\bar{\sigma}_0, \bar{\tau}_0)^T$ and the strain vector (ε_{ij}) under the loading paths where the principal stress direction remains constant.

4.2.1 Flow rule No.1 and determination of isotropic stiffness

As the stiffness matrix becomes isotropic and symmetric in the reversible process (See Section 3.3.3), we have

$$\begin{bmatrix} \varepsilon_{e1} \\ \varepsilon_{e2} \end{bmatrix} = \frac{1}{E^*} \begin{bmatrix} 1 & -\nu^* \\ -\nu^* & 1 \end{bmatrix} \begin{bmatrix} \sigma_1 \\ \sigma_2 \end{bmatrix} \tag{39}$$

According to the isotropic and symmetric form of secant stiffness matrix in Eq.(39), the relation of the elastic strain vector and the total stress vector does not depend on the coordinate transformation. Therefore, using Eqs.(11),(12) and (16), in any coordinate system Eq.(39) becomes

$$\begin{bmatrix} \bar{\varepsilon}_0 \\ \bar{\gamma}_0 \end{bmatrix} = \frac{1}{E^*} \begin{bmatrix} 1-\nu^* & 0 \\ 0 & 1+\nu^* \end{bmatrix} \begin{bmatrix} \bar{\sigma}_0 \\ \bar{\tau}_0 \end{bmatrix}_{\delta_{ij}=\varepsilon_{eij}} \quad \text{... Flow Rule No.1} \tag{40}$$

This constitutive equation which formulates the directional correlation between the stress and elastic strain invariant vector is named as flow rule No.1 which was experimentally determined. The flow rule No.1 includes two parameters, say, reversible Poisson's ratio ν^* and reversible stiffness E*.

The reversible Poisson's ratio is the most important material parameter to control the flow rule No.1. The relationship between this isotropic Poisson's ratio in the reversible process and the experimental maximum value of the equivalent total strain is shown in Fig.47. This relationship was obtained from the data of the compression-tension loadihng tests under the reversible process (See Section 2.).

When the maximum level of deformation in the strain hystory is low, say Emax $<$ 0.5, the reversible Poisson's ratio is nearly contant and equal to the initial value. When the maximum equivalent strain Emax exceeds 0.5, it increases linearly.

As shown in Fig.47, the unique relationship between the reversible Poisson's ratio 'ν^*' and maximum level of deformation Emax is observed in the low level of Emax. However, strictly speaking, the assumption of linearity of stress-strain relations in the reversible process is not correct and the value of the isotropic Poisson's ratio 'ν^*' changes a little within the reversible process, especially when concrete has the hysteresis of large deformation in the strain paths (Emax=1.0) as shown in Fig.47. Then, the reversible Poisson's ratio is also influenced by equivalent total strain. But, the scattering of the experimentally obtained reversible Poisson's ratio is small compared with its sensitibity to the change of the maximum equivalent strain, so that the unique relationship between the reversible Poisson's ratio and the maximum equivalent strain is assumed at any time of the reversible process for simplicity as

$$\nu^* = \nu_0 \qquad \text{Emax} < 0.5$$

$$\nu^* = \nu_0(1.8(\text{Emax} - 0.5) + 1.0) \qquad 0.5 \leqq \text{Emax} \tag{41}$$

where $\nu^* \leqq 0.5$ $\qquad \nu_0 = 0.17$

The data of the reversible Poisson's ratio in case of the large deformation level, such as Emax $>$ 1, are lacking, therefore, for the time being, the value of ν^* is limited within 0.5 as Eq.(41), where the volume expansion is idealized not to occur in the reversible process even if the uniaxial compressive stress is applied.

The coefficient E* controls the scalar relations of the stress and elastic strain invarint vectors. Therefore, the reversible stiffness E* can be obtained by solving this flow rule No.1 and the elasto-plastic and fracture constitutive equation simultaneously. Substituting Eq.(40) into Eq.(35), we find that E* must satisfy

$$S\left(\frac{E^*}{1-\nu^*}\bar{\varepsilon}_0,\ \frac{E^*}{1+\nu^*}\bar{\gamma}_0\right)\Big|_{\delta_{ij}=\varepsilon_{eij}} = K(E_{\max})E_0E_e(\bar{\varepsilon}_0,\ \bar{\gamma}_0)|_{\delta_{ij}=\varepsilon_{eij}} \tag{42}$$

Using the function S and F(Ee=F) given in Eq.(13) and Eq.(16) respectively, the reversible stiffness E* can be explicitly solved as

$$E^* = \left.\frac{\sqrt{(c\bar{\varepsilon}_0)^2+(d\bar{\gamma}_0)^2}}{\sqrt{\left(\frac{a\bar{\varepsilon}_0}{1-\nu^*}\right)^2+\left(\frac{b\bar{\gamma}_0}{1+\nu^*}\right)^2}}\right|_{\delta_{ij}=\varepsilon_{eij}} \cdot E_0 K(E_{\max})$$

$$= \left.\frac{E_0 E_e K(E_{\max})}{S\left(\frac{\bar{\varepsilon}_0}{1-\nu^*},\ \frac{\bar{\gamma}_0}{1+\nu^*}\right)}\right|_{\delta_{ij}=\varepsilon_{eij}} \tag{43-1}$$

$$E^* = \frac{\sqrt{(c(1-\nu^*)\bar{\sigma}_0)^2+(d(1+\nu^*)\bar{\tau}_0)^2}}{\sqrt{(a\bar{\sigma}_0)^2+(b\bar{\tau}_0)^2}} E_0 K(E_{\max}) \tag{43-2}$$

Let us now consider the reversible process. In this condition, the plastic strains are idealized constant, that is, the increment of the elastic strains are equal to the increment of the total strains. Accordingly, when the values of stresses and strains at time t are known and the values of the total strains at time t+dt are given, the stress invariant vectors at time t+dt can be calculated by the flow rule No.1(Eq.(40)). The flow rule system in the reversible process is constructed only with the Flow rule No.1.

4.2.2 Flow rule No.2 and No.3, and directions of stress and strain invariant vectors in irreversible process

In the case of the reversible process, fracture parameter and equivalent plastic strain (state values) are constant and independent of the strain paths, so that, the flow rule No.1 can be explicitly formulated in the integlated form of stress and strain vectors. But, in the case of the irreversible process, the fracture parameter and the equivalent plastic strain are not constant, moreover these values are evaluated by the path-integretion, therefore, it is impossible to formulate the flow rule with the integrated stress and strain formats in the irreversible process.

Accordingly, the author chose the approach to construct the system of the flow rule in difference forms from experimental data and next, to generalize the system to the simultaneous system of differential constitutive equations.

Increment of the stress invariant vector $(\Delta\bar{\sigma}_0, \Delta\bar{\tau}_0)^T$ in the irreversible process can be calculated from experimental data using Eq.(11) and Eq.(12). In this process, the finite difference of stress increments were 2 - 5 % of the uniaxial compressive strength. The increment of the stress invariant vector can be divided into two vectors, say, V1 which does not change the equivalent stress and V2 which increases the value of the equivalent stress as shown in Fig.48. The component vector V1 is defined to converge the tangent vector which touches the envelope at the stress point ($\bar{\sigma}_0^t$, $\bar{\tau}_0^t$), where the equivalent

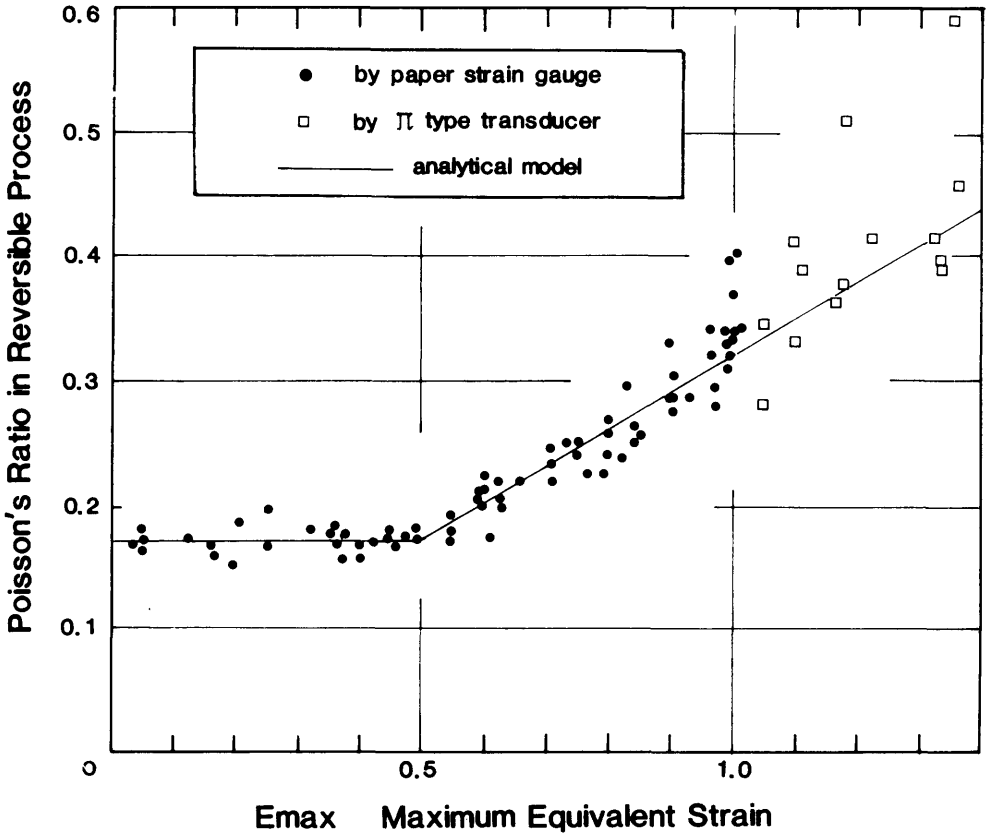

Fig.47. Relation between maximum equivalent strain and Poisson's ratio in the reversible process.

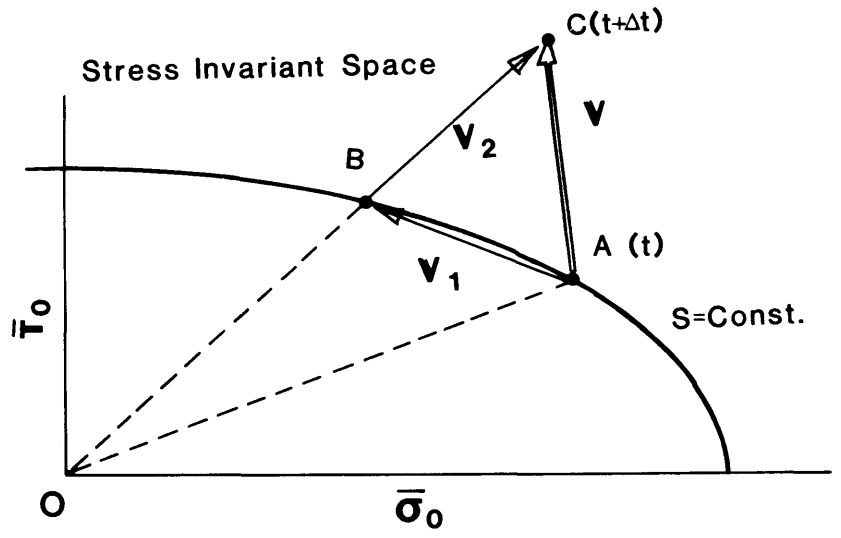

Fig.48. Direction of incremental stress invariant vector and component vector.

stress S is constant and equal to $S(\bar{\sigma}_0^t, \bar{\tau}_0^t)$, when the stress increment becomes infinitely small. V2 is defined as the component vector at point B on this envelope as shown in Fig.48. In this paper, this dividing rule of stress invariant vector is named as flow rule No.2.

The mathematical definition of the flow rule No.2 can be written in the form

$$V = \begin{bmatrix} \Delta\bar{\sigma}_0 \\ \Delta\bar{\tau}_0 \end{bmatrix} = V_1 + V_2 = \begin{bmatrix} \Delta\bar{\sigma}_{on} \\ \Delta\bar{\tau}_{on} \end{bmatrix} + \begin{bmatrix} \bar{\sigma}_0^t + \Delta\bar{\sigma}_{on} \\ \bar{\tau}_0^t + \Delta\bar{\tau}_{on} \end{bmatrix} \Delta l \qquad (44\text{-}1)$$

... Flow Rule No. 2

$$S(\bar{\sigma}_0^t + \Delta\bar{\sigma}_{on},\ \bar{\tau}_0^t + \Delta\bar{\sigma}_{on}) = S(\bar{\sigma}_0^t,\ \bar{\tau}_0^t) \qquad (44\text{-}2)$$

where, the position vector of point B on the stress space is defined as $(\bar{\sigma}_0^t + \Delta\bar{\sigma}_{on},\ \bar{\tau}_0^t + \Delta\bar{\tau}_{on})$, accordingly the vector V2 is defined to be parallel to the position vector of point B. Δl is the propotional coefficient. In the biaxial experimental data, incremental stress invariant vector are given values, therefore, unknown values $\Delta\bar{\sigma}_{on}$, $\Delta\bar{\tau}_{on}$ and Δl can be easily and uniquely determined by solving Eq.(44-1) and Eq.(44-2) simultaneously.

In the irreversible process, the incremental strain invariant vector $(\Delta\bar{\varepsilon}_0, \Delta\bar{\gamma}_0)^T$ which indicates the degree of the incremental total strain vector is

$$\bar{\varepsilon}_0^t \equiv \bar{\varepsilon}_0(\delta_{ij} = \varepsilon e_{ij}^t) \qquad (45\text{-}1)$$

$$\bar{\gamma}_0^t \equiv \bar{\gamma}_0(\delta_{ij} = \varepsilon e_{ij}^t) \qquad (45\text{-}2)$$

$$\Delta\bar{\varepsilon}_0 \equiv \bar{\varepsilon}_0(\delta_{ij} = \varepsilon e_{ij}^t + \Delta\varepsilon_{ij}) - \bar{\varepsilon}_0^t \qquad (45\text{-}3)$$

$$\Delta\bar{\gamma}_0 \equiv \bar{\gamma}_0(\delta_{ij} = \varepsilon e_{ij}^t + \Delta\varepsilon_{ij}) - \bar{\gamma}_0^t \qquad (45\text{-}4)$$

Similar to the case of vector V, the author considered to divide the strain invariant vector $X=(\Delta\bar{\varepsilon}_0, \Delta\bar{\gamma}_0)^T$ into component vector X1, which does not change the equivalent total strain and X2, which increases the value of the equivalent total strain.

If the constitutive equations, which indicate the directional correlations between X1 and V1 and between X2 and V2, are formulated, the system of flow rule is completed under an arbitrary strain path in the irreversible process.

According to this consideration, it is reasonable to define the component vector X1 as the tangent vector which touches the envelope at point $(\bar{\varepsilon}_0^t, \bar{\gamma}_0^t)$, where the equivalent strain E is constant, when the strain increment becomes infinitely small as shown in Fig.49. The mathematical definition is written as

$$X = \begin{bmatrix} \Delta\bar{\varepsilon}_0 \\ \Delta\bar{\gamma}_0 \end{bmatrix} = X_1 + X_2, \qquad X_1 \equiv \begin{bmatrix} \Delta\bar{\varepsilon}_{on} \\ \Delta\bar{\gamma}_{on} \end{bmatrix} \tag{46-1}$$

$$F(\bar{\varepsilon}_0^t + \Delta\bar{\varepsilon}_{on},\ \bar{\gamma}_0^t + \Delta\bar{\gamma}_{on}) = F(\bar{\varepsilon}_0^t,\ \bar{\gamma}_0^t) \tag{46-2}$$

where, the component vector X2 is still unknown.

Let us now consider the condition where the stress incremental vector V is indicated only by the component V1. This stress path corresponds to the hysteresis in which the equivalent stress remains constant, therefore, the corresponding incremental strain vector must be devided only with X1 due to Eq.(35). This loading path exists on the boundary of reversible area whose functional corresponds to the irreversible criterion in Eq.(30) (This loading hysteresis is defined as 'neutral pocess'.). In this case, the flow rule in the irreversible process must coincide with that in the reversible process (the requirement of continuity condition). Therefore, the directional correlation between stress and strain invariant vector in this neutral process must be described by the flow rule No.1 as

$$\begin{bmatrix} \bar{\varepsilon}_0^t + \Delta\bar{\varepsilon}_{on} \\ \bar{\gamma}_0^t + \Delta\bar{\gamma}_{on} \end{bmatrix} = \frac{1}{E^*} \begin{bmatrix} 1-\nu^* & 0 \\ 0 & 1+\nu^* \end{bmatrix} \begin{bmatrix} \bar{\sigma}_0^t + \Delta\bar{\sigma}_{on} \\ \bar{\tau}_0^t + \Delta\bar{\tau}_{on} \end{bmatrix} \tag{47}$$

The values of ν^* and E* in Eq.(47) are determined by Eq.(41) and Eq.(42). From this continuity condition, the author define to apply the flow rule No.1 (Eq.(47)) as the flow rule equation which formulates the directional correlation between the stress component vector V1 and the strain component vector X2 not only in this neutral process but in the general irreversible one.

Accordingly, the strain component vector X1 is calculated from the stress component vector V1, and the other component vector X2 can be experimentally obtained by Eqs.(46-1),(45). The formulation of the direction of the strain component vector X2 completes the system of flow rule as the directional correlation of total stress and strain vectors mathematically.

The component vector V2 on the point B in the stress space (Fig.48) and the corresponding strain component vector X2 on the point B' in the strain space (Fig.49) are respectively plotted in each strain level as shown in Fig.50(a)- Fig.50(e), where the coordinate of point B' is defined as $(\bar{\varepsilon}_0^t + \Delta\bar{\varepsilon}_{on},\ \bar{\gamma}_0^t + \Delta\bar{\gamma}_{on})$. The arrows in these figures represent the directions of V2 and X2 respectively, points B4-B6 and B4'-B6' correspond to the stress and strain points B and B' in biaxial compression stress states, and poimts B1-B3 and

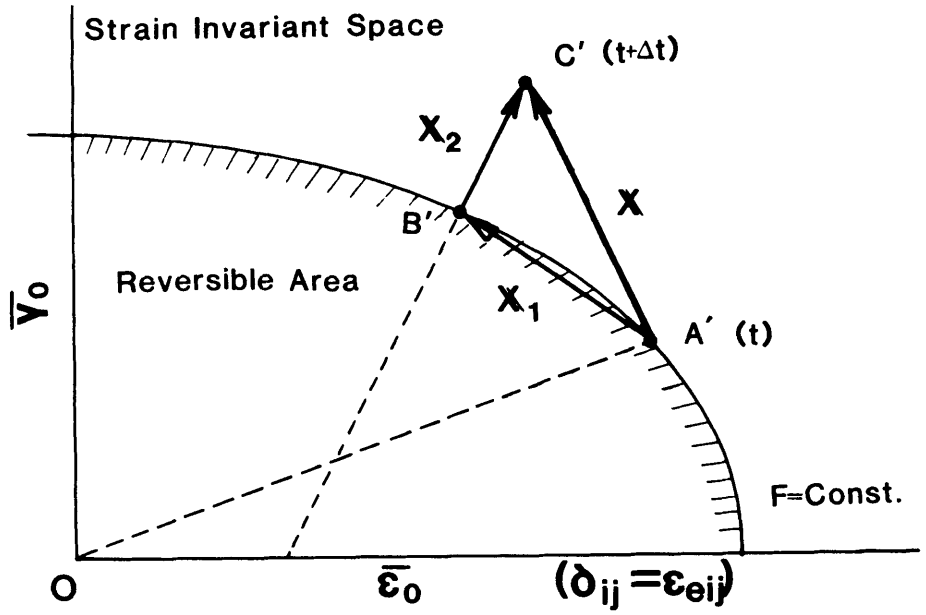

Fig.49. Direction of incremental strain invariant vector and component vectors.

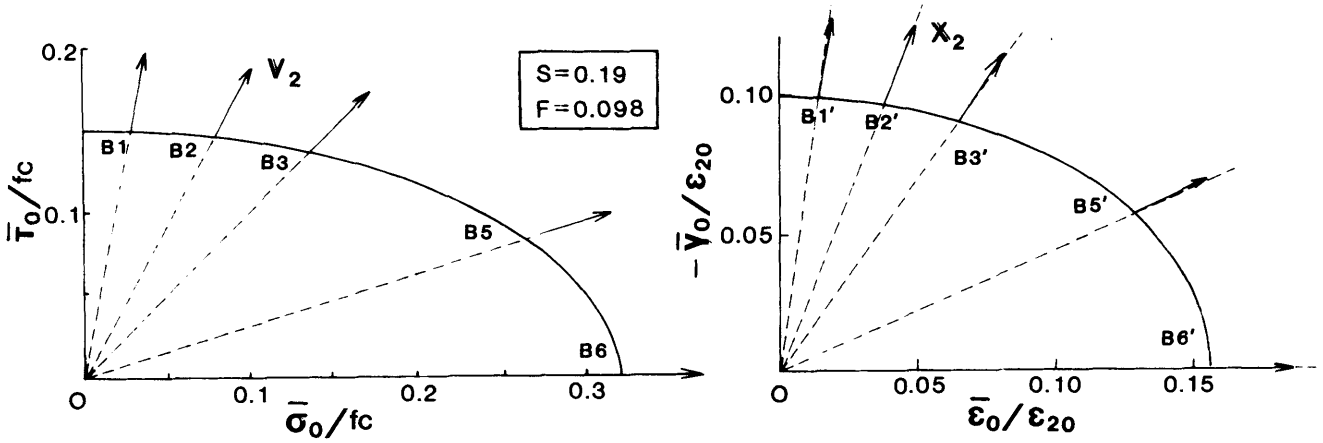

Fig.50. (a)

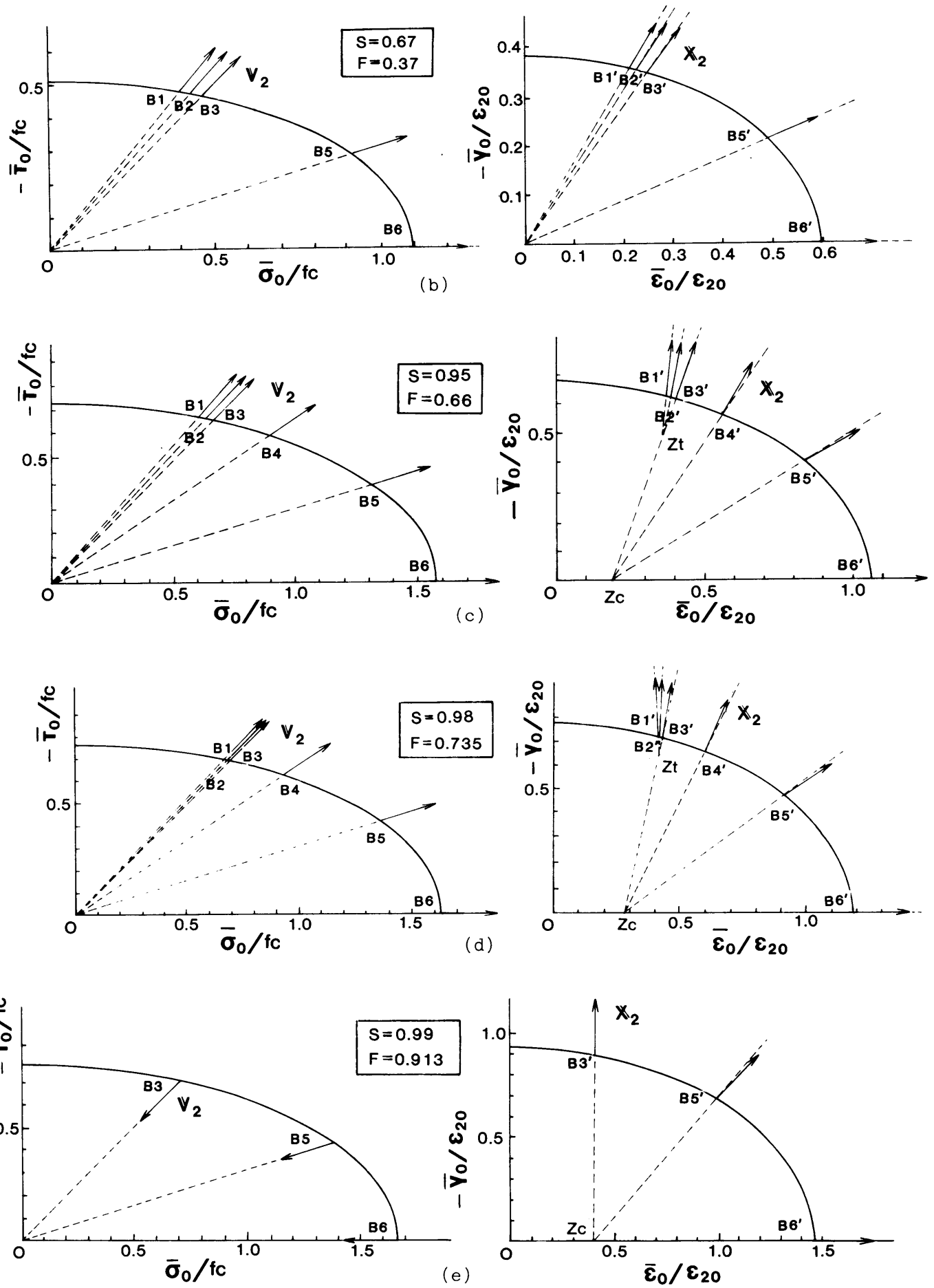

Fig.50. Direction of component vector X2.

B1'-B3', the compression-tension stress states on the stress and strain spaces respectively. In the irreversible process at the low equivalent elastic strain levels, vector X2 is almost parallel to the position vector of B' ($\bar{\varepsilon}_0^t+\Delta\bar{\varepsilon}_{on}$, $\bar{\gamma}_0^t+\Delta\bar{\gamma}_{on}$) at all the ratios of the principal stresses (B1-B6, B1'-B6').

However, as the equivalent elastic strain level becomes larger, the directions of the vector X2 become non-parallel to the direction of the position vector B' as shown in Fig.50(c)-50(e). Then, the following interesting fact is observed that, the extentions of vectors X2 on B' converge to the common point Zc on the mean stress axis in biaxal compression stress states (B4-B6, B4'-B6'), and to the other convergence point Zt in case of the compression-tention stress state (B1-B3, B1'-B3').

According to this indication, convergence points Zc and Zt coincide with the origin on the strain space when X2 is parallel to the position vector of point B'. Therefore, the direction of the vector X2 can be unifiedly formulated using the coordinate values (α, β) of these convergence points without any stress component in the form

$$\boldsymbol{X}_2=\begin{bmatrix}\bar{\varepsilon}_0^t+\Delta\varepsilon_{on}-\alpha\\ \bar{\gamma}_0^t+\Delta\bar{\gamma}_{on}-\beta\end{bmatrix}\Delta m \tag{48}$$

Substituting Eq.(48) into Eq.(46-1), we can find the direction of the strain invariant vector in the irreversible process and flow rule No.3 is defined by

$$\boldsymbol{X}=\boldsymbol{X}_1+\boldsymbol{X}_2=\begin{bmatrix}\Delta\bar{\varepsilon}_{on}\\ \Delta\bar{\sigma}_{on}\end{bmatrix}+\begin{bmatrix}\bar{\varepsilon}_0^t+\Delta\bar{\varepsilon}_{on}-\alpha\\ \bar{\gamma}_0^t+\Delta\bar{\sigma}_{on}-\beta\end{bmatrix}\Delta m \quad \text{....Flow Rule No.3} \tag{49}$$

In this newly proposed flow rule system, proportional coefficients m and l are the unknown values, which control the "lengths" of stress and strain vectors(See Section 3). Therefore, the scalar relation of the parameter m and l should be determired by the elasto-plastic and fracture constitutive law which formulates the relations between the scalar invariant vector of the stress and the strain vectors.

As a result, the flow rule system to predict the direction of the stress invariant vector is organized with flow rule equations No.1-No.3 as shown in Fig.51.

Let us now consider the case where (α, β)=(0,0). From the flow rule No.1, No.2 and No.3, the isotropic relationship similar to the flow rule No.1 is also derived in the irreversible process as

$$\begin{bmatrix} \bar{\varepsilon}_0^t + \Delta\bar{\varepsilon}_0 \\ \bar{\gamma}_0^t + \Delta\bar{\gamma}_0 \end{bmatrix} = \frac{1+\Delta m}{1+\Delta l}\frac{1}{E^*}\begin{bmatrix} 1-\nu^* & 0 \\ 0 & 1+\nu^* \end{bmatrix}\begin{bmatrix} \bar{\sigma}_0^t + \Delta\bar{\sigma}_0 \\ \bar{\tau}_0^t + \Delta\bar{\tau}_0 \end{bmatrix} \tag{50}$$

which describes the direction of the stress and strain invariant vector at time t+Δ t. But, when the convergence points Zc and Zt shift from the origin in the strain space, the isotropic relationship as Eq.(50) in the irreversible process does not hold, but the anisotropic and non-symmetric matrix of tangent stiffness is derived from the system of the flow rule (Mathematical derivations of general anisotropic constitutive equations will be discussed in Section 4.3.5.). Therefore, the parameters (α, β) represents the degree of the anisotropy of concrete. When these parameters are nearly zero, the behavior of concrete is nealy isotropic, and the larger values of these anisotropy parameters describe the level of the anisotropic behavior of concrete.

4.2.3 Formulation of the anisotropy

The kinematic shift of these convergence points Zc and Zt represents the relatively large strain in the maximum principal stress direction compared with the strain in the minimum one, and corresponds to the anisotropy in the large deformational level. The existence of two convergence points concerning the ratios of the principal stresses reflects the characteristics of the more anisotropic behaveior of concrete under high compression tention stress state. According to Fig.52, the anisotropy parameters (α, β) in biaxial compression stresses are given by

$$(\alpha, \beta) = (gEe/c\ ,\ 0) \tag{51}$$

The compression-tension convergence point Zt is located on the line between point Zc and the uniaxial compression point on the envelope where equivalent total strain is constant. Therefore, the coodinate values of point Zt on the strain space in biaxial compression-tension, tension-tension stress states is

$$(\alpha, \beta) = \left(gE_e/c + h\left(\frac{-E_e}{\sqrt{c^2 + \left(\frac{1+\nu^*}{1-\nu^*}d\right)^2}} - gE_e/c \right),\ h\frac{E_e}{\sqrt{\left(\frac{1-\nu^*}{1+\nu^*}c\right)^2 + d^2}} \right) \tag{52}$$

These coefficients g and h which are named as 'flow rule parameters' are shown in Fig.53, where those coefficients were calculated by the author's biaxial test data (Section 2) and Kupfer's one(2). The values of g and h can be formulated with reasonable accuracy by the equivalent elastic strain as

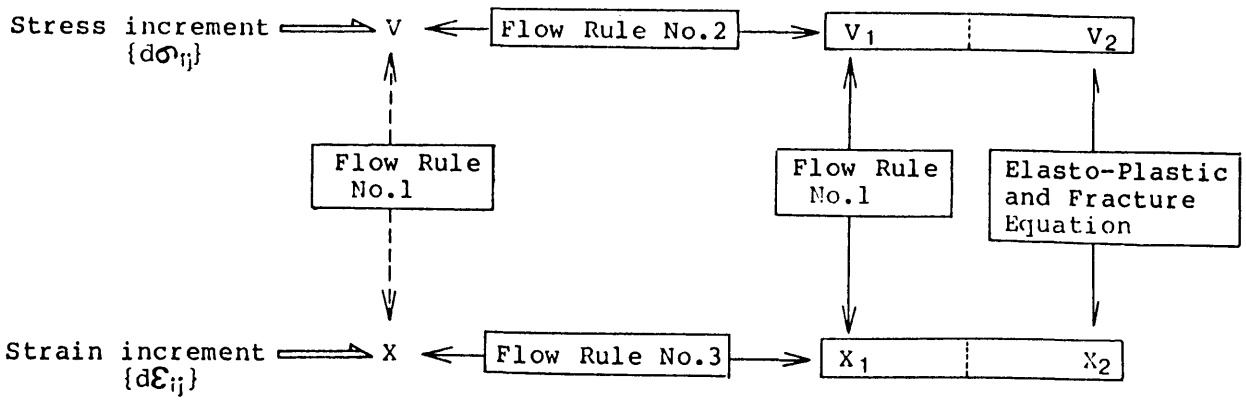

Fig.51. System of flow rule predicting the direction of stress invariant vector.

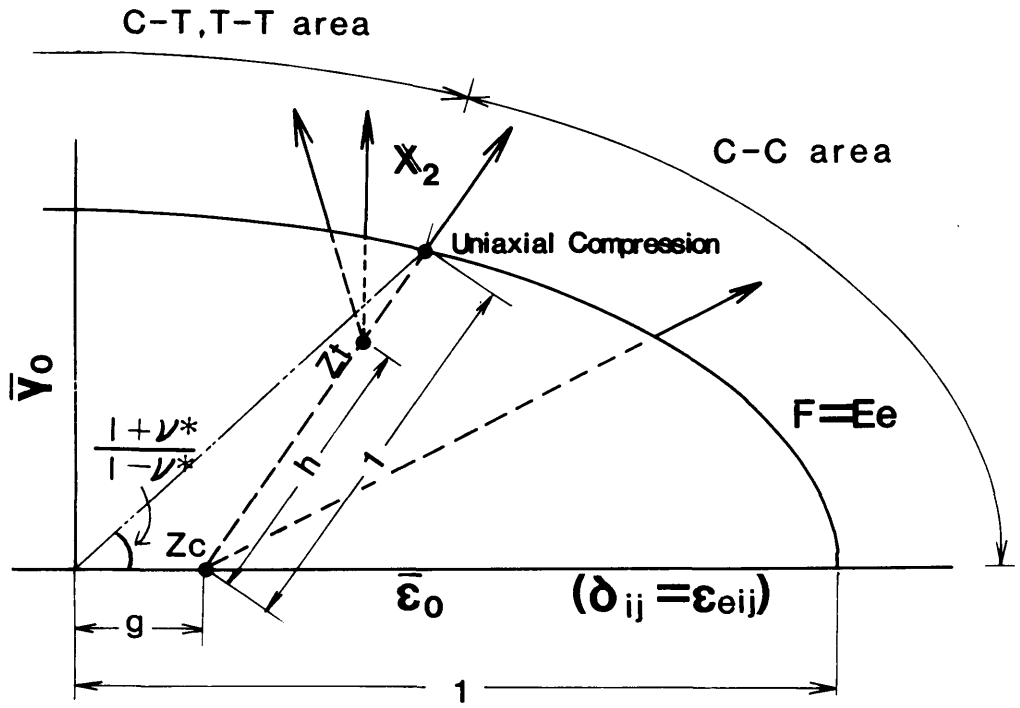

Fig.52. Formulation of component vector X2 and focus points Zc and Zt.

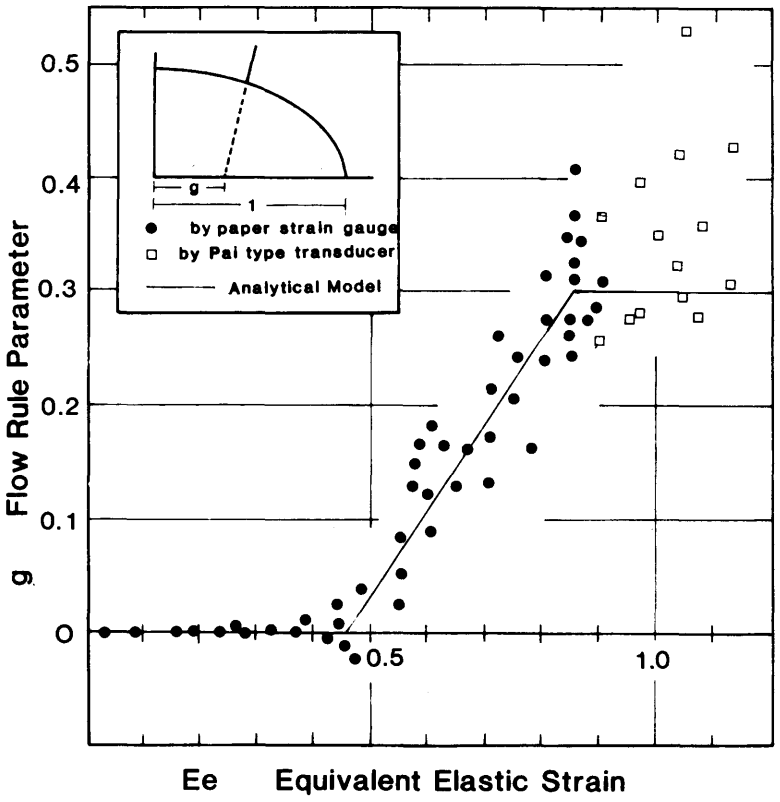

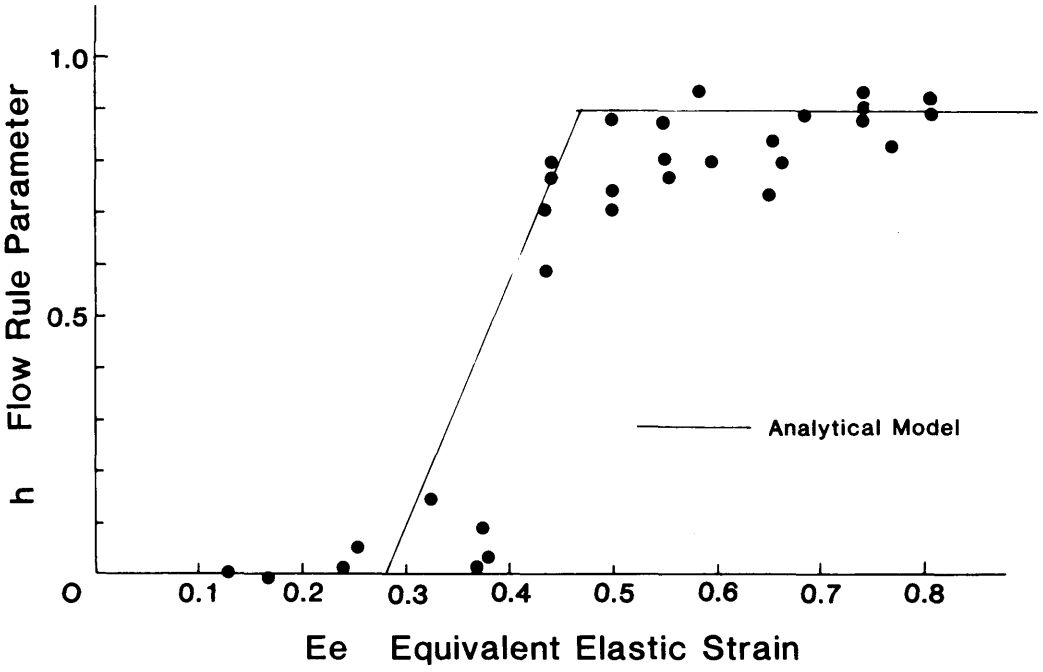

Fig.53. Flow rule parameter (a): for biaxial compression stress states
(b): for compression-tension stress states.

$$
\begin{aligned}
g &= 0 && Ee \leqq 0.46 \\
&= 0.3(2.6Ee - 1.2) && 0.46 < Ee \\
g &\leqq 0.3
\end{aligned} \tag{53}
$$

$$
\begin{aligned}
h &= 0 && Ee \leqq 0.28 \\
&= 5Ee - 1.4 && 0.28 < Ee \\
h &\leqq 0.9
\end{aligned} \tag{54}
$$

4.2.4 Differential forms of flow rules

In this section, the linearization of the nonlinear difference flow rules No.1-No.3 is carried out to generalize these flow rule equations mathematically, and the constitutive equation which predict the stress invariant vector under general strain paths will be formulated by solving these flow rule equations and the previouly formulated elasto-plastic and fracture equation simultaneously.

The flow rule No.2 is linearized by disregarding differential terms of higher orders as

$$
\begin{bmatrix} d\bar{\sigma}_0 \\ d\bar{\tau}_0 \end{bmatrix} = [S1] \begin{bmatrix} dj \\ dl \end{bmatrix}, \quad [S1] = \begin{bmatrix} -\dfrac{\partial S}{\partial \bar{\tau}_0} & \bar{\sigma}_0 \\ \dfrac{\partial S}{\partial \bar{\sigma}_0} & \bar{\tau}_0 \end{bmatrix}, \quad \begin{bmatrix} d\bar{\sigma}_{on} \\ d\bar{\tau}_{on} \end{bmatrix} = \begin{bmatrix} -\dfrac{\partial S}{\partial \bar{\tau}_0} \\ \dfrac{\partial S}{\partial \bar{\sigma}_0} \end{bmatrix} dj \tag{55}
$$

where dj dl : proportional coefficients

$[Si]$: stress transformation matrix

Similarly, we can write the differential form of the flow rule No.3 as

$$
\begin{bmatrix} d\bar{\varepsilon}_0 \\ d\bar{\gamma}_0 \end{bmatrix} = [M] \begin{bmatrix} dk \\ dm \end{bmatrix}, \quad [M] = \begin{bmatrix} -\dfrac{\partial F}{\partial \bar{\gamma}_0} & \bar{\varepsilon}_0 - \alpha \\ \dfrac{\partial F}{\partial \bar{\varepsilon}_0} & \bar{\gamma}_0 - \beta \end{bmatrix}_{\delta_{ij} = \varepsilon_{eij}},
$$

$$
\begin{bmatrix} d\bar{\varepsilon}_{on} \\ d\bar{\gamma}_{on} \end{bmatrix} = \begin{bmatrix} -\dfrac{\partial F}{\partial \bar{\gamma}_0} \\ \dfrac{\partial F}{\partial \bar{\varepsilon}_0} \end{bmatrix}_{\delta_{ij} = \varepsilon_{eij}} dk \tag{56}
$$

$$
\begin{bmatrix} d\bar{\varepsilon}_0 \\ d\bar{\gamma}_0 \end{bmatrix} = [D]\{d\varepsilon_{ij}\} \qquad [D] = \begin{bmatrix} \dfrac{1}{\sqrt{2}} & \dfrac{1}{\sqrt{2}} & 0 \\ \dfrac{\delta_{xx} - \delta_{yy}}{2\bar{\gamma}_0} & \dfrac{\delta_{yy} - \delta_{xx}}{2\bar{\gamma}_0} & \dfrac{2\delta_{xy}}{\bar{\gamma}_0} \end{bmatrix}_{\delta_{ij} = \varepsilon_{eij}}
$$

where, dk, dl : proportional coefficients

$[M]$: strain transformation matrix

$[D]$: strain matrix

Incremental stress and strain invariant vectors are linearly transformed into the local coordinate systems which have the origins at $(\bar{\sigma}_0^t, \bar{\tau}_0^t)$ and $(\bar{\varepsilon}_0^t, \bar{\gamma}_0^t)$ on the stress and strain space respectively. (dj,dl) and (dk,dm) represent the local coordinate values and two columns of stress and strain transformation matrices are the base vectors of each coordinate system as shown in Fig.54.

The flow rule No.1 at time t+dt is described in the differential form

$$\left.\frac{\bar{\varepsilon}_0 + d\bar{\varepsilon}_{on}}{\bar{\gamma}_0 + d\bar{\gamma}_{on}}\right|_{\delta_{ij}=\varepsilon^t_{ij}} = \frac{1-\nu^*}{1+\nu^*}\frac{\bar{\sigma}_0^t + d\bar{\sigma}_{on}}{\bar{\tau}_0^t + d\bar{\tau}_{on}} \tag{57}$$

Similarly, the flow rule No.1 at time t is

$$\left.\frac{\bar{\varepsilon}_0}{\bar{\gamma}_0}\right|_{\delta_{ij}=\varepsilon^t_{ij}} = \frac{1-\nu^*}{1+\nu^*}\frac{\bar{\sigma}_0^t}{\bar{\tau}_0^t} \tag{58}$$

Therefore, when the neutral loading path is chosen as the differential path, as the general form of flow rule No.1 in the irreversible process, we have

$$d\left(\frac{\bar{\varepsilon}_0}{\bar{\gamma}_0}\right) = d\left\{\left(\frac{1-\nu^*}{1+\nu^*}\right)\frac{\bar{\sigma}_0}{\bar{\tau}_0}\right\} \tag{59}$$

Eq.(55), Eq.(56) and Eq.(59) are the generalized flow rule equations. Solving these flow rule equations with the elasto-plastic and fracture constitutive equation simultaneously, we can get the constitutive equation which gives the stress invariant vector in the form

$$\begin{bmatrix} d\bar{\sigma}_0 \\ d\bar{\tau}_0 \end{bmatrix} = [[S1][S21][M]^{-1}[D] + [S1][S22][M]^{-1}[D]] \begin{bmatrix} d\varepsilon_{xx} \\ d\varepsilon_{yy} \\ d\varepsilon_{xy} \end{bmatrix} \tag{60}$$

$$S21 = \begin{bmatrix} P1 & 0 \\ 0 & P2 \end{bmatrix} \quad \text{Fracture matrix} \qquad S22 = \begin{bmatrix} P1 & 0 \\ 0 & P3 \end{bmatrix} \quad \text{Plasticity matrix}$$

where, the process of the mathematical derivation and the functional forms of P1, P2, P3 are given in Appendix.II.

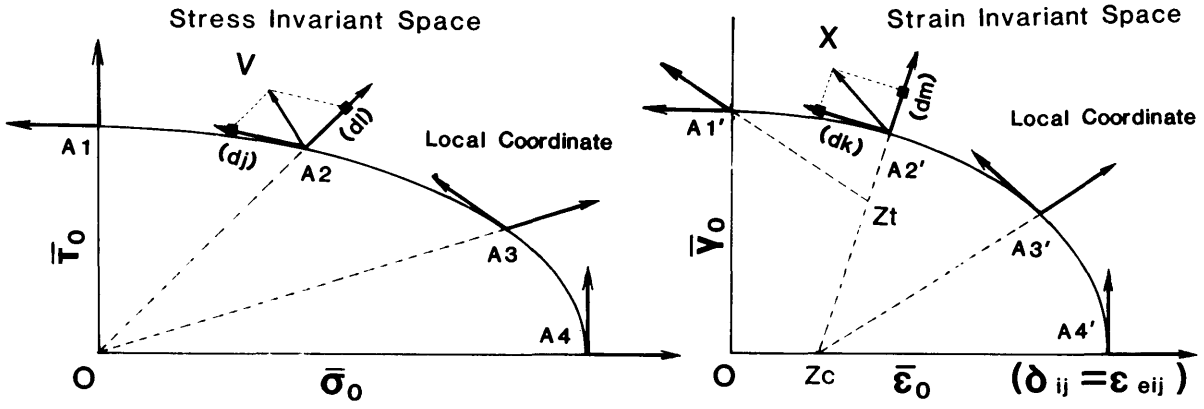

Fig.54. Local coordinates and base vectors on the stress and strain spaces.

4.3 Loading hysteresis including principal axis rotation and floe rule No.4

The stress invariant vector under an arbitrary strain path can be determined mathematically by Eq.(60), but its applicability has been verified only by the experimental data in the loading paths under fixed principal stress direction. The application of Eq.(60) in the irreversible process to the more general cases including principal axis rotation requres the following conditions.

(1) The elasto-plastic and fracture constitutive equation is independent of the rotation of the principal stress axis. Similarly, the criterion of the irreversible process is not influenced by the strain paths of axis rotation.

(2) Flow rules No.1-No.3 hold even when the rotation of the principal axis occurs, in other words, flow rule parameters g,h and reversible Poisson's ratio must be independent of the effect of axis rotation for the more general cases.

In the first place, this section discusses the applicability of the elasto-plastic and fracture law and the flow rules No.1-No.3 to the case of the principal axis rotation.

In the second place, this section proposes a flow rule which describes the maximum principal stress direction in the general strain paths. The predicting precision of the principal stress direction has not been also verified in the previously reported contitutive models because of lack of experimental data, and because their mathematical forms are in general not suitable to take the deformational characteristics concerning the direction of the principal stress axis into the mathematical description.

4.3.1 Experiments

The loading paths including the rotation of the principal stress axis was introduced by the following method.

(1) Uniaxial compressive stress was monotonically applied to a certain strain level and unloaded completely (the first loading).

(2) A concrete piece was cut off the uniaxially compressed concrete plate in (1) and re-shaped as shown in Fig.55.

(3) Uniaxial compressive stress was applied to the cut-off concrete specimen (the second loading). In this case, the direction of principal stress was different from that in the first loaeding.

The mixture of concrete plates used is shown in Table 1. Four faces of the cut-off concrete plates were recapped by the super high early portland

cement mortar whose uniaxial one-day compressive strength was almost equal to the strength of concrete used as shown in Fig.55. In the process of cutting, the concrete plate was splitted statically with round steel bars as shown in Fig.56. The diamondcutter was not used because it has the possibility to introduce the extra microcracking by its hard vibrations. The cut concrete plates and recapped one are shown in Fig.57. The same procedures in Chapter 2 were applied for elimination of contact friction and for measurement of stress and strains. In order to check the method of cutting, the uniaxial stress-strain curve was measured using the cut-off concrete plates from a vergin concrete specimen. The stress-strain diagram of cut-off concrete practically coincides with that of the original one. The compressive level at the first loading and rotation angles are summarized in Table 2.

4.3.2 Experimental verification of elasto-plastic and fracture law and the flow rules

The experimental results including principal axis rotation tests are given as shown in Fig.58. The coordinate system used is set as shown in Fig.55. When the compressive stress was reloaded within the maximum experimental stress of the first loading, there exists the practical linear relationship between the increments of stress and strain even in the hysteresis including stress axis rotation. However, when the concrete was compressed to the level of the uniaxial strength, the stress-strain relationship in the reversible process becomes nonlinear and the peak strength at the second loading decreases due to the effect of cyclic loading, regardless of the axis rotation. The effect of cyclic loading to the stress-strain relationships will be discussed in another papers.

The equavalent stress-strain diagrams of the test sereies in Table 2 are shown in Fig.59. Concrete subjected to the loading hysteresis where the maximum equivalent total strain is approximately 0.46 behaves linearly when the equivalent total strain E in the second loading is smaller than the maximum value of the equivalent total strain Emax, but the nonlinearity in the diagrams in Fig.59(a) appears when the value of E exceeds Emax in the first loading, where this process satisfies the irreversible condition.

From experimental results, the constitutive equation of the elasto-plastic and fracture model in Eq.(35) and irreversible criterion in Eq.(30) is successful to predict these nonlinear behavior of concrete quantitatively. It is observed from these experiments that the equivalent stress-strain relationship is independent of the hysteresis of principal stress rotation.

In case of the loading hystory where the maximum level of the equivalent

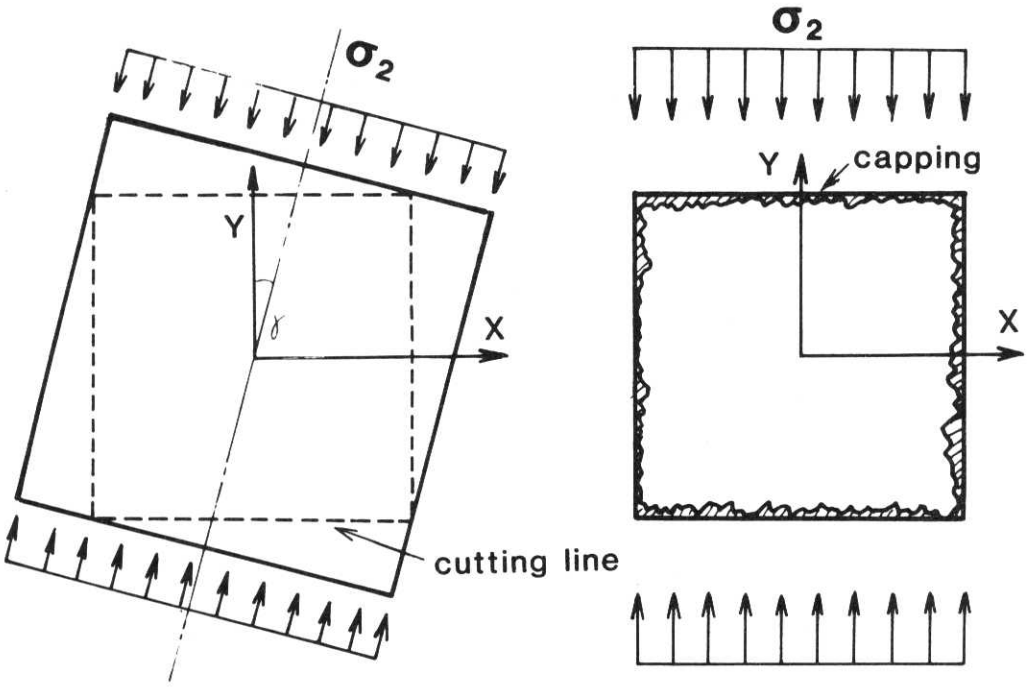

Fig.55. Principal axis rotation and coordinate system.

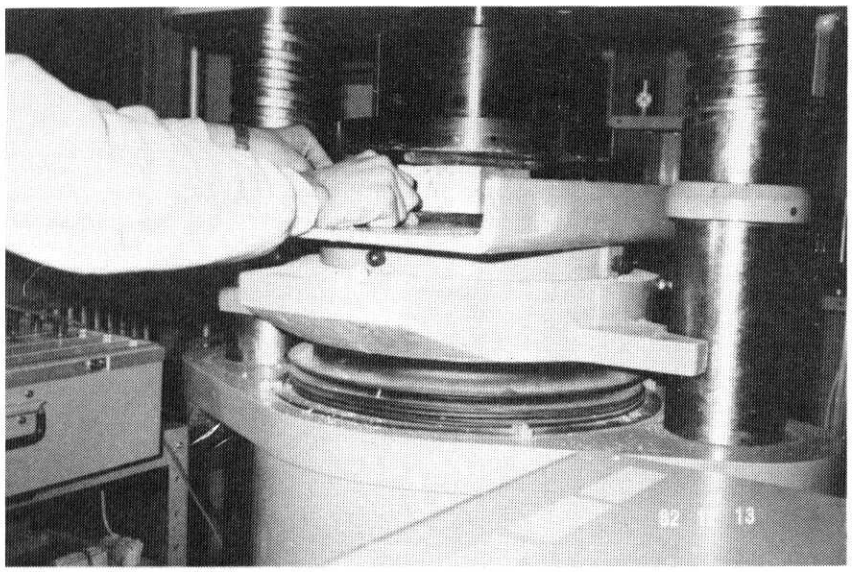

Fig.56. Method of cutting concrete by splitting.

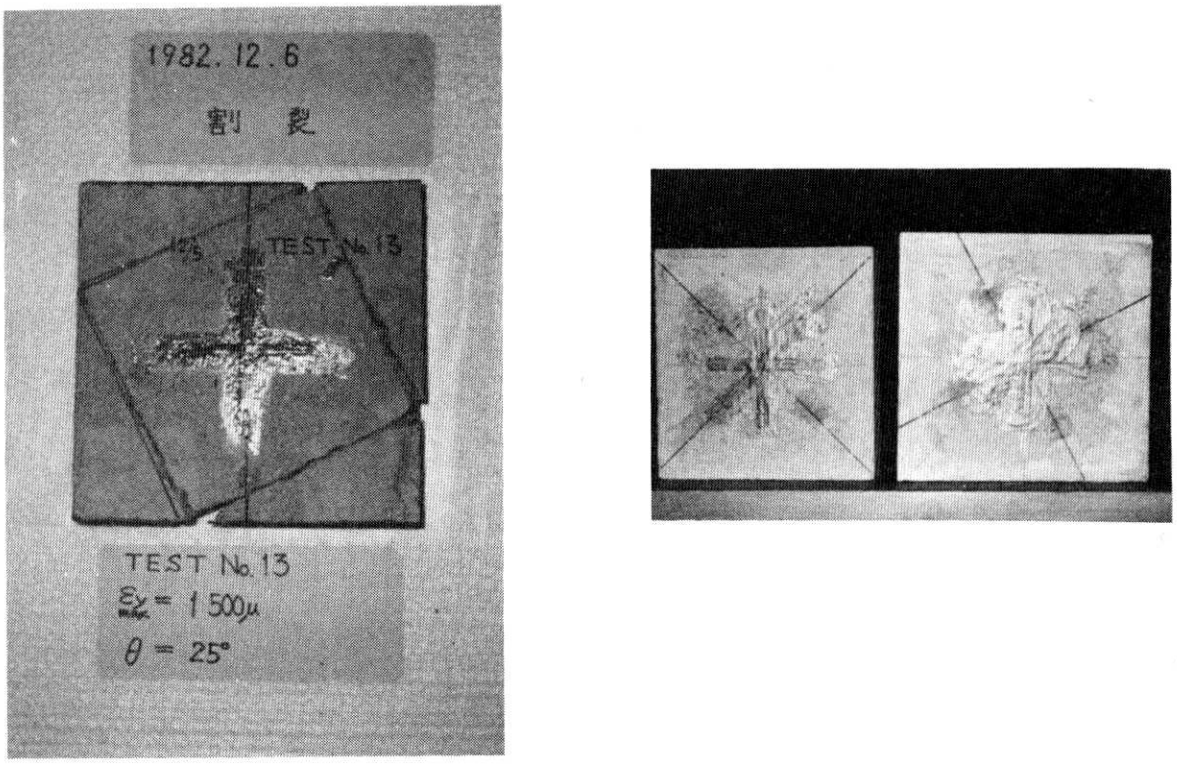

Fig.57. Cut concrete and capped concrete specimens.

Table 2. Specimens and loading program of principal axis rotation tests.

Exp. No.	γ (deg.)	Mix. Type*	F_C (Mpa)	$\in_{20}$ (micro)	E_{max} (First)
RT1	15	B	−27.4	−2100	0.46
RT2	25	B	−27.4	−2180	0.41
RT3	45	B	−28.0	−2200	0.46
RT4	65	B	−28.0	−2200	0.46
RT5	15	B	−26.9	−2100	0.58
RT6	25	B	−28.0	−2200	0.56
RT7	45	B	−26.9	−2200	0.66
RT8	65	B	−27.7	−2200	0.55
RT9	21	A	−34.4	−2350	0.95
RT10	28.4	A	−35.1	−2350	0.85
RT11	45	A	−34.0	−2350	0.95

* See Table 1

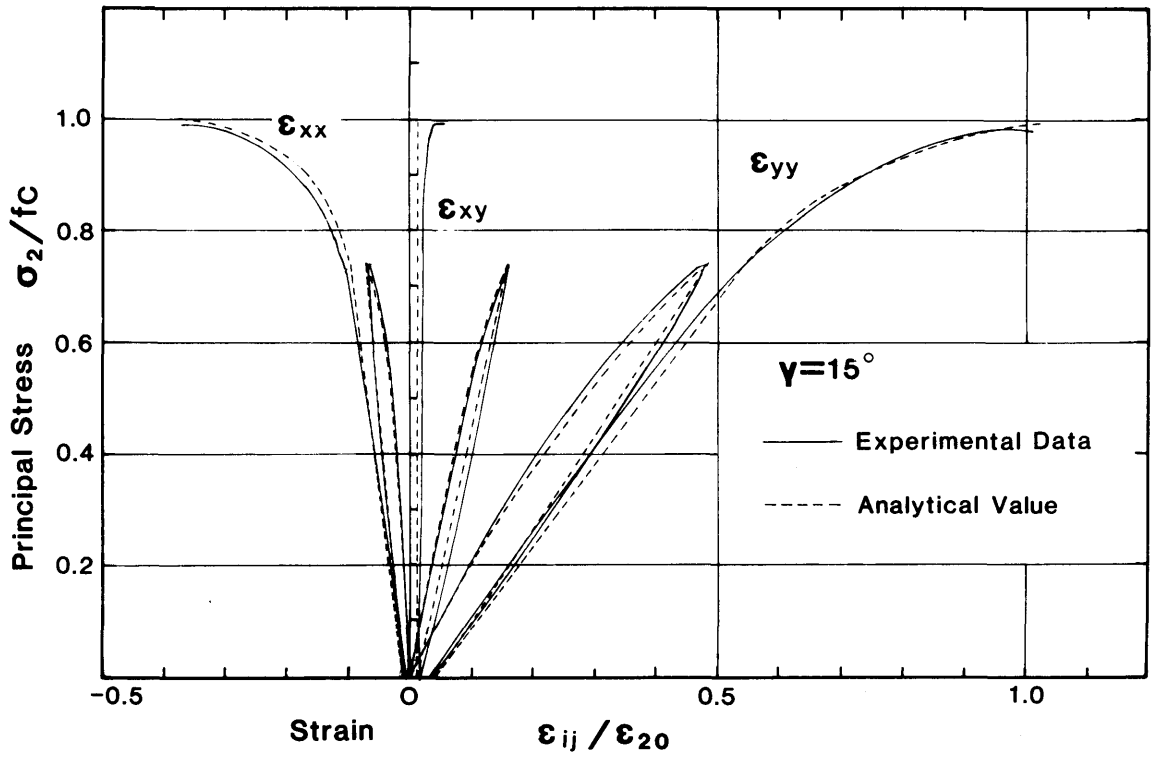

Fig.58. (a)

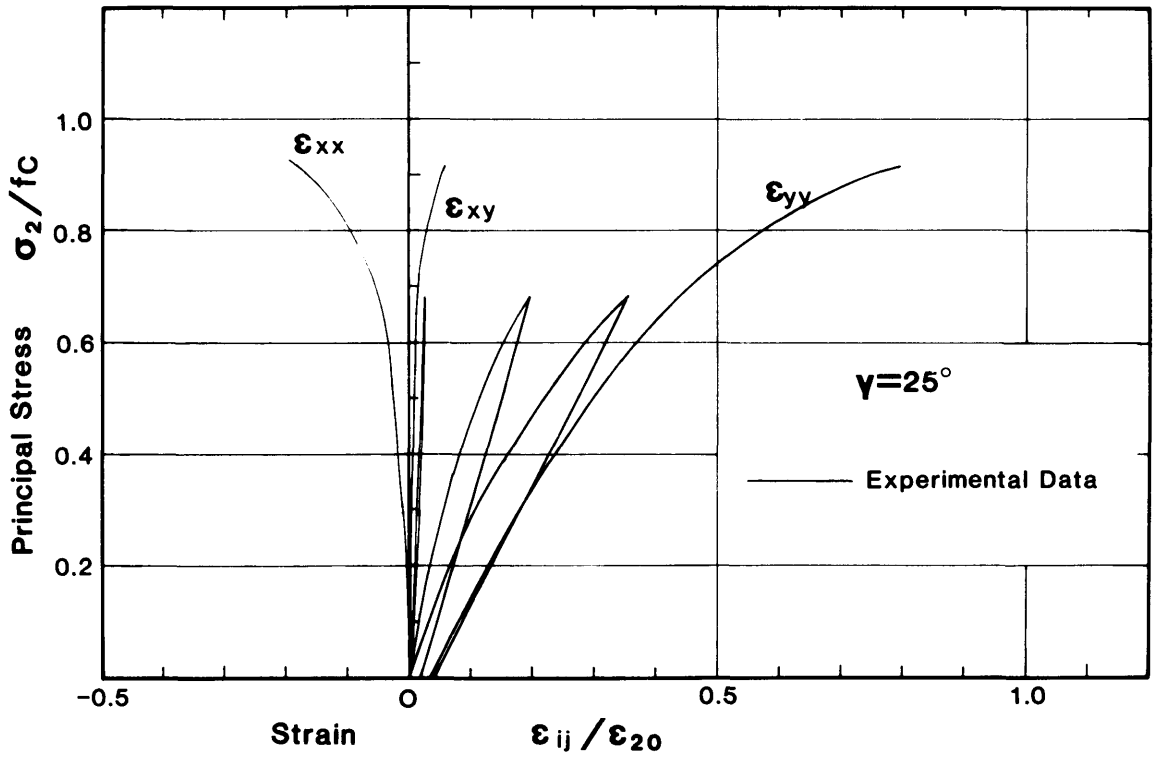

Fig.58. (b)

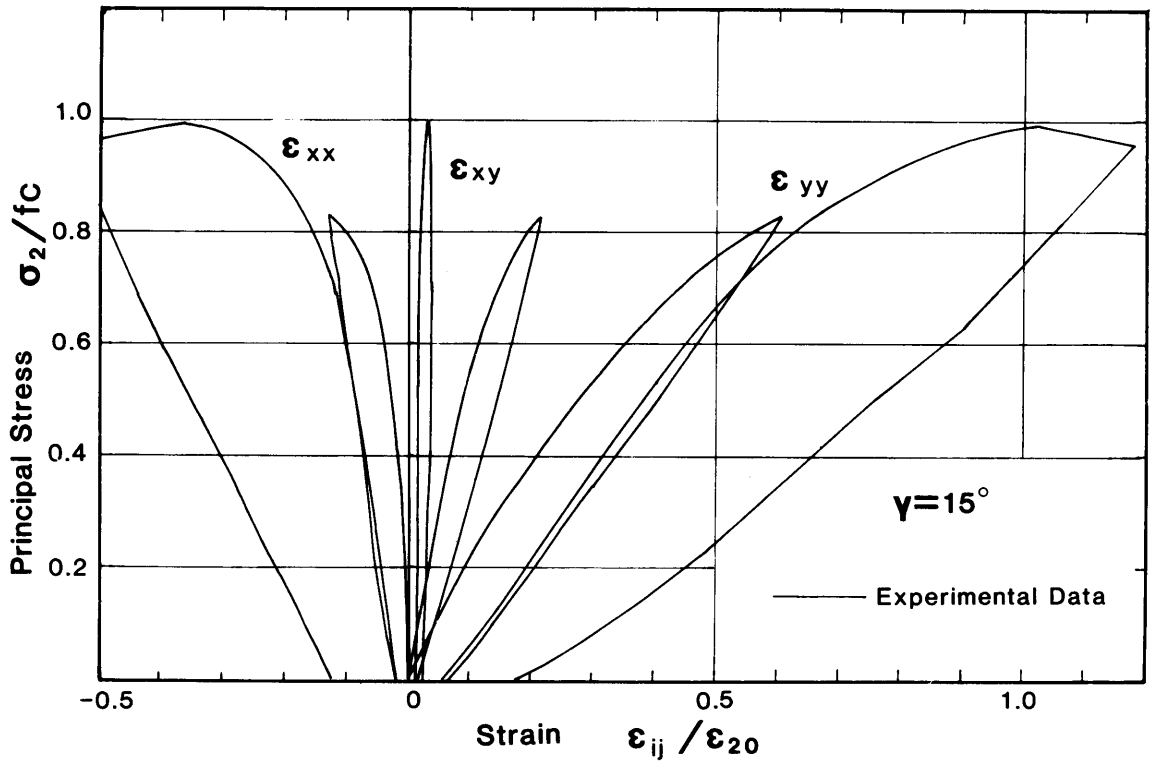
1.0
0.8
0.6
0.4
0.2
Principal Stress σ2/fc
εxx
εxy
ε yy
γ=15°
Experimental Data
-0.5
0
0.5
1.0
Strain εij /ε20

Fig.58. (c)

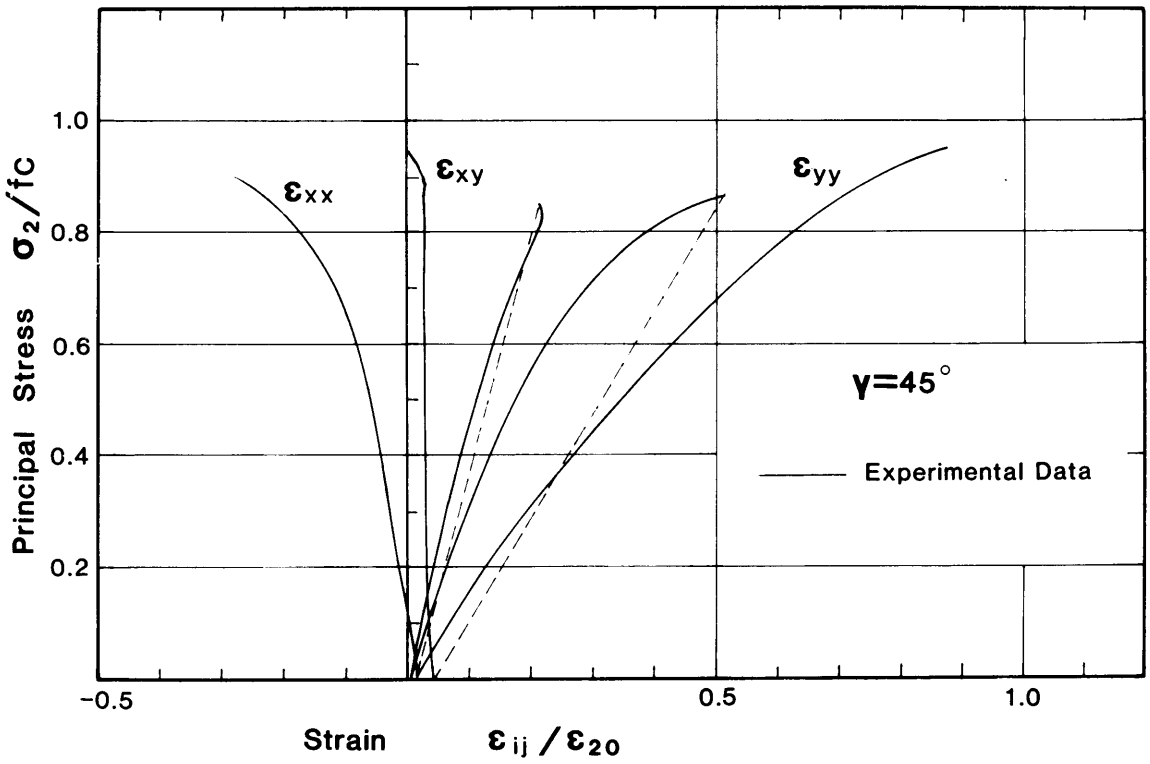
1.0
0.8
0.6
0.4
0.2
Principal Stress σ2/fc
εxx
εxy
εyy
γ=45°
Experimental Data
-0.5
0.5
1.0
Strain εij /ε20

(d)

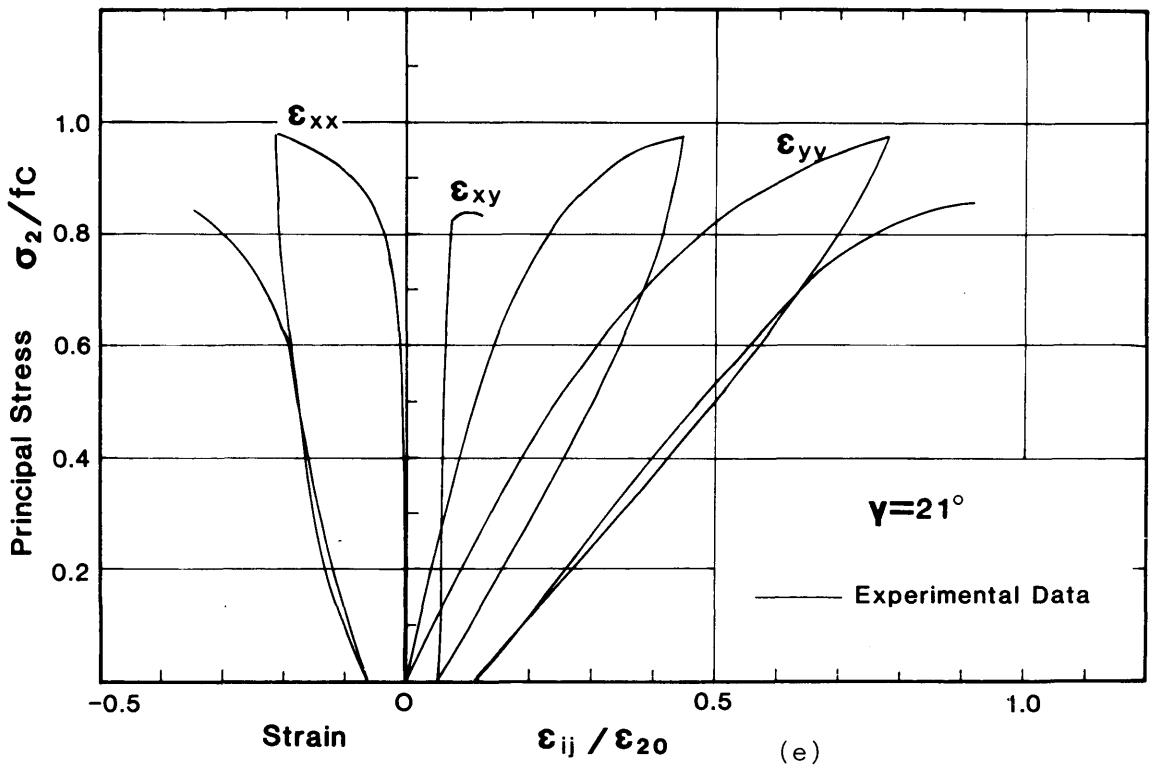

Fig.58. Stress-strain diagrams of rotation tests: (a) RT1, (b) RT2, (c) RT5, (d) RT7 and (e) RT9.

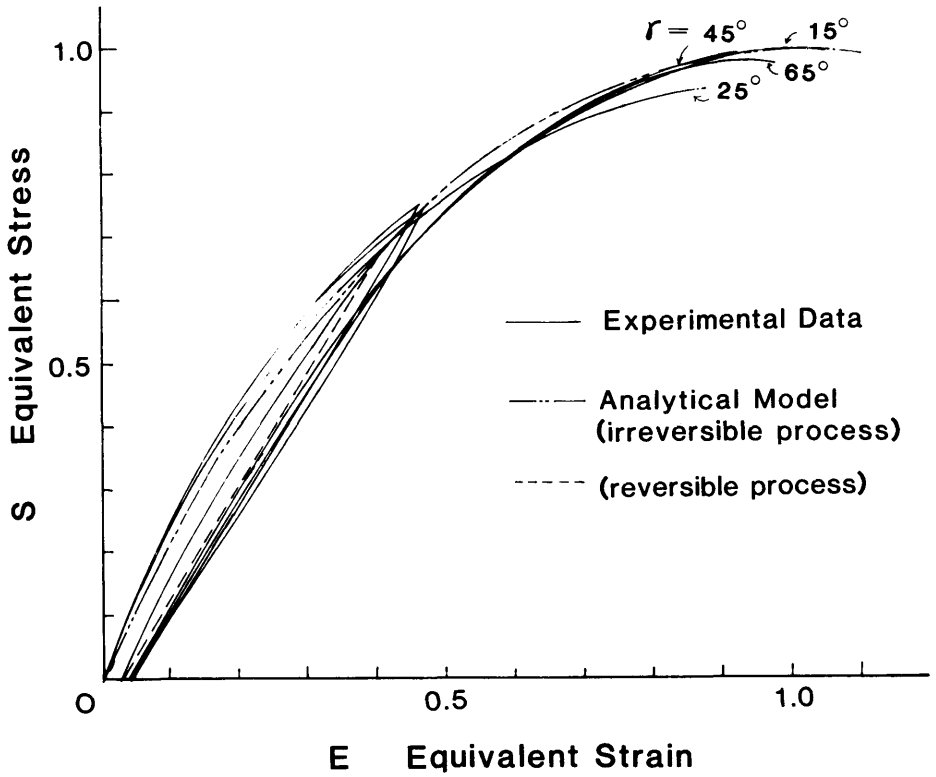

Fig.59. (a)

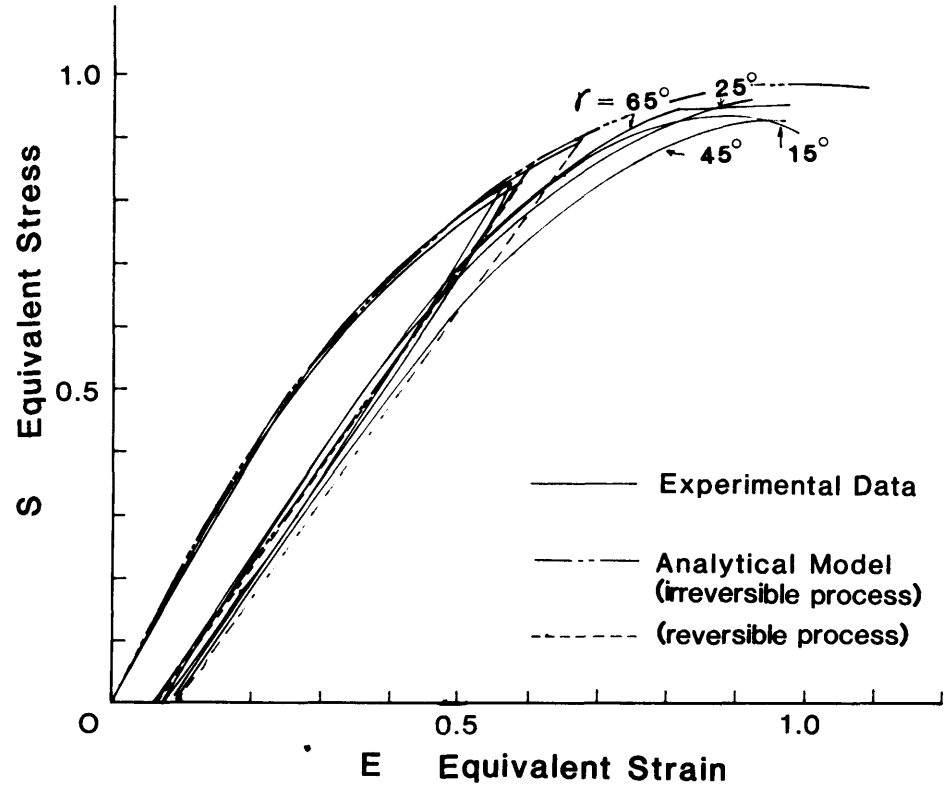

(b)

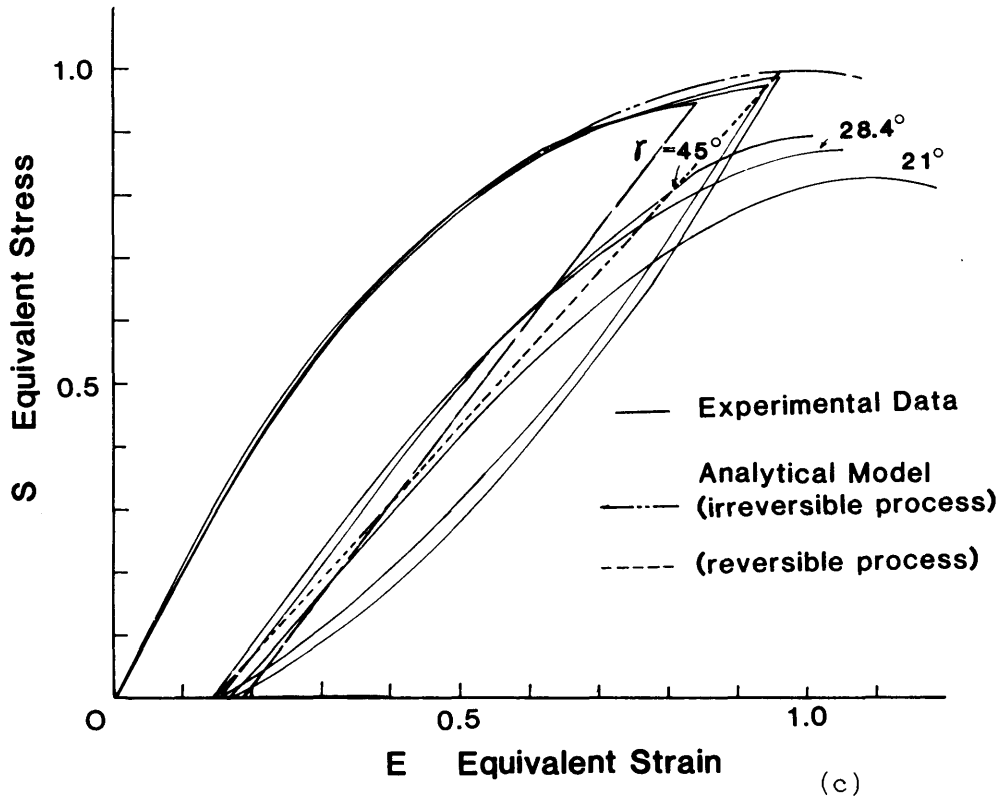

(c)

Fig.59. Equivalent stress-strain relationship of rotation tests

(a) RT1 - RT4, (b) RT5 - RT8, (c) RT9 - RT11.

total strain is 0.6, the similar facts are observed from experiments as shown in Fig.59(b). When the high deformation level was applied to concrete, say Emax=0.9, the influence of the principal axis rotation on the equivalent stress-strain diagrams is observed in Fig.59(c).

However, the difference between the experimental data and the predicted values is not so large to discuss the effect of stress axis rotation, moreover, the experimental data are not sufficient to formulate this small effect of the hysteresis of stress axis rotation. Accordingly, the elasto-plastic and fracture law can be applied to the nonlinear behavior of concrete in the generel condition including principal axis rotation.

In the next step, let us discuss the applicability of the flow rule equations which formulate the directional correlation of stress and strain invariant vectors. The relationship between the reversible Poisson's ratio ν^* in the second loading and the rotation angle γ are shown in Fig.60, where the value of the reversible Poisson's ratio at γ=0 is the predicted one by Eq.(41).

The Poisson's ratio in the reversible process seems to be dependent only on the maximum equivalent total strain Emax, not on the degree of the stress axis rotation. Therefore, also in case of these experiments, the directional relationship between stress and elastic strain vector satisfies the flow rule No.1 with acceptable accuracy.

At any time of loading, the stress condition are under uniaxial stress state, that is, the direction of the stress invariant vector $(\Delta\bar{\sigma}_0, \Delta\bar{\tau}_0)^T$ is constant and equal to the direction of the stress position vector $(\bar{\sigma}_0, \bar{\tau}_0)^T$ (See Section 4.2.2). As a result, the component vector V1 always becomes a zero vector, so that, the corresponding incremental strain invariant vector $(\Delta\bar{\varepsilon}_0, \Delta\bar{\gamma}_0)^T$ is indicated only by the component vector X2 according to the definition of the flow rule No.3.

The direction of the vector X2 in the irreversible process is determined by the flow rule No.2, or actually by flow rule parameter g. Then, the value of g, when the equivalent total strain coincides with the maximum level of the equivalent strain in the second loading (E=Emax, irreversible process), are plotted from experimental data in each test as shown in Fig.61. The value of g when the rotation angle is zero is the predicted value by Eq.(53) which was derived from the data with the fixed principal stress direction, say γ=0.

As far as the test results are concerned, the correlation between the rotation angle of the principal stress direction and the flow rule parameter can not be observed. Within the range of experiments in this report, it is reasonable to assume that the flow rules No.1-No.3 can predict the direction of the stress invariant vectors even in case of the stress axis rotation.

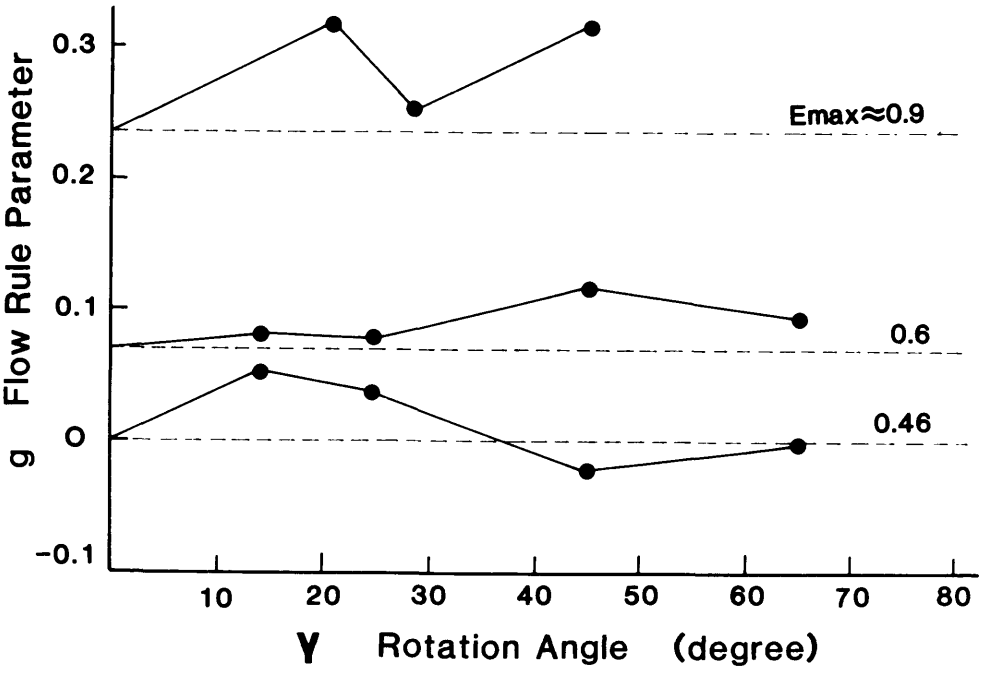

Fig.61. Flow rule parameter under the principal axis rotation.

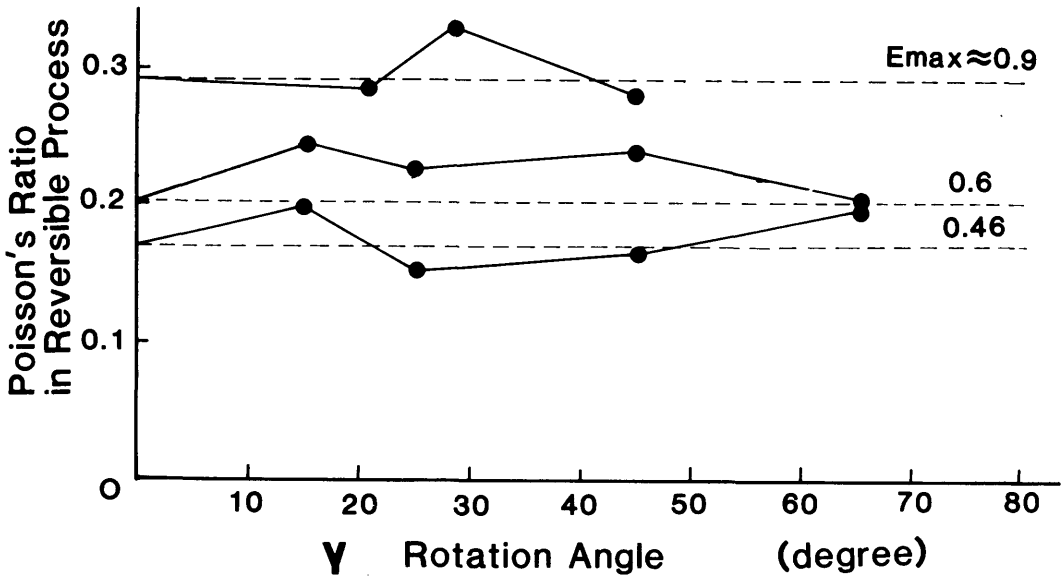

Fig.60. Poisson's ratios in the reversible process under the principal axis rotation.

4.3.3 Flow rule No.4 for the direction of the maximum principal stress

The objective of this section is to find the flow rule No.4 which determines the angle of the maximum principal stress direction under arbitrary strain paths. In the case of the reversible process, the principal stress direction must coincides with that of the elastic strain, because the secant stiffness matrix in the reversible process is isotropic and symmetric. This deformational behavior of concrete is verified by the experimental data(See Section 3.3.3.). The difference between the principal stress direction θ and the principal elastic strain direction θe are shown in Fig.62. Here, strain component $\varepsilon_{ij} - \varepsilon_{pij}^{to}$ was used for calculating the angle θe with the function T in Eq.(37). ε_{pij}^{to} indicates the plastic strains just before the second loading.

In the reversible process of the second reloading, the increment of plastic strain is pracitically equal to zero, so that the plastic strain in the reversible process agrees with the plastic strain at the beginning of the second loading. Therefore, θe represents the direction of the principal elastic strain. Actually, the deviation of stress and elastic strain direction is certainly almost equal to zero.

$$\theta - \theta e = 0$$

$$\theta = \theta e = T(\delta_{ij} = \varepsilon_{eij}) \quad , \text{ in reversible process} \tag{61}$$

Differentiating Eq.(61) under the condition where $d\varepsilon pij = 0$, we obtain

$$d\theta = \left.\frac{\partial T}{\partial \delta_{ij}}\right|_{\delta_{ij}=\varepsilon_{eij}} \cdot (d\varepsilon_{ij} - d\varepsilon_{pij}) = \left.\frac{\partial T}{\partial \delta_{ij}}\right|_{\delta_{ij}=\varepsilon_{eij}} \cdot d\varepsilon_{ij} \tag{62}$$

On the other hand, the principal direction of total strain does not coincide with that of total stress. However, even when the equivalent strain E exceeds Emax in the irreversible process, the deviatoric direction of principal stress and principal elastic strain '$\theta - \theta e$' is almost equal to zero (See Fig.62). Therefore, the following flow rule which describes the principal stress direction is derived in the difference forms

$$\theta^{t+\Delta t} = T(\delta_{ij} = \varepsilon_{ij}^{t+\Delta t} - \varepsilon_{pij}^{t})$$

or

$$\Delta\theta = T(\delta_{ij} = \varepsilon_{ij}^{t} + \Delta\varepsilon_{ij} - \varepsilon_{pij}^{t}) - T(\delta_{ij} = \varepsilon_{ij}^{t} - \varepsilon_{pij}^{t}) \tag{63}$$

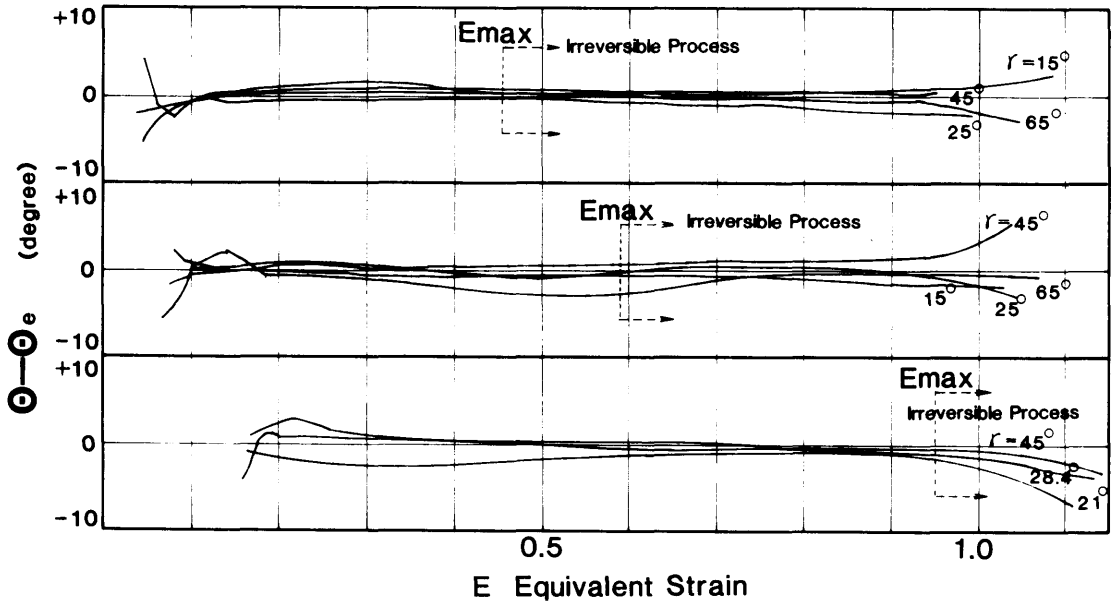

Fig.62. The difference between the principal stress direction and the principal elastic strain direction.

Linearizing Eq.(63) into the differential equation, we find

$$d\theta = T(\delta_{ij} = \varepsilon^t_{ij} - \varepsilon^t_{pij}) + \left.\frac{\partial T}{\partial \delta_{ij}}\right|_{\delta_{ij}=\varepsilon_{eij}} \cdot d\varepsilon_{ij} - T(\delta_{ij} = \varepsilon^t_{ij} - \varepsilon^t_{pij})$$

$$= \left.\frac{\partial T}{\partial \delta_{ij}}\right|_{\delta_{ij}=\varepsilon_{eij}} \cdot d\varepsilon_{ij}$$

which has the same mathematical form as Eq.(62). Accordingly, the author assumes that the floe rule No.4 is given by Eq.(62) in all the case of the strain paths. The precision of this flow rule has been verified in the loading paths where strain moves from the reversible to the irreversible cases. However, the applicability of flow rule No.4 is not completely verified because of the lack of experimental data in the irreversible process where the principal axis rotates(21),(22). This problem is discuseed in Chapter 7. The matrix form of flow rule No.4 is

$$d\theta = [Q]\{d\varepsilon_{ij}\}$$

$$[Q] = [\sin 2\theta, \ -\sin 2\theta, \ -2\cos 2\theta]/A$$

$$A = 2((\varepsilon_{eyy} - \varepsilon_{exx})\cos 2\theta - 2\varepsilon_{exy}\sin 2\theta) \qquad (64)$$

4.4 Concluding remarks

From the experimental approach in Chapter 2, the anisotropic behaviors of concrete were quantitatively made clear in compression-tension stress states. However, previously reported flow rules do not take the investigated anisotropy into account.

Then, in order to formulate the anisotropy of concrete systematically, four flow rule equations concerning the directional correlation between stress and strain vectors were newly derived from experimental data.

As the reported flow rules are described by 3 or 6 dimensional tensors and constructed in taking the simple mathematical treatment into account, it is difficult to verify their applicability and to include the experimental results into the previously constructed mathematical frames. Then, the author represented the direction of stress vector by the ratio of two stress invariants and the direction of the maximum principal stress.

By adopting this type of formulation, it became easy to use experimental

data directly for deriving the mathematical forms as to the stress invariant vectors as follows.

(1) The experimentally investigated isotropic relationship between stress and elastic strain vectors was mathematically expressed by flow rule No.1. In this formulation, it was made clear that the isotropic (reversible) Poisson's ratio is not constant but changes under high compression-tension stress state, moreover, influenced by the strain paths.

By adopting the equivalent total strain as the index of strain hysteresis, the flow rule No.1 could successfully describe the isotropic relationship in reversible process.

(2) The anisotropic behavior of concrete in the irreversible process was systematically formulated by flow rule No.2 and No.3.

In these formulations, the anisotropy parameters were newly introduced. In using thees parameters, it became possible to express the effect of strain paths on the degree of anisotropy.

(3) Based on the newly developed experimental data on the rotation of principal stress direction, it is made clear that the direction of principal elastic strain coincides with that of the principal stress, but the direction of principal total strain does not agree with that of principal stress. According to these results, the direction of principal stress was formulated by Flow rule No.4.

5. Linearlized Differential Equations under Plane Stress State

Linearlized plane stress differential equation can be obtained by solving the constitutive equations derived in Section 4.2 and 4.3 in the matrix forms. In reversible process, the plastic strain is assumed to remain constant and stress-strain relationship is described explicitly in the integrated format. Substituting Eq.(60) and Eq.(64) into Eq.(37), we obtain the stress increments undre arbitrary strain changes, where

$$\{\sigma_{ij}\} = [De]\{\varepsilon_{ij} - \varepsilon_{pij}\}$$

$$[De] = \frac{E^*}{1-\nu^{*2}} \begin{bmatrix} 1 & \nu^* & 0 \\ \nu^* & 1 & 0 \\ 0 & 0 & 1-\nu^* \end{bmatrix} \tag{65}$$

where E^*, ν^* are determined by Eqs.(41),(42).

In the irreversible process, the behavior of concrete is path-dependent, accordingly, the plane stress constitutive equations can be formulated in the differential equations. The effects of strain hysteresis to the stress-strain relationship is introduced mathematically by the integration paths. Substituting Eq.(60) and Eq.(64) into Eq.(37), we obtain the stress increments under arbitrary strain changes, where

$$\{d\sigma_{ij}\} = [Dep]\{d\varepsilon_{ij}\}$$

$$[Dep] = [Dp] + [Df] + [Dr]$$

$$[Dp] = [C(\theta)][S\,1][S\,22][M]^{-1}[D]$$

$$[Df] = [C(\theta)][S\,1][S\,21][M]^{-1}[D] \tag{66}$$

$$[Dr] = \frac{d}{d\theta}[C(\theta)]\begin{bmatrix} \bar{\sigma}_0 \\ \bar{\tau}_0 \end{bmatrix}[Q]$$

The constructed constitutive law in this paper does not formulate the relations between the plastic strain and total stress , such as the formulation type of the theory of plasticity, but between the total strain and total stress. Accordingly, this constitutive model is classified as a differencial total strain theory. In order to proceed the calculation, the plastic strain must be calculated in each integration step for the next step. Integrated plastic strain can be easily calculated by

$$\{\varepsilon_{pij}\} = \{\varepsilon_{ij}\} - [De]^{-1}\{\sigma_{ij}\} \tag{67}$$

6. Numerical Integration and Experimental Verification

Generally speaking, the step-by-step integration method of differential equations with certain time intervals accumulates the numerical errors. Especially, if equations to be integrated numerically express the high order nonlinear bohaviors, the disregarded differential terms of higher orders are directly connected with the integration errors, therefore, the integration intervals should be selected to be as small as possible within the acceptable calculation cost.

Fortunately, these constitutive equations in this paper were originally formulated in the nonlinear difference equations, so that, in the nonlinear finite element method, it is reasonable and desirable not to use the linearized differential equations but to adopt the original nonlinear difference equations directly derived from the experimental data for the stress estimation. Moreover, this model is easy to be programmed in the nonlinear iterative routine such as Newton Raphson Method and Modified Newton Method, which require the true stress evaluation corresponding to the assumed finite strain increments in the program. These methods have a merit that the integration error is not accumulated during the load steps when the true stress is given corresponding to the inputed finite strain increments.

The process flow how to calculate the stress at $t+\Delta t$ with the information of the values at time t, where σ_{ij}^{t}, ε_{ij}^{t}, ε_{pij}^{t}, E^{t} and $Emax^{t}$ is shown in Appendix III. This type of calculation method in Appendix III was originally given by Yamada(19) as r-miminum method. Authors applied this method to the numerical integration of the derived plane stress constitutive equations.

The material coefficients used in this modelling are compiled as follows.

(1) a , b .... weight constants which represent the influences of mean and deviatoric stresses on the equivalent stress function S.
(2) c , d .... weight constants which represent the influences of mean and deviatoric straines on the strain measure function F.
(3) K(Emax) .. fracture parameter which represents the rate of the fracture.
(4) Ep ..... equivalent plastic strain which represents the rate of the plastic deformation.
(5) ν^{*} ..... Poisson's ratio which controls the flow rule in the reversible process.
(6) (α, β) .... coordinate values of the convergence points which controls the flow rule in the irrecoverable process.

Material parameters (3) and (4) represent the macroscopic behavior of the

plasticity and the fracture. (5) and (6) are the main parameters which control the flow rules. (1) and (2) make it possible to apply the basic concept of the plasticity and the fracture to two dimentional problems. In order to check the constitutive equations, typical examples and analytical predictions by FEM (Appendix III) are given as follows.

Stress-strain diagrams under biaxial compressive loadings(2) and analytical results are shown in Fig.63. The accuracy of the prediction concerning the ultimate values of biaxial stresses and strains is dependent most on the precision of the material parameters (1) and (2). The predicted ratio of biaxial strains $\varepsilon_1 / \varepsilon_2$ is mainly influenced by the flow rule, that is, the material parameter (6). According to the good fittness between the experimental and analytical results, it is verified that this system of the constitutive equations has the ability to express these behaviors.

The strain paths on the biaxial total strain space under the uniaxial cyclic loading are shown in Fig.64. The dotted lines in this figure represent the strain paths when the compressive stress is completely unloaded. In this analysis, the value of equivalent plastic strain (parameter (4)) and the Poisson's ratio in reversible process (parameter (5)) have much infuluences on the analytical results. According to Fig.64, this model is successful to predict the kinematic movement of the biaxial plastic strains. But, the nonlinearity in the reversible process is not included in this modelling. This problem should be studied from now on.

The incremental stress-strain relationship is shown in Fig.65 when the tensile principal uniaxial stress is applied to the concrete which has the loading hystory of compression in the direction normal to the applied tensile stress. In this case, material parameters (3) and (5) have large influences on the results of the analysis. The stiffness under the tensile stress decreases as the preloaded comressive level becomes higher. This constitutive equations express the decreasing stiffness quantitatively with reasonable accuracy. However, as shown in Fig.65, this model does not especially take the plasticity and the fracture under the tensile stress into account near the cracking failure, so that, the predicting accuracy near the cracking failure decreases a little. The difference of deformational mechanics under tensile and compressive stresses should be investigated and more experimental data are necessary.

The analytical results of concrete behavior under the stress paths including the principal axis rotation are demonstrated by the dotted lines in Fig.58(a). There exists a good coincidence between the analytical and experimental results. Accordingly, this fact is one of the verifications of the applicability of the flow rule related to the direction of the principal

axis, and the accuracy of material parameters (5) and (6) is confirmed.

The strain paths on the biaxial strain space are shown in Fig.66 when the uniaxially compressed concrete was loaded by the orthogonal tensile principal stress. The results of both the analytical and experimental data indicate the characteristic behaveior of anisotropy under compression-tention stress state. The analytical results of strain paths are much influenced by the system of flow rule in the irreversible process or the precision of material parameter (6). According to this figure, the flow rule equations in this research have acceprtable ability to predict the directional correlations between the direction of stress vector and that of strain vector.

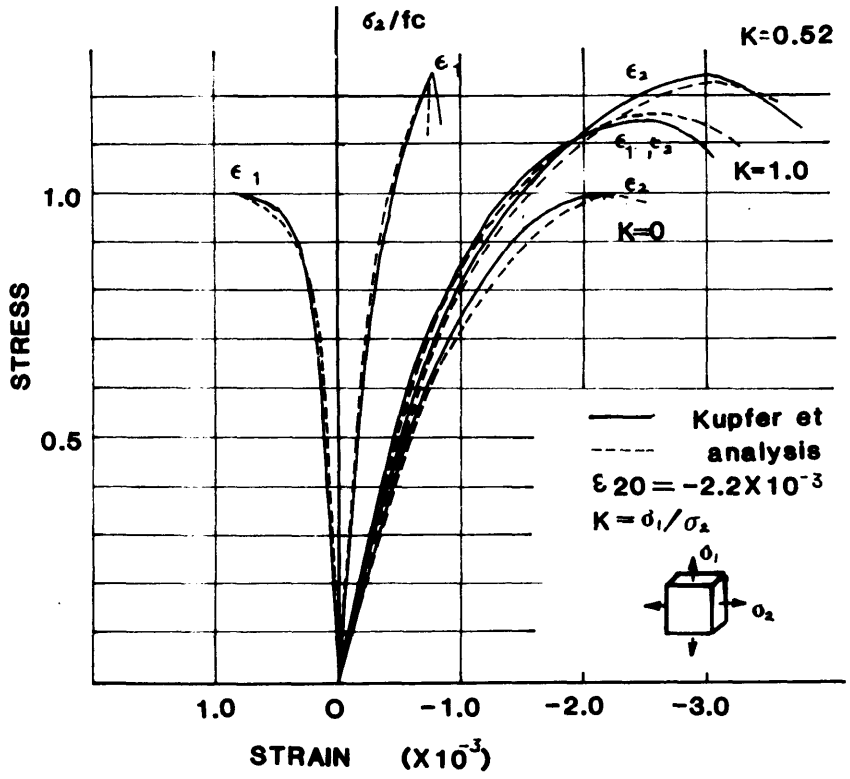

Fig.63. Stress-strain diagrams under biaxial compression.

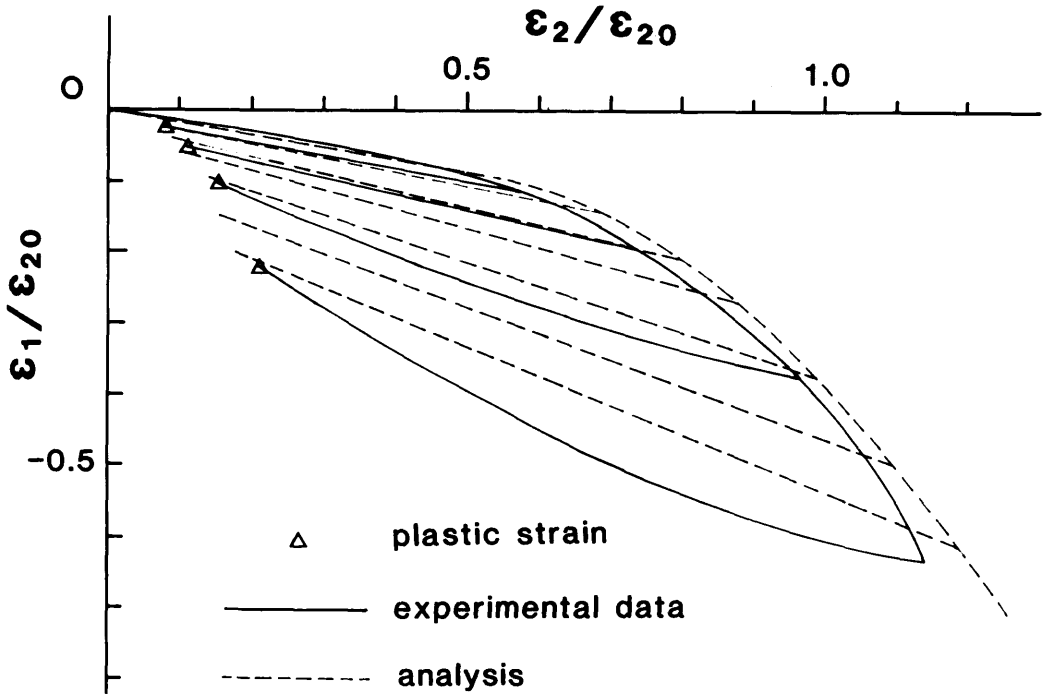

Fig.64. Biaxial total and plastic strain paths under cyclic uniaxial compressive stress state.

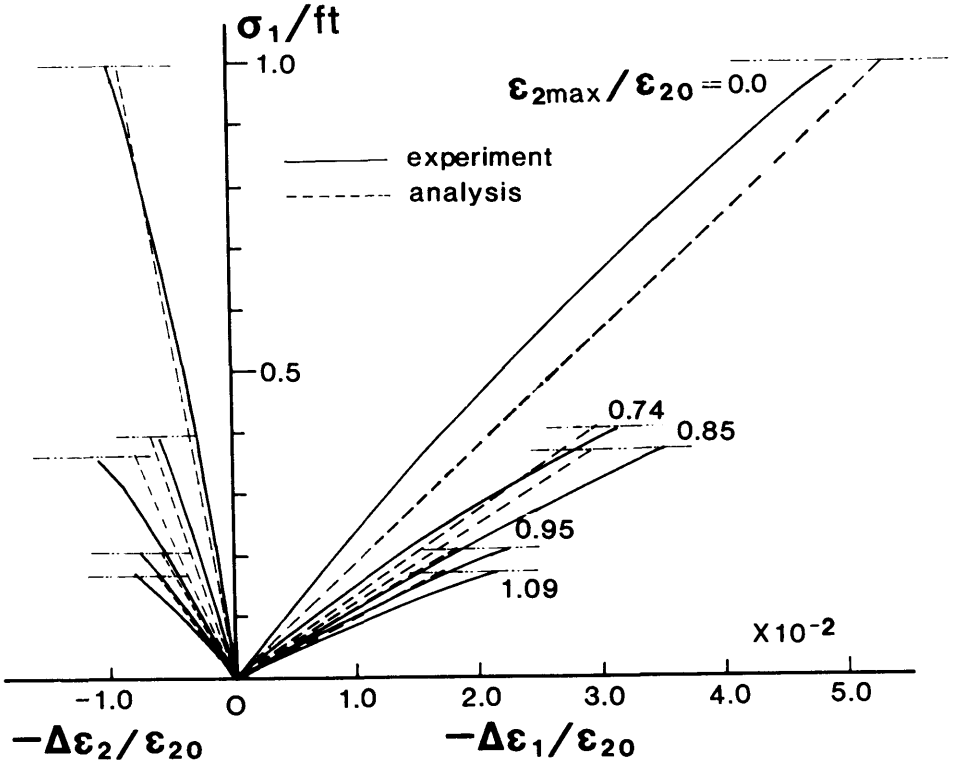

Fig.65. Relations between tensile principal stress and incremental biaxial strains of concrete with compression histories.

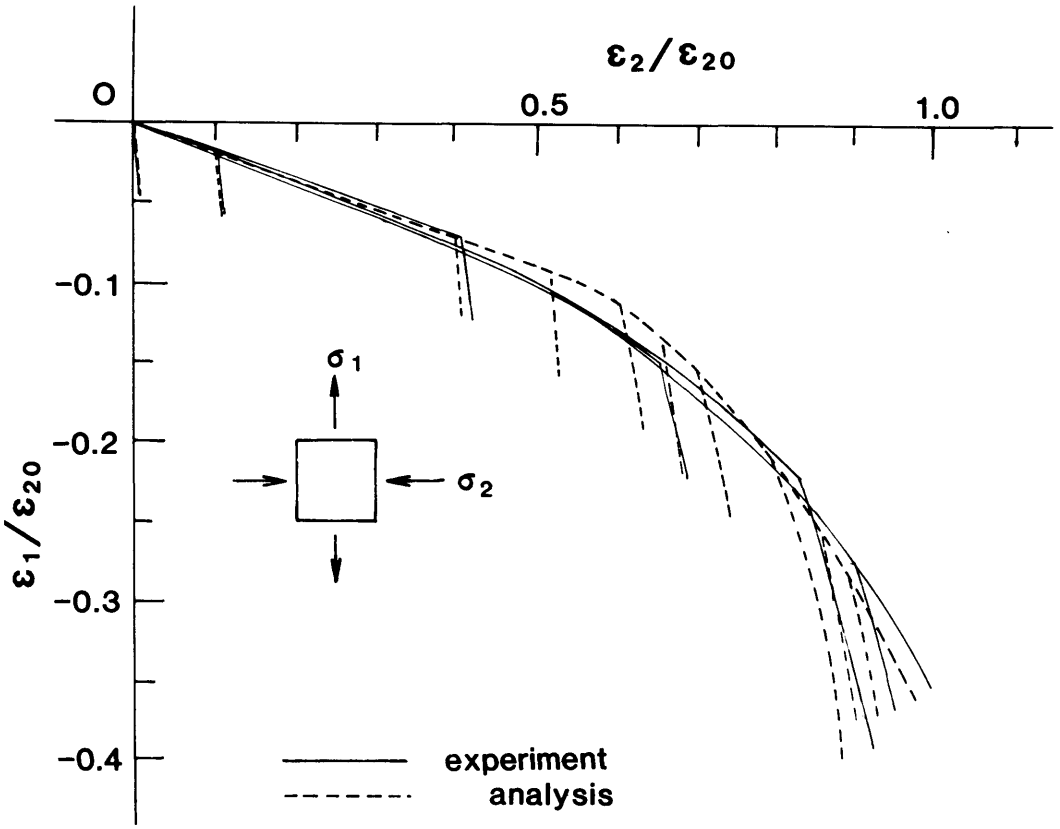

Fig.66. Biaxial strain paths under biaxial compression tension stress states.

7. APPLICABILITY OF THE PROPOSED ELASTO-PLASTIC AND FRACTURE MODEL - - GENERAL LOADING PATH WHERE PRINCIPAL STRESS AXES CONTINUOUSLY ROTATE - -

7.1 General

In Chapter 6, the experimental verification of the elasto-plastic and fracture model was made, but the stress-strain diagrams which were used for checking the precision are the grounding of the proposed constitutive laws. Therefore, the good coincidence of the predicted behavior with the actual one is proper and natural. The author considers that the check in Chapter 6 is not enough to apply the derived constitutive laws to the structural analyses, because the experimental verification in Chapter 6 does not cover all stress paths which are produced in reinforced concrete structures. In meeting the many-sided demands on the function of RC structures, path-dependent characteristics of concrete and applicability of constitutive laws should be investigated. Then, it is indispensable to check the proposed equations by different type of experimental data from that utilized for establishing the proposed equations.

The main subject of this chapter is on the experimental verification of the elasto-plastic and fracture model related to the deformational behavior of concrete under the conditions where principal stress axis "continuously" rotates. This type of experiments were not adopted at all for deciding the constitutive equations proposed. In case of the 2D reinforced concrete members, the rotation of principal stress direction is usually produced by the anisotropic stiffness change such as cracking of concrete and by the existence of reinforcement. In some cases, failure of concrete element under the axis rotation causes the catastropic failure of RC beams. Taking these cases into account, the prediction ability of this modelling under the principal axis rotation paths cannot be ignored, and continuous rotation paths are appropriate for checking the applicability of the proposed model.

According to the main point of this chapter, biaxial loading tests with the histories of continuous rotation of stress axes were carried out. The author checked the applicability of the elasto-plastic and fracture model in using this experimental data and discussed the deformational behavior of concrete under continuous rotation paths.

7.2 Experiment

Principal axis rotation paths under compression-tension stresses were introduced by applying compressive force and torsional moment independently to the cylindrical shell specimens (23,24) (320mm diameter (D), 950mm height (H) and 35mm thickness (W), 35160mm^2 area (A). See Fig. 67). Mixture of concrete used is Type B in Table 1. Specimens were fixed on the base plate. Torsional moment was transmitted to concrete by the steel arm which sticked to the specimen with epoxy adhesive agency. As it is impossible to eliminate the effect of restriction from the steel arm and the base plate completely, the greater height to diameter ratio ($\fallingdotseq$3) was adopted. The thickness was decided in taking the maximum aggregate size (15mm) and the formation of uniform strain field into account. With this geometry of specimens, the disorder of strain field was limited within the same acceptable order as discussed in Chapter 2.

In order to eliminate the friction between the steel arm and the compression-loading apparatus, bearing balls, silicon grease and teflon sheets were placed between them. Shear and normal stress in the global coordinate defined in fig. 67 are calculated by the compression force C (negative) and torsional moment T (negative) as

$$\sigma_{xx}=0 \quad \sigma_{yy}=C/A, \quad \sigma_{xy}=T/(DW) \tag{68}$$

The loss of shear stress due to the friction was not greater than 0.05Mpa. The strains were measured by wire strain gauges and forces were picked up by load cells. The measured strains and forces were transformed into the principal stresses and strains by the computer-aided measuring system, and displayed instantaneously. The compressive force and torsional moment were controlled by the manual operation in accordance with the loading program and corresponding strains from the system console. Because of the experimental technique, the same loading speed of shear and normal stresses ($|d\sigma xy/dt|$, $|d\sigma yy/dt|$ =0.2Mpa/sec) was adopted as the rate in the case of compression-tension loading tests in Chapter 2.

7.3 Anisotropic deformational characteristics under principal stress rotation

The author obtained stress-strain diagrams as shown in Fig. 68 where the shear stress increased monotonically ($d\sigma xy\neq 0$) with the principal stress rotation under the fixed normal compressive stress ($d\sigma yy=0$). In this type of loading paths as shown in Fig. 68, the principal stresses and their directions

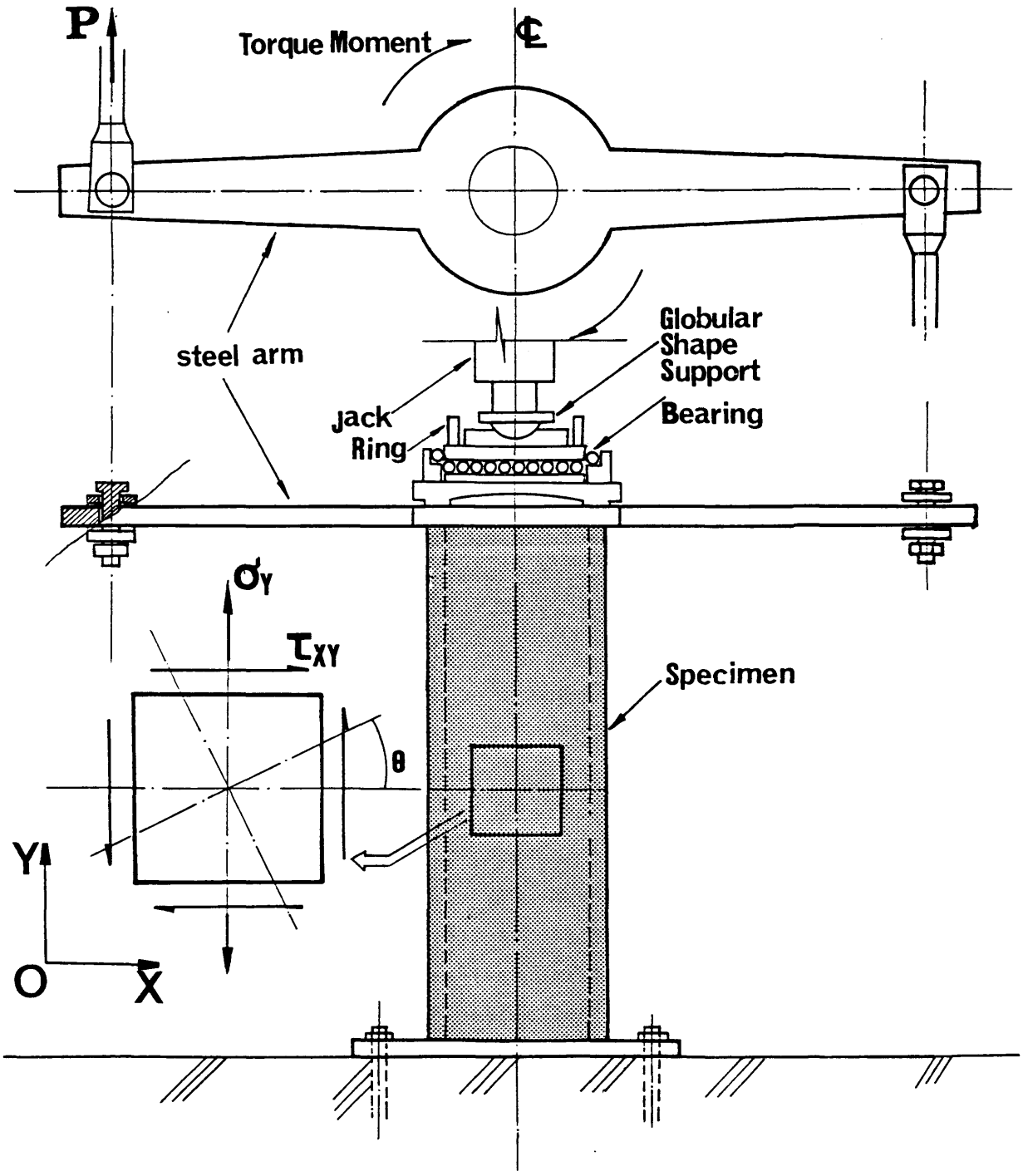

Fig.67. Loading set-up for compression-shear tests.

are calculated by

$$\sigma 1 = \sigma yy/2 + \sqrt{(\sigma yy)^2/4 + \sigma xy^2}$$
$$\sigma 2 = \sigma yy/2 - \sqrt{(\sigma yy)^2/4 + \sigma xy^2}$$
$$\theta = T(\delta ij=\sigma ij) \qquad (69)$$

The calculated stress-strain correlation by the proposed constitutive equation is shown in Fig. 68 with dotted lines. The predicted shear stress-strain diagrams agree with the experimentally obtained diagrams. When the fixed compressive level $\sigma yy/fc$ is less than 0.86, the predicted incremental normal strains are a little small compared with the actual strain increments, but the proposed constitutive equation expresses the actual deformational behavior with reasonable accuracy in appearance. However, in the case where $\sigma yy/fc=0.86$, the elasto-plastic and fracture model estimates normal strain increments to be small. The proposed constitutive modelling has the ability to predict the shear response of concrete even in the high stress range, but does not offer the correct normal strains in greater stress conditions. Accordingly, it is necessary to make clear the applicability of modelling.

For deeper discussions related to the applicability of concrete modelling, the author lets the following compliances for the convenience denote the relation between incremental total strains and stresses as

$$\begin{bmatrix} d\varepsilon xx \\ d\varepsilon yy \\ d\varepsilon xy \end{bmatrix} = \begin{bmatrix} \phi 11 & \phi 12 & \phi 13 \\ \phi 21 & \phi 22 & \phi 23 \\ \phi 31 & \phi 32 & \phi 33 \end{bmatrix} \begin{bmatrix} d\sigma xx \\ d\sigma yy \\ d\sigma xy \end{bmatrix} \qquad (70)$$

The tangential shear and normal stiffnesses $E(=1/\phi 22)$, $2G(=1/\phi 33)$ normalized by the initial stiffnesses (Eo, Go) in each compressive level are shown in Fig. 69. These stiffnesses are represented by the secant stiffnesses corresponding to the small stress increment 0.05fc at the start of axis rotation. Fig. 69 illustrates the anisotropic decrease of both stiffnesses according to the increase of compressive stress level $\sigma yy/fc$. There exists the interesting fact that the tangential shear stiffness does not decrease so remarkably as the compressive normal stiffness does. In other words, concrete is more rigid concerning the shear deformation including principal axis rotation. The predicted value by the elasto-plastic and fracture equation (66) is shown in Fig. 69 with experimental data. The anisotropic decrease of both stiffnesses can be simulated with reasonable accuracy.

In order to discuss the fitness of concrete modelling, the ratio of non-diagonal compliances $\phi 13$ to $\phi 23$ as shown in Fig. 70 should be adopted for

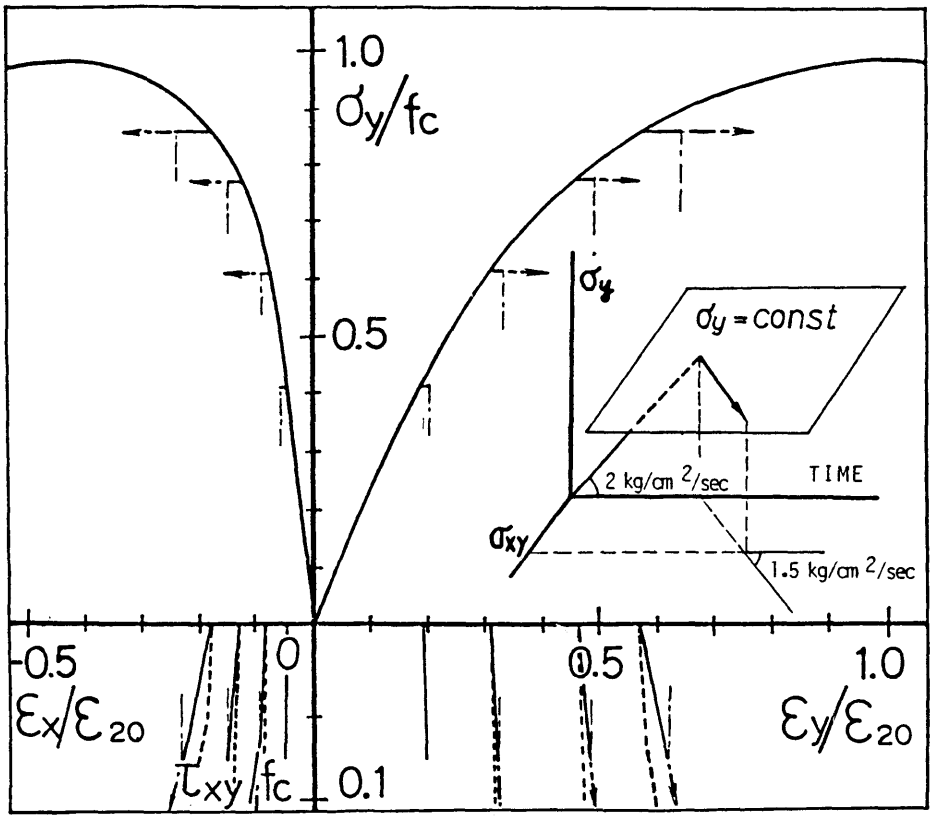

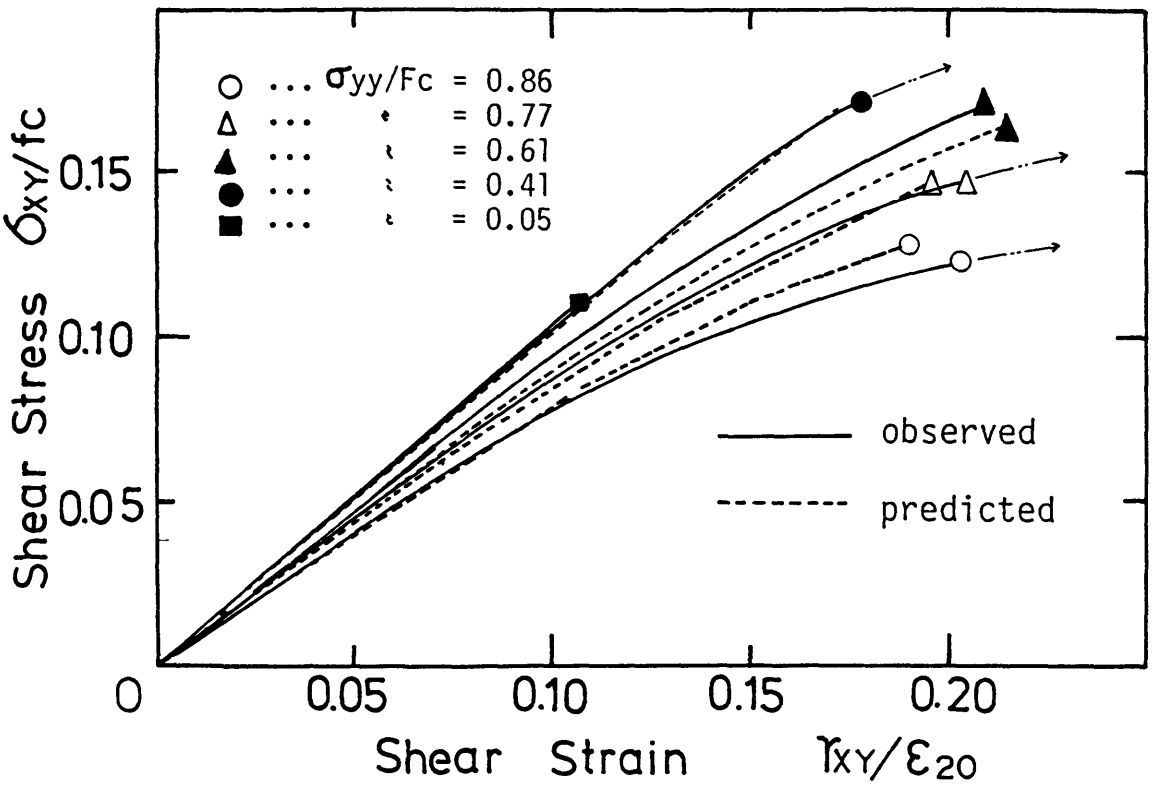

Fig.68. Stress-strain diagrams under continuous rotation of principal stress axes.

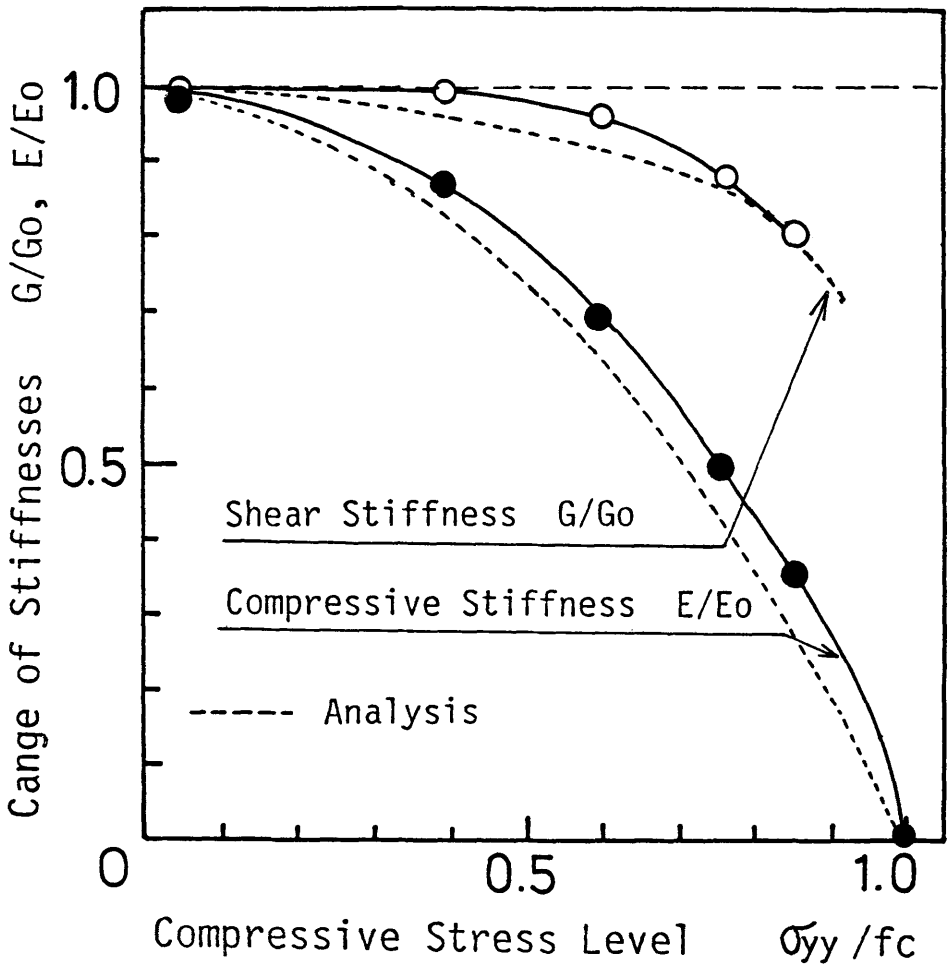

Fig.69. Anisotropic change of shear and normal stiffnesses.

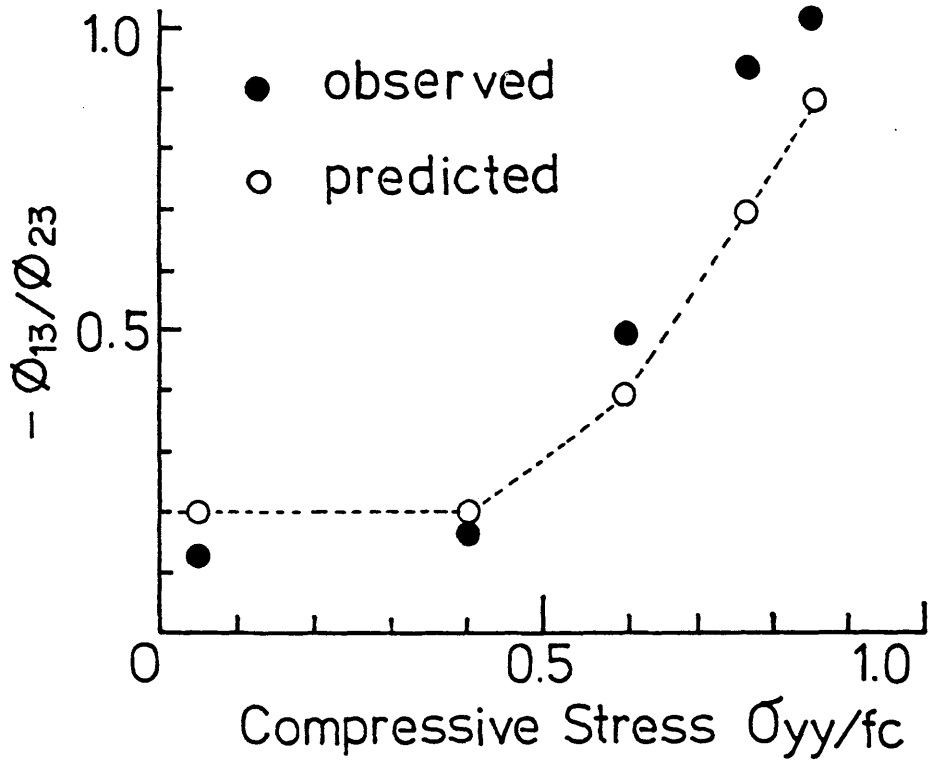

Fig.70. Ratio of non-diagonal compliances under principal axes rotation.

checking, because the ratio of compliances is one of the parameters to represent the direction of deformation, and influenced very much by the accuracy of flow rules. In case of high compressive stress levels, $\phi 13/\phi 23$ at the beginning of the axis rotation varies in accordance with the increase of compressive stress level $\bar{\sigma}yy/fc$. The direction calculated numerically in obedience to Appendix III is almost the same as that obtained from the experiments discussed here. However, the absolute change of normal strains were predicted small in the high compressive level as shown in Fig. 68.

As mentioned above, the proposed constitutive law has the ability to explain the overall deformational behavior under more general stress paths where the axis of principal stress continuously rotates, but includes some insufficient points. In order to evaluate the capacity of the proposed model more correctly, it might be effective to check the behavior predicted by popular and representative concrete models as follows.

1) Nonlinear Isotropic Elasticity

The previously reported constitutive laws (3,4,5) within this category are generally formulated or transformed as

$$\varepsilon_o = K_{in}(I1)\bar{\sigma}_o, \qquad e_{ij} = G_{in}(J2)s_{ij} \tag{71}$$

where, $\bar{\sigma}_o = \bar{\sigma}_{kk}$ (mean stress), $\varepsilon_o = \varepsilon_{kk}$ (mean strain), $e_{ij} = \varepsilon_{ij} - \delta_{ij}*\varepsilon_o/3$, $s_{ij} = \bar{\sigma}_{ij} - \delta_{ij}*\bar{\sigma}_o/3$, $I1 = \bar{\sigma}_o$ and $J2 = 0.5*s_{ij}*s_{ij}$ (the first and second stress invariants). Kin and Gin are explicit functions of I1 and J2.

This modelling is recognized as the nonlinear modification of the wellknown linear isotropic elasticity (25). The compliances are respectively calculated by differentiating Eq. (71) as

$$\begin{aligned}
\phi 33 &= G_{in}(J2) + (dG_{in}(J2)/dJ2)*\bar{\sigma}_{xy}*\bar{\sigma}_{xy} \\
\phi 13 &= s_{xx}*s_{xy}*(dG_{in}(J2)/dG2) \\
\phi 23 &= s_{yy}*s_{xy}*(dG_{in}(J2)/dJ2)
\end{aligned} \tag{72}$$

Eq. (72) is described in the global coordinate system where y-axis corresponds to the compressive normal stress and sxy ($=\bar{\sigma}_{xy}$) is equal to zero at the beginning of the principal stress rotation. According to this modeling for concrete, the shear compliance $\phi 33$ in Eq. (72) increases rapidly and nonlinearly as the shear stress increases because J2 is almost constant under high stress levels during axis rotation paths. However, according to the increase of shear stress level $\bar{\sigma}_{xy}/fc$, the actual shear compliance changes linearly when axis rotation starts as shown in Fig. 71. The prediction by Eq. (72) contradicts the

actual behavior. On the other hand, the shear compliance under greater shear stress conditions increases nonlinearly as predicted by Eq. (72).

The non-diagonal compliances $\phi 13$ and $\phi 23$ are idealized to be zero because shear stress is zero at the beginning of the axis rotation. However, $\phi 13$ and $\phi 23$ are not zero when concrete is compressed in greater levels.

2) Classical elasto-plastic model

The plasticity criterion described by stress tensors estimates this type of loading paths as the irreversible one where plastic deformation flows in general. Accordingly, the compliances defined by Eq. (70) are expressed as the sum of the elastic and plastic components of compliances. Let us consider the plasticity model including the plastic potential function P formulated by the first and the second invariants of stresses I1 and J2 (17). Plastic incremental vector is expressed parallel to the normal and outer vector which stands on the plastic potential face where P=const. as follows.

$$d\varepsilon_{pij} = g*(dP/d\sigma_{ij}) \qquad g : \text{scalar value} \qquad (73)$$

When only shear stress changes with fixed normal stresses, the compliances defined by Eq. (70) are

$$\begin{aligned} \phi 33 &= 1/2G_o + g*PJ2\ sxy \\ \phi 13 &= g*(PI1+PJ2*Sxx) \\ \phi 23 &= g*(PI1+PJ2*Syy) \end{aligned} \qquad (74)$$

where Go is the initial shear stiffness and PJ2 and PI1 are the partial differential coefficients of the plastic potential function P by J2 and I1. The value of g is determined by the strain-hardening rule in the theory of plasticity.

The shear compliance $\phi 33$ is not equal to $1/2G_o$ in general as formulated in Eq. (74), but in this case becomes zero at the beginning of axis rotation because sxy is equal to zero. Accordingly, the shear stiffness does not change in the case of stress paths as shown in Fig. 68. This behavior is quantitatively different from the experimental results demonstrated in Fig. 69. As the shear stress sxy increases, however, the shear compliance varies in a linear fashion because PJ2 changes very little in these rotation paths under high stress levels. The simulated behavior by elasto-plasticity concordes with the experimental results as shown in Fig. 71.

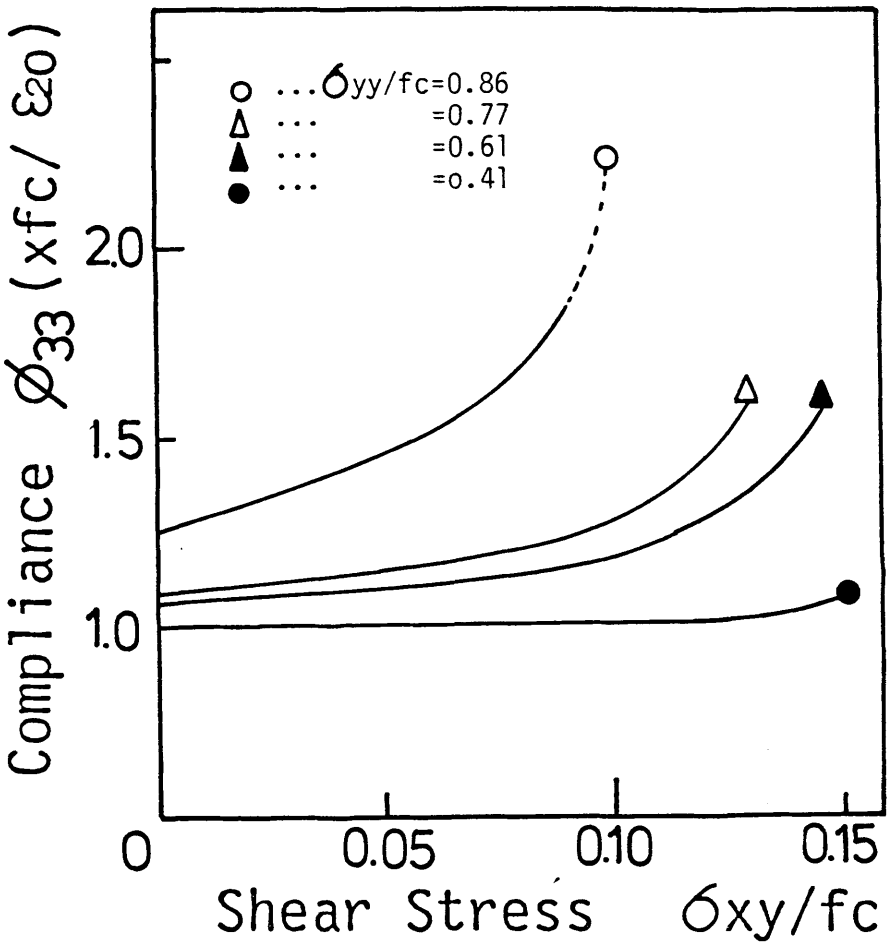

Fig.71. Shear compliance and shear stress increment.

3) Orthogonally anisotropic model

At the beginning of the principal stress rotation, this type of modeling (6,7) specifies the concrete tangential stiffness as

$$\begin{Bmatrix} d\sigma_{xx} \\ d\sigma_{yy} \\ d\sigma_{xy} \end{Bmatrix} = \frac{1}{1-\nu^2} \begin{bmatrix} E1 & \nu\sqrt{E1E2} & 0 \\ \nu\sqrt{E1E2} & E2 & 0 \\ 0 & 0 & (E1+E2-2\nu\sqrt{E1E2})/4 \end{bmatrix} \begin{Bmatrix} d\varepsilon_{xx} \\ d\varepsilon_{yy} \\ d\varepsilon_{xy} \end{Bmatrix} \quad (75)$$

where, $d\bar{\sigma}_{xy} \neq 0$ and $d\bar{\sigma}_{xx}$, $d\bar{\sigma}_{yy} = 0$

Accordingly, the compliances $\phi 13$, $\phi 23$ and the volumetric strain increment are explicitly equal to zero, but actual compliances are not zero in high stress levels as shown in Fig. 68.

As mentioned above, the quantitative behavior under principal axis rotation is predicted in different manners. Each concrete constitutive model is considered to have physically appropriate concepts for concrete deformation but is not sufficient respectinely. In order to verify the applicability of the elasto-plastic and fracture concept, it is necessary to discuss the proposed constitutive laws again as to the reversible and irreversible strains in Chapters 3 and 4.

7.4 Reversible deformation under principal stress rotation

This paper defines the reversible (elastic) strain as that decided explicitly by stresses and the fracture parameter and the irreversible (plastic) one as total strain when stresses are instantaneously and completely released. In order to analyze the total strain increments introduced by the principal stress rotation, unloading paths were supplemented to the monotonic loading histories as shown in Fig. 72. The plastic strain increment is the change of total strains at non-stress conditions corresponding to points A and B in Fig. 72.

According to the definition, the reversible shear and normal strain increments were separated from total strain increments as shown in Fig. 72(b), where there exists the interesting fact that the reversible shear strain increment account for the greater part of the total strain increment. On the contrary, increments of the reversible normal strains takes very little under principal stress rotation. Here, the change of fracture parameter K during the shear stress increase was not observed.

From the separation of strains, the tangential shear stiffness($2G=1/033$) is recognized as the elastic one at the beginning of the axis rotation because

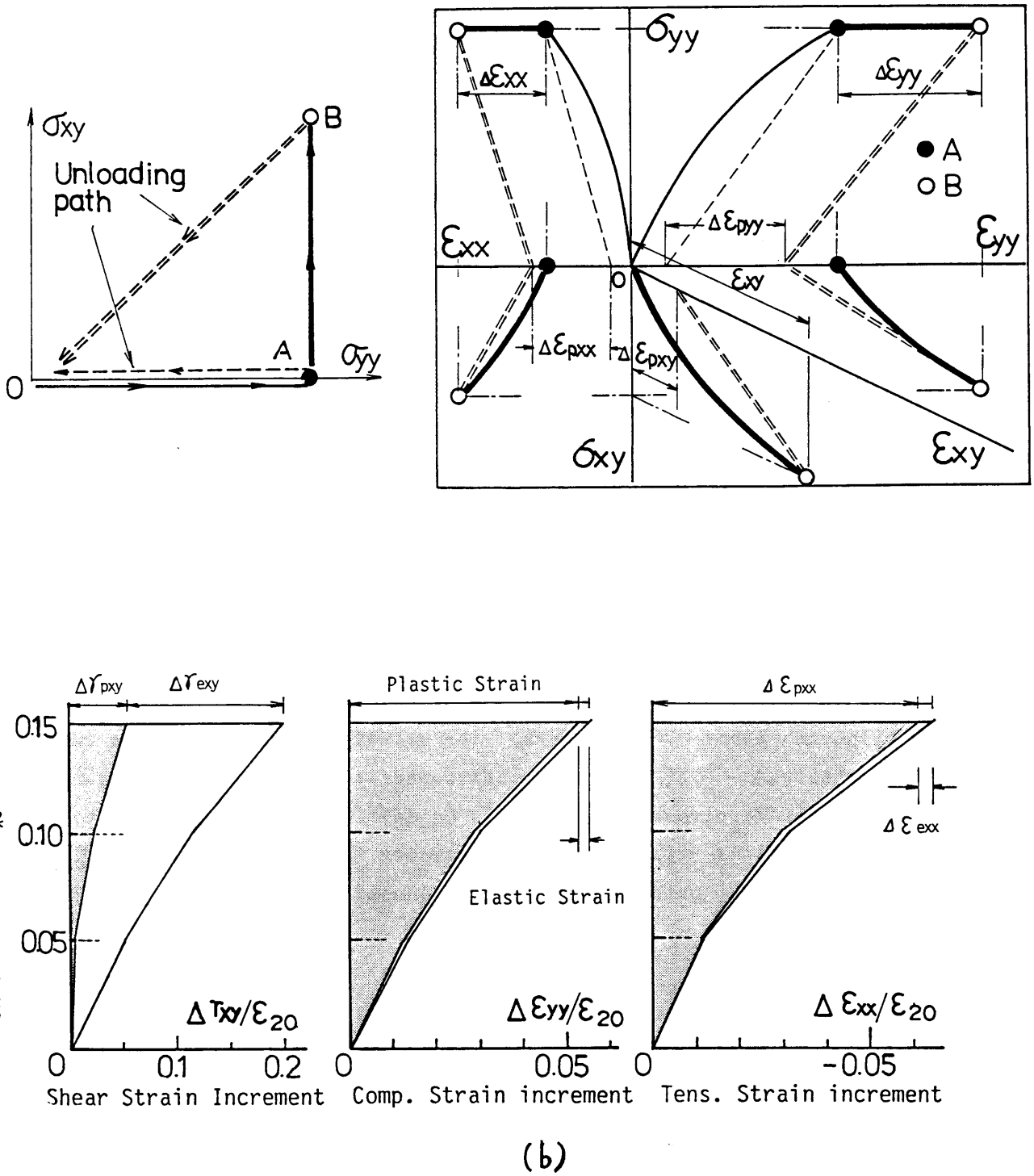

Fig.72. Elastic and plastic strain increments under axes rotation paths.

the increment of shear strain is almost the same as that of the elastic strain. In case of the elasto-plastic and fracture model proposed, the elastic stiffness changes according to the fracture parameter as predicted by Eq. (33). The decrease of shear stiffness which was correctly predicted as shown in Fig. 69 is due to the fracturing of concrete. Classical theory of plasticity does not take the effect of the decrease of elastic stiffness into account, therefore, it could not simulate the correct response of concrete, but the proposed model has the capacity to represent this effect.

For checking the applicability of elastic constitutive equation proposed, isotropic assumption should be strictly proved to this problems under continuous rotation of axis. The author introduced the biaxial unloading paths to concrete shell specimens as shown in Fig. 73. From the strain response corresponding to the release of compressive normal stress $\bar{\sigma}yy$, the hypothetical shear stiffness can be calculated in assuming the isotropy as

$$G_{cal}=Ese/(1+\nu se) \tag{76}$$

where, Ese and νse are the same compressive stiffness and Poisson's ratio as defined by Eq. (3). The actual and hypothetical shear stiffnesses are illustrated in Fig. 74. From an engineering point of view, two shear moduli coincide with each other. Furthermore, the normal strain increments were not still more observed. This behavior corresponds to the isotropic response of reversible strains to stress increments in Eq. (47). Accordingly, the proposed constitutive equations related to the elasticity is applicable to the loading history where principal axis of stresses continuously rotates.

7.5 Irreversible deformation under principal stress rotation

The elastic strain expresses the reversible deformation and corresponding constitutive law was verified isotropic and path-independent when the fracture parameter is constant in Section 7.4. Accordingly, separated irreversible plastic strain represents the path-dependent nonlinearlity concerning normal strain increments as discussed in Section 7.3. Therefore, the plastic strain increment should be exactly formulated. Taking more intuitive understanding of plastic flow into account, the author expresses the experimentally obtained plastic flow as

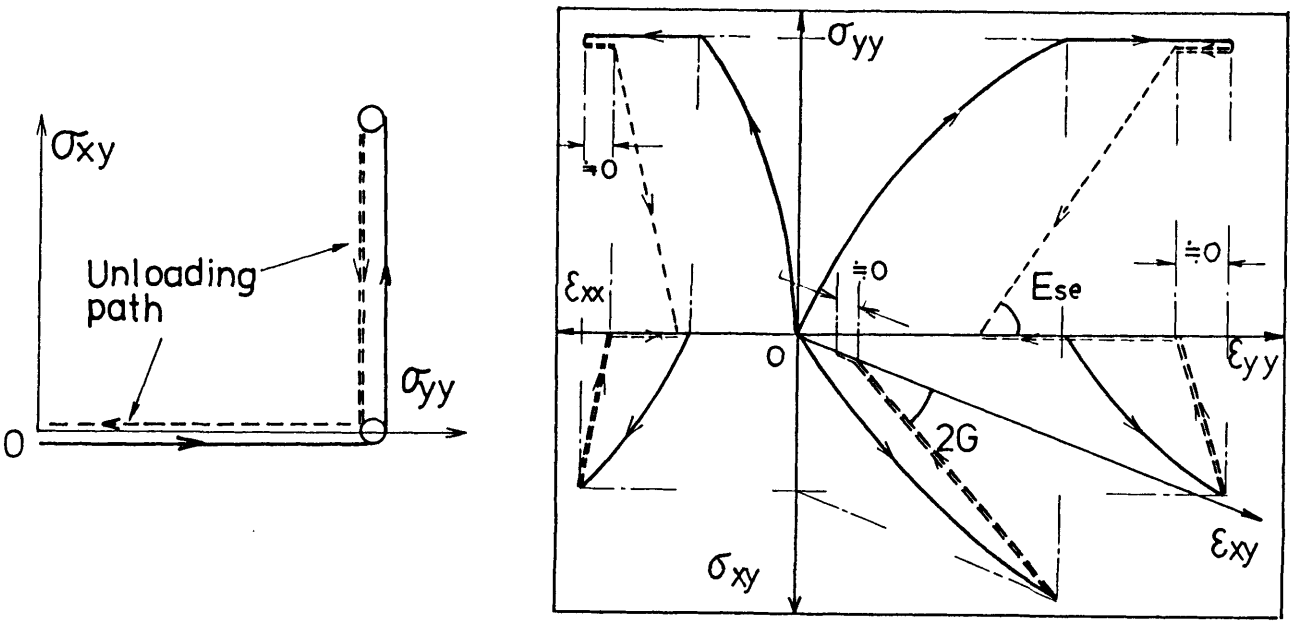

Fig.73. Biaxial unloading path for the investigation of elastic response.

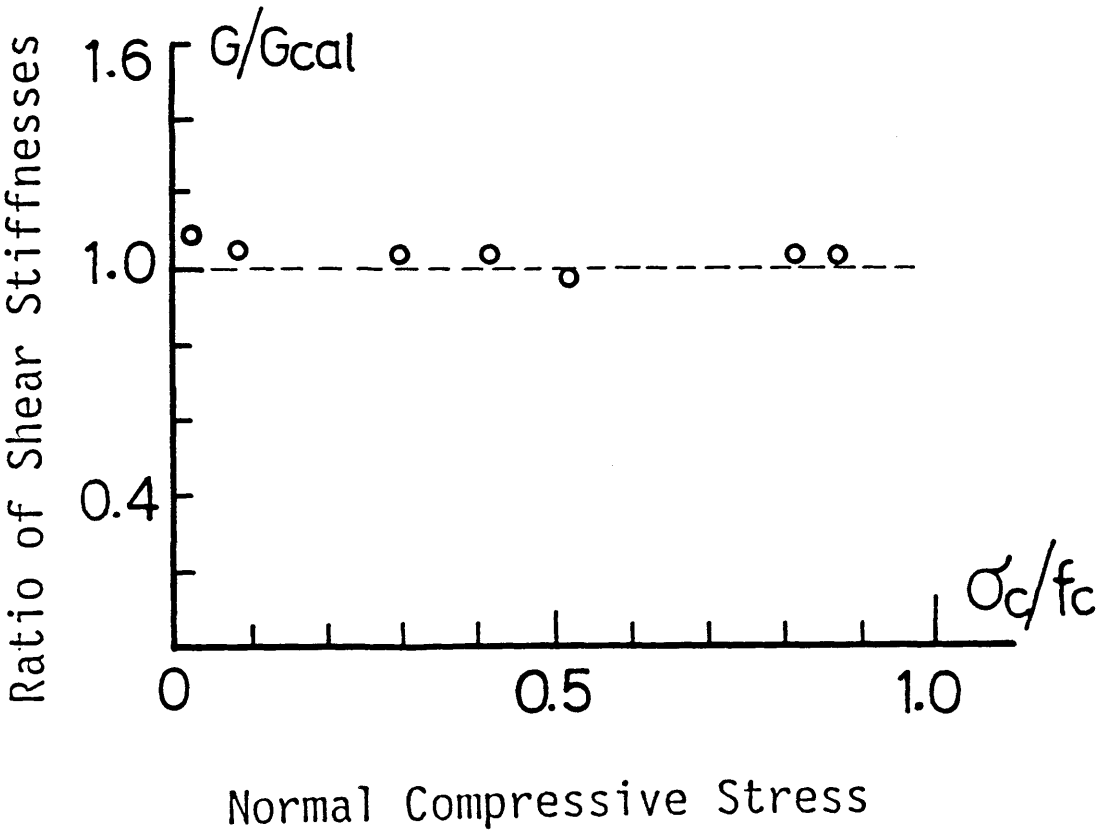

Fig.74. The shear stiffness and the calculated one using the isotropy of elasticity.

$$\begin{Bmatrix} d\varepsilon_{pxx} \\ d\varepsilon_{pyy} \\ d\varepsilon_{pxy} \end{Bmatrix} = \left[C(\theta_p) \right] \begin{Bmatrix} d\varepsilon_{p1} \\ \\ d\varepsilon_{p2} \end{Bmatrix} \tag{77}$$

where, C : coordinate transformation matrix in Eq. (37)

θ_p : angle of principal axis 1 to the X coordinate axis, $=T(\delta_{ij}=d\varepsilon_{pij})$

ε_{p1}, ε_{p2} : maximum and minimum principal plastic increments

7-5-1 Principal direction

Rotation tests by cut-off method in Section 4.3 were carried out under the uniaxial compression stress state only and the abrupt rotation hysteresis of stress axis was enforced due to the experimental technique. As a result, experimental information as to the flow direction of deformation could not be obtained under biaxial compression-tension and continuous rotation of stress axis. However, this compression-shear loading test offers the effective information as to flow rule No. 4 in Eq. (64).

As the applicability of Eq. (64) was verified only within the limited conditions, it is significant to check the flow rule No. 4 with this experimental data. When the principal axis starts to rotate, the shear plastic strain increment was not observed as shown in Fig. 72, say, the principal direction of plastic strain increment agrees with the principal stress direction as

$$T(\sigma ij)=T(d\varepsilon_{pij}) \tag{78}$$

Because of the isotropic relationship between elastic strain and total stress, the principal elastic strain direction agrees with the principal stress direction as

$$T(\varepsilon_{eij})=T(\sigma ij)=T(d\varepsilon_{pij}) \tag{79}$$

On the global coordinate system as shown in Fig. 67, shear tensorial components ε_{exy} and $d\varepsilon_{pxy}$ are equal to zero at the beginning of axis rotation respectively, in effect, shear component of $\varepsilon_{exy}+d\varepsilon_{pxy}$ is also equal to zero. Accordingly, combined tensors $\varepsilon_{eij}+d\varepsilon_{pij}$ has the same principal direction as the elastic one.

$$T(\varepsilon_{eij}+\varepsilon_{pij})=T(\varepsilon_{eij}) \tag{80}$$

Developing Eq. (11) in total differential form

$$(dT/d\varepsilon_{eij}) * d\varepsilon_{pij} = 0 \tag{81}$$

The plastic incremental vector stands normal to the envelope where F is constant. In this type of stress paths, the change of principal stress direction dH is expressed as

$$d\theta = d\theta_e = (dF/d\varepsilon_{eij}) * d\varepsilon_{eij} + (dF/d\varepsilon_{eij}) * d\varepsilon_{pij} = dF/d\varepsilon_{eij} \cdot d\varepsilon_{ij} \tag{82}$$

Eq. (82) coincides with the flow rule constitutive equation (64), say, the flow rule no. 4 is applicable to more general strain paths including continuous rotation of principal axis. The agreement of principal direction of plastic flow with that of principal stress is mathematically equivalent to flow rule No. 4 when isotropy of elasticity holds. However, it is reasonable and beneficial to express the flow rule No. 4 in terms of strain tensors as Eq. (64) because of the harmony of other constitutive laws such as Eq. (33) related to the prediction of fracture rate.

7_5_2 Directional vector of plasticity on principal strain space

In order to express the plastic flow ratio on principal space, it is convenient to define the unit directional vector of plastic flow, PF, as

$$PF = (d\varepsilon_{p1},\ d\varepsilon_{p2}) / \sqrt{d\varepsilon_{p1}^2 + d\varepsilon_{p2}^2} \tag{83}$$

Vectors PF which were experimentally obtained under the axis rotation are drawn on the principal stress space as Fig. 75. The directional tangent of PF, $(d\varepsilon_{p1}/d\varepsilon_{p2})$, under uniaxial stress states is calculated as the ratio of the normal strain increment xx to yy because each normal strain increment is equivalent to the plastic strain increment respectively. Even if the direction of principal stress vector, (σ_1, σ_2) is fixed, the corresponding direction of PF is not constant but varies according to the absolute stress levels. PF tilts to the principal tensile direction when stress reaches to higher level as shown in Fig. 75. Even in case of the continuous rotation of axis, the existence of tensile stress accelerates this tendency very much. Experimentally observed behavior in Fig. 75 is not peculiar to the case of axis rotation but characteristic of concrete under compression-tension stress states as discussed in Chapter 2.

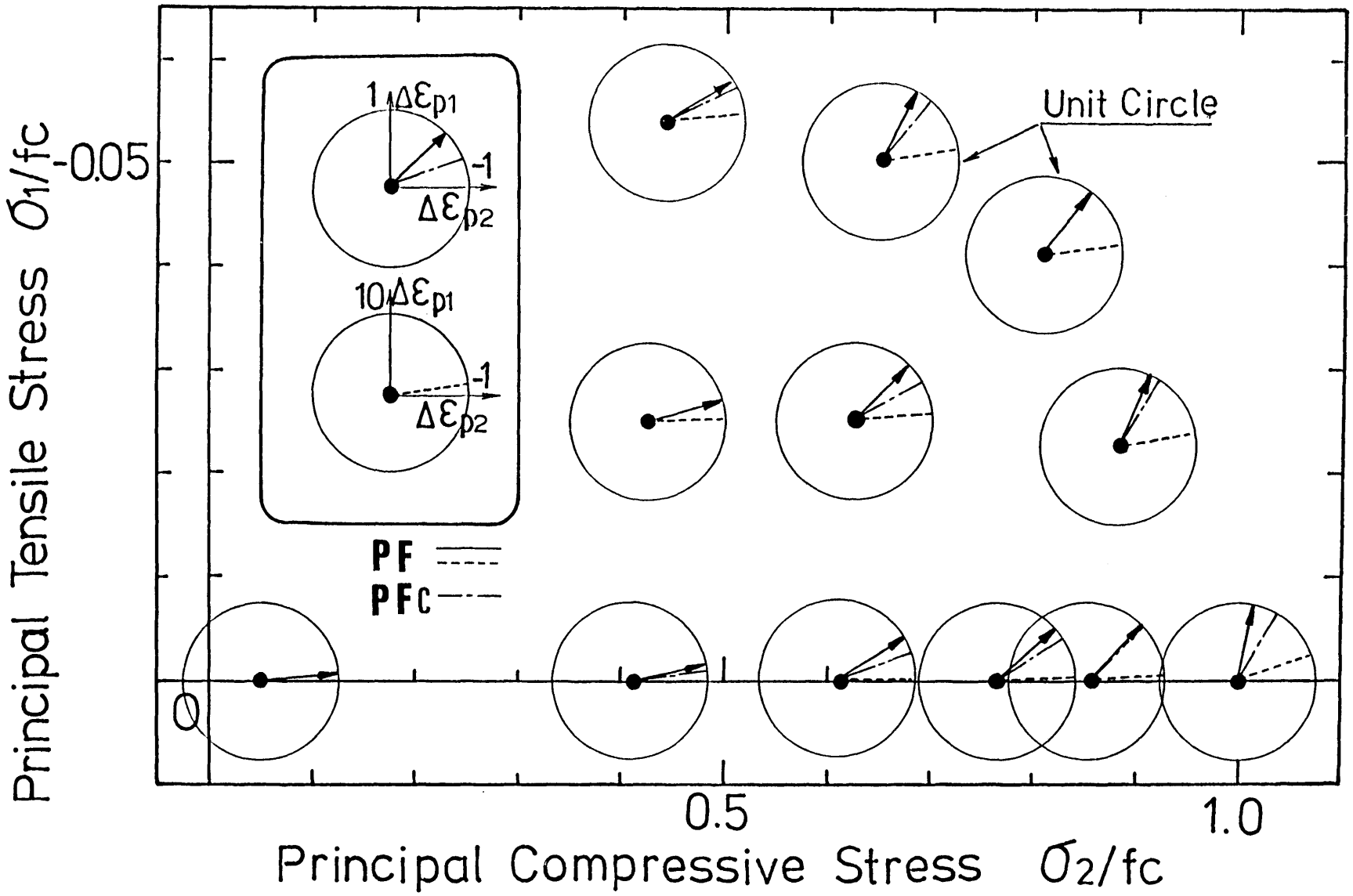

Fig.75. The direction of plastic flow on the principal stress space.

The estimation of the direction of vector PF on the principal strain space has to do with the proposed flow rules No. 2 and No. 3. The prediction of PF by Eq. (67) are included in Fig. 75. There exists some scatter between the actual and predicted directions but the effect of axis rotation is not especially observed. Let us note that the precision for differences, ratios or slopes of directly obtained data drops in general compared with the accuracy of non-processed data. Accordingly, it is appropriate to use rules as to the principal direction of flow based on experiments subjected to non-rotation paths of stress as formulated in Chapter 4.

7.5.3 Plastic flow rate

In case of the elasto-plastic and fracture model, the length of the incremental plastic strain vector is expressed by the equivalent plastic strain Ep as discussed in Section 3.4. The equivalent plastic strain is calculated by the total equivalent strain E in Eq. (32). Therefore, the rate of plastic flow "PR" can be easily obtained by differentiating Eq. (32) as

$$PR=dEp/dE=1-\exp(-0.35E), \quad \text{when } Emax=E \tag{84-1}$$

Using the finite difference of Eq. (84-1), we can calculate the actual plastic flow rate under continuous axis rotation paths as follows.

$$PRc=\left(F(\varepsilon_{ei_j}+\Delta\varepsilon_{pi_j})-F(\varepsilon_{ei_j})\right)/\left(F(\varepsilon_{ei_j}+\Delta\varepsilon_{\tilde{i}_j})-F(\varepsilon_{ei_j})\right) \tag{84-2}$$

Eq. (84-1) was directly verified under biaxial compression-tension tests without rotation of principal stress axes. The experimentally obtained plastic flow rate PRc with rotation paths by Eq. (84-2) is plotted in Fig. 76 normalized by the predicted value by Eq. (84-1). As shown in Fig. 76, the axis rotation of principal stresses has an effect on the plastic flow rate in appearance. Especially, under the high stress condition, the axis rotation accelerates the plastic deformation effectively.

Investigating the influences of axis rotation on the plasticity, let us consider the difference of loading conditions concerning the "time-path". In case of the compression-shear test, the shear stress rate was 0.15Mpa/sec, but the corresponding loading speed of principal stresses is not greater than 0.015Mpa/sec (1/10 - 1/50 times). Accordingly, greater time-dependent plasticity (creep) may be included in the experimentally obtained plastic strain than the plasticity introduced by the non-rotation tests.

On the other hand, the plastic flow rate by Eq. (84-1) was derived from

loading tests with the principal stress rate 0.2Mpa/sec. In this type of loading paths, the normal strain increments are nearly equal to the plastic flow. Therefore, the difference of the time effect causes the disagreement between analytical and experimental results related to the normal strain increments as shown in Fig.68.

Using the loading system as shown in Fig.3, the author obtained the plastic flow rate Ept from experiments where the principal loading speed agreed with the compression-shear tests but the principal axis did not rotate. The actual plastic flow rate normalized by Ept was shown in Fig.76 where the delayed plasticity (creep) was eliminated. We can understand from this test result that the effect of time-path is great under high stress conditions. Then, the advanced plastic flow rate due to the axis rotation history is almost explained by the difference of time-paths. Taking these situations into account, it is indispensable to formulate the time-path dependent palsticity for the wide-ranged applicability of constitutive equations for concrete.

However, we can recognize another effect of axis rotation on the plasticity as shown in Fig.76. In order to understand the effect of rotation on the plastic flow rate, let us consider the extreme case, that is to say, "orthogonal" rotation. The loading path and corresponding equivalent plastic strain are shown in Fig.77. When concrete is strained to a higher level introduced by the cyclic loading, the excessive plastic flow owing to the orthogonally rotating path was observed when the directional angle θ varied 90deg. Especially, the flow rate is remarkable under low stress state after rotation. However, this anisotropic flow rate cannot be expressed because hardening formulation by Eq.(32) is an explicit function of invariants. It is imagined that the tensile plastic strain easily flows due to compressive stress normal to the distributed microcracking until enough recontact between cracking faces is ensured. The accelerated plastic flow subjected to rotation histories is considered one of substantial properties of concrete. Unfortunately, we do not have enough data to formulate this behavior of concrete. Systematically arranged program of experiments for this purpose is expected.

In the case of 2D structural members, actually reproduced angle of stress rotation is not so great as to take their additional flow rate due to axis rotation into account. When concrete is biaxially loaded until Emax=unity, plastic flow rate may be described mathematically by invariants of strains which are independent of the coordinate transformation as Eq.(32).

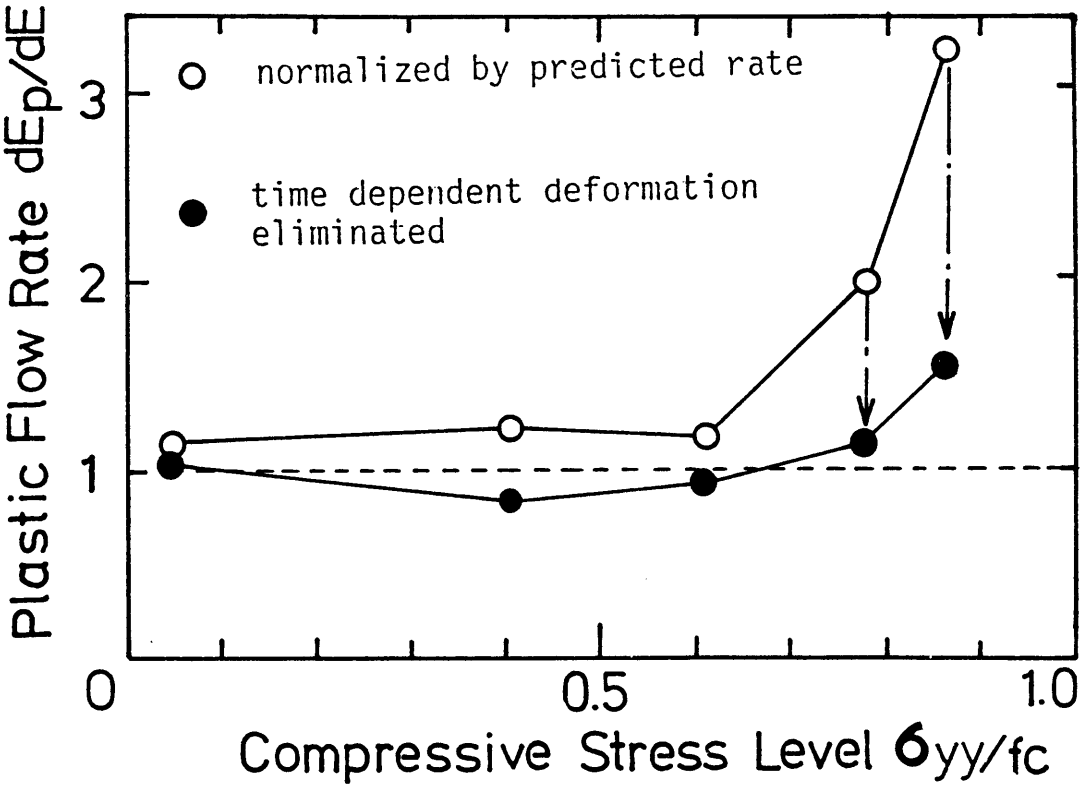

Fig.76. Accelerated plastic flow rate introduced by rotation paths.

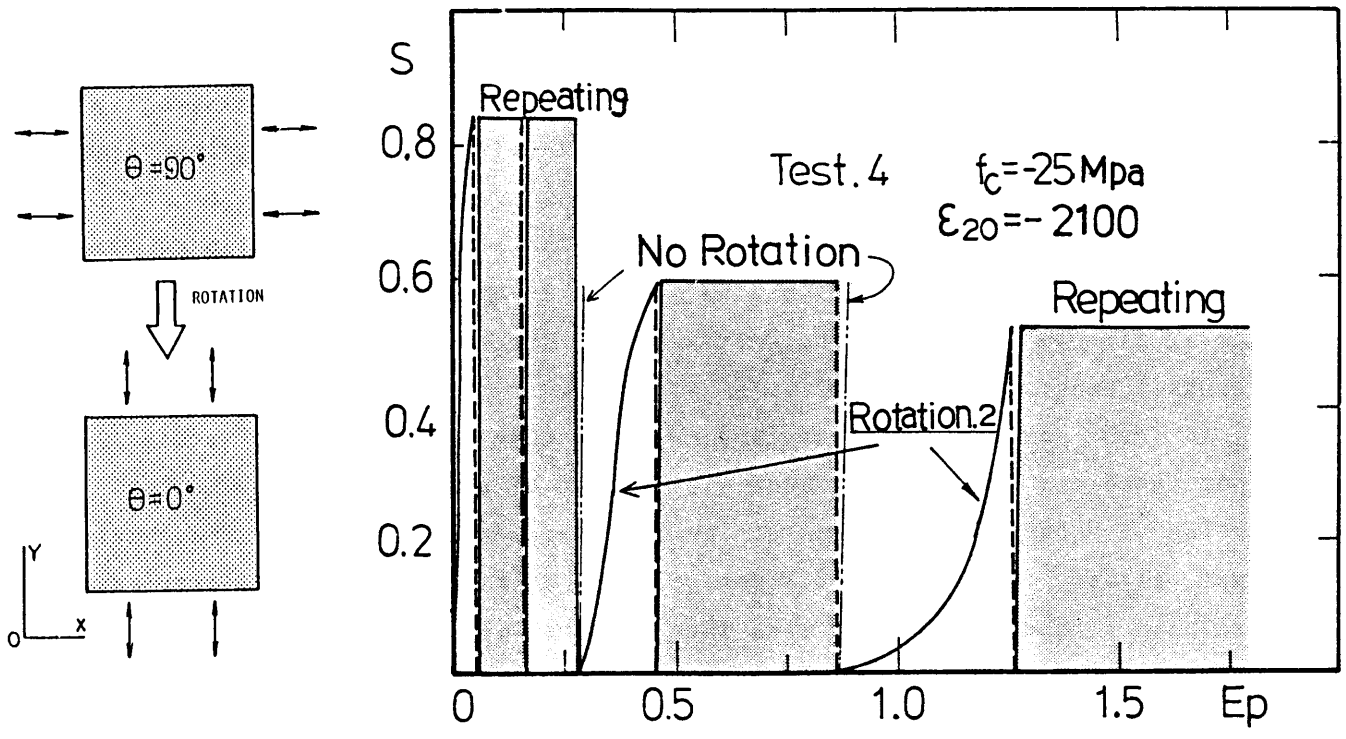

Fig.77. Orthogonal rotation paths and corresponding equivalent plastic strain.

7.6 Concluding remarks

The loading tests including axis rotation were executed in order to verify the elasro-plastic and fracture model for concrete subjected to the continuous rotation of principal axes under compression-tension stress states. The author obtained the anisotropic behavior of concrete as follows.

(1) Anisotropy.

When the shear stress is applied to concrete under the fixed normal stresses (The principal stress axis rotates), the normal stiffness parallel to the principal stress axis and the shear stiffness decrease according to the increase of compressive stress level, but the shear stiffness does not drop so great as the normal one decreases in appearance. This behavior can be quantitatively simulated by the proposed modelling. But, the normal strain increments introduced by the axis rotation were estimated to be small under high stress conditions.

In order to understand this anisotropy, the author introduced unloading paths and it was made clear that very little shear plastic strain flows but normal plastic strain increments account for nearly 100 per cent of the normal total strain increments parallel to the principal stresses when concrete receives the axis rotation. This behavior was correctly predicted by the elasto-plastic and fracture model.

(2) Elasticity.

The relationship between elastic strains and stresses was verified isotropic under continuous rotation of principal axes, and the constitutive law concerning the fracture parameter was also effective with reasonable accuracy.

(3) Plasticity.

The flow rule No.4 correctly predicted the principal direction of plastic strain increment and the calculated plastic flow direction on the principal space by flow rules No.2 and No.3 agreed with the actual plastic direction with reasonable accuracy.

In the compression-shear loading paths under high stress states, the author observed the apparent accelerated rate of plastic flow due to the axis rotation. Because of the restriction of experimental technique, the shear and normal stress rates 0.15, 0.20Mpa/sec were adopted, but the corresponding principal stress rate became less than 0.015Mpa/sec (nearly 1/10 - 1/50 times the stress component speed). However, the plastic flow rate and fracture rate are based on the experiments under constant principal stress rate 0.2Mpa/sec. The fact is that the effect of the axis rotation in appearance is practically caused by the difference of time hysteresis. Therefore, it is natural that the proposed model without time parameter could not predict the normal strain

increments under axis rotation because normal strain increments were almost the same as the plastic increments.

We should carefully use the elasto-plastic and fracture model when we apply this model to FEM analyses of RC structures where the direction of stress increments is produced greatly different from the updated stress direction. It is indispensable to formulate the time path-dependent deformation of concrete when we seek for the wide applicability of constitutive laws for concrete.

8. CONCLUSION

The biaxial loading tests under various types of stress paths were carried out and corresponding strain paths were precisely measured. Adopted stress paths were summarized as

(1) Monotonic non-proportional and compression-tension loading where the ratio of principal stresses is not constant.

(2) Cyclic non-proportional and compression-tension loading where unloading stress paths were included in the loading programs.

(3) Cyclic uniaxial compression loading where the direction of principal stress rotates.

By choosing three types of loading paths, it became possible to verify the following deformational behavior of concrete which have been qualitatively predicted but not quantitatively described.

(1) Anisotropy of biaxial stiffnesses.

When the deformational level is low, concrete behaves isotropically. But under high compression-tension stress state, the biaxial stiffnesses do not coincide with each other and the stiffness in the principal tensile direction decreases rapidly.

(2) Isotropic relation between stress and elastic strain.

Biaxial stresses and elastic strains are linked by the isotropic stiffness matrix in the integrated form. Accordingly, the stress-strain relationship in the reversible process (elastic condition) is not influenced by strain paths.

(3) The direction of principal elastic strain and total strains.

The direction of principal elastic strain coincides with the direction of principal stress. However, under high stress level, the direction of principal total strain does not agree with that of principal stress.

Moreover, these biaxial loading experiments were successful in making clear the following characteristics of concrete newly and quantitatively.

(4) Non-symmetry of biaxial stiffness matrix.

When the deformational level is low, the tangential stiffness matrix is symmetrical, but under high compression-tension stress state, the stiffness matrix becomes non-symmetrical.

(5) Plastic flow rate.

Under high compression-tension stress states, the increment of the principal tensile stress accelerates the plastic deformation more effectively than that of principal compressive stress.

(6) Direction of plastic flow.

Under high compression-tension stress states, the plastic strain in the principal tensile stress direction flows more rapidly than that in the

direction normal to the principal tensile stress.

In order to formulate the investigated deformational behavior above, the equivalent stress and strain (equivalent elastic, plastic and total strains), fracture parameter and anisotropy parameter were introduced under arbitrary strain paths. These invariant values were successful in indicating the degrees of plasticity, fracture and anisotropy of concrete. Moreover, with these values, the elasto-plastic and fracture constitutive law and new flow rule system could be organized in simplified mathematical forms.

By solving these two types of constitutive laws, plane stress constitutive equations could be derived. Then, the effective numerical integration method of derived equations were given for FEM analysis and analytical results were checked by experimental data including stress paths where principal stress axes "continuously" rotate.

From experimental verification, it was confirmed that the formulated constitutive laws are able to express the overall nonlinear deformational behavior of concrete with reasonable accuracy.

ACKNOWLEDGMENTS

The author expresses his sincere gratitude to Professor Hajime Okamura for his invaluable advice and suggestion throughout all stages of this research. The author has received good instruction related to the basic philosophy toward scientific research from Dr. Hajime Okamura.

The author wishes to thank Associate Professor Kyuichi Maruyama, Technological University of Nagaoka, for his encouragement and support.

The author thanks his colleagues and students for their warm and devoted cooperation . Mr. Matuji Enomoto (University of Tokyo) and Mr. Yugo Nakamura (Technological University of Nagaoka) assisted the author in the experimental planning. Mr. Kazuto Kamisakoda, Mr. Masanobu Tabata, Mr. Baolu Li and Mr. Masashi Odagawa, undergraduate and graduate students, supported experiments and data processing jobs. The author is grateful to their kindness.

Finally, the author appreciates the financial support by the Grant-in-aid for the scientific research No.56460123 (Okamura and Maekawa in 1983), No.58750382 (Maekawa in 1983) and No.59750372 (Maekawa in 1984) from Japan Ministry of Education.

REEERENCES

(1) Ngo,D. and Scordelis,A.C. : Finite Element Analysis of Reinforced Concrete Beams, Journal of ACI, Vol.64, No.3, pp.152 - 163, March, 1967.

(2) Kupfer,H.B., Hirsdorf,H.K. and Rusch,H. : Behavior of Concrete Under Biaxial Stresses, Journal of ACI, Vol.66, No.8, pp.656-666, August, 1969.

(3) Kotsovos,M.D. and Newmann,J.B. : Generalized Stress-Strain Relations for Concrete, Proceedings of ASCE, Vol.104, No.EM4, pp.845-856, August, 1978.

(4) Kupfer,H.B. and Gerstle,K.H. : Behavior of Concrete Under Biaxial Stresses, Proceedings of ASCE, Vol.99, No.EM4, pp.852-866, August, 1973.

(5) Kotsovos,M.D. and Newmann,J.B. : A Mathematical Description of the Deformational Behavior of Concrete under Complex Loading, Magazine of Concrete research, Vol.31, No.107, June, 1979.

(6) Isobata,S. : The Orthogonal Anisotropic Model for Concrete Structures and Application, Proceedings of AIJ, No.265, pp.11-18, March, 1978.

(7) Darwin,D. and Pecknold,D.A. : Nonlinear Biaxial Stres-Strain Law of Concrete, Proceedings of ASCE, Vol.103, No.EM2, pp.229-241, April, 1977.

(8) Chen,A.T.C. and Chen,W.F. : Constitutive Relations for Concrete, Proceedings of ASCE, Vol.101, No.EM4, August, 1975.

(9) Chen,W.F. : Constitutive Equations and Yield Criterion, IABSE Colloquium, Copenhagen, 1979.

(10) Chen,A.T.C. and Chen,W.F. : Constitutive Equations and Punch Identitation of Concrete, Proceedings of ASCE, Vol.101, No.EM6, pp.889-906, December, 1975.

(11) Bazant,Z.P. : Endochronic Inelasticity and Incremental Plasticity, Int. Journal of Solids and Structures, Vol.14, 1978.

(12) Bazant,Z.P. and Kim,S. : Plastic Fracturing Theory for Concrete, Proceedings of ASCE, No.EM3, June, 1979.

(13) Tasuji,M.E., Slate,F.O. and Nilson,A.H. : Stress-Strain Response and Fracture of Concrete in Biaxial Loading, Journal of ACI, Vol.75, No.7, pp.306-312, July, 1978.

(14) Tasuji,M.E., Nilson,A.H. and Slate,F.O. : Biaxial Stress-strain Relationships for Concrete, Magazine of Concrete Research, Vol.31, No.109, pp.324-337, December, 1979.

(15) Niwa,J., Maekawa,K. and Okamura,H. : Non-linear Finite Element Analysis of Deep Beams, IABSE Colloquium, Final Report, Delft, pp.625-638, 1981.

(16) Nelissen,L.J.M. : Biaxial Testing of Normal Concrete, HERON, Vol.18, No.1, Delft, 1972.

(17) Chen,W.F. : Plasticity in Reinforced Concrete, McGraw-Hill, 1982.

(18) Owen and Hinton : Plasticity in Finite Elements, John Wiley & Sons, 1981.

(19) Yamada,Y. : Plasticity and Visco-Elasticity, Lecture of Structural Analysis by Computers, Vol.II-2-A, Baifu-Kan Co. (in Japanese).

(20) Vecohio,F. and Collins,M.P. : Stress-Strain Characteristics of Reinforced Concrete in Pure Shear, IABSE Colloquium, Final Report, Delft, pp.211-225, June, 1981.

(21) Tohata,I. : The Effect of the Principal Axis Rotation on the Deformational Behavior of Sand under the Cyclic Shear, Dissertation for the Degree of Doctor of Engineering, submitted to the University of Tokyo, March, 1982.

(22) Bazant,Z.P. : Final Report of IABSE Colloquium, 1981, General Discussion, Session 2, Part II, pp.490-491, 1981.

(23) Okajima,T. : The Strength of Concrete Under Combined Axial Force (Compression and Tension) and Torsional Moment, Transaction of AIJ, No.178, pp.1-8, December, 1970.

(24) Bresler,B. and Pister,K.S. : Strength of Concrete Under combined Stresses, Journal of ACI, Sept. 1958, pp.321-345.

(25) Chen,W.F. and Saleeb,A.F. : Constitutive Equations for Engineering Materials, Volume 1, John Wiley & Sons, 1982.

Appendix I Derivation of Equivalent Total Strain in Monotonic and Proportional Biaxial Compressive Stress Paths

--- Derivation of Eq.(36)---

Using the strain measure function in Eq.(16) and the definition of equivalent total strain in Eq.(28), we can calculate the increment of the equivalent total strain in the form

$$dE = \frac{c\bar{\varepsilon}_0}{F}\frac{\partial\bar{\varepsilon}_0}{\partial\delta_{ij}}\Big|_{\delta_{ij}=\varepsilon_{eij}}\cdot d\varepsilon_{ij} + \frac{d\bar{\gamma}_0}{F}\frac{\partial\bar{\gamma}_0}{\partial\delta_{ij}}\Big|_{\delta_{ij}=\varepsilon_{eij}}\cdot d\varepsilon_{ij} \qquad \text{(A-1-1)}$$

Eq.(A-1-1) holds in any coordinate system. Taking the coordinate axes in the principal stress directions (Principal directions are constant.), we find

$$\frac{\partial\bar{\varepsilon}_0}{\partial\delta_{ij}}\Big|_{\delta_{ij}=\varepsilon_{eij}}\cdot d\varepsilon_{ij} = \frac{1}{\sqrt{2}}d\varepsilon_{xx} + \frac{1}{\sqrt{2}}d\varepsilon_{yy} = \frac{\partial\bar{\varepsilon}_0}{\partial\delta_{ij}}\Big|_{\delta_{ij}=\varepsilon_{ij}}\cdot d\varepsilon_{ij} \qquad \text{(A-1-2)}$$

where, $\varepsilon_{xy} = \varepsilon_{exy} = 0$

$$\frac{\partial\bar{\gamma}_0}{\partial\delta_{ij}}\Big|_{\delta_{ij}=\varepsilon_{eij}}\cdot d\varepsilon_{ij} = \frac{\delta_{xx}-\delta_{yy}}{2\bar{\gamma}_0}\Big|_{\delta_{ij}=\varepsilon_{eij}}\cdot(d\varepsilon_{xx}-d\varepsilon_{yy}) + \frac{2\delta_{xy}}{\bar{\gamma}_0}\Big|_{\delta_{ij}=\varepsilon_{eij}}\cdot d\varepsilon_{xy}$$

$$= \frac{\delta_{xx}-\delta_{yy}}{\bar{\gamma}_0}\Big|_{\delta_{ij}=\varepsilon_{eij}}\cdot\left(\frac{1}{2}d\varepsilon_{xx}-\frac{1}{2}d\varepsilon_{yy}\right) + \frac{2\delta_{xy}}{\bar{\gamma}_0}\Big|_{\delta_{ij}=\varepsilon_{ij}}\cdot d\varepsilon_{xy} \qquad \text{(A-1-3)}$$

Let us now consider the uniaxail stress state (one of the ultimate condition in biaxial compression stress states.). When E is less than unity in this condition, the direction of the total strain vector is approximately equal to that of the plastic strain vector as shown in Fig.A1, that is

$$(\varepsilon_{exx}, \varepsilon_{eyy}) \fallingdotseq k1(\varepsilon_{xx}, \varepsilon_{yy}) \qquad k1:\text{constant} \qquad \text{(A-1-4)}$$

Otherwise, in the case of the biaxial isotropic compressive stress state (another ultimate condition) where $\varepsilon_{xx}=\varepsilon_{yy}$, $\varepsilon_{exx}=\varepsilon_{eyy}$, the directions of total strain and plastic strain vectors satisfy Eq.(A-1-4) strictly. Therefore, it is reasonable to use Eq.(A-1-4) in the biaxial compressive stress state.

Substituting Eq.(A-1-4) into Eq.(A-1-2), we have

$$\frac{\partial\bar{\gamma}_0}{\partial\delta_{ij}}\Big|_{\delta_{ij}=\varepsilon_{eij}}\cdot d\varepsilon_{ij} = \frac{\delta_{xx}-\delta_{yy}}{\bar{\gamma}_0}\Big|_{\delta_{ij}=\varepsilon_{ij}}\left(\frac{1}{2}d\varepsilon_{xx}-\frac{1}{2}d\varepsilon_{yy}\right) + \frac{2\delta_{xy}}{\bar{\gamma}_0}\Big|_{\delta_{ij}=\varepsilon_{ij}}\cdot d\varepsilon_{xy}$$

$$= \frac{\partial\bar{\gamma}_0}{\partial\delta_{ij}}\Big|_{\delta_{ij}=\varepsilon_{ij}}\cdot d\varepsilon_{ij} \qquad \text{(A-1-5)}$$

Similarly, Eq.(A-1-6) and Eq.(A-1-7) are derived as follows.

$$\left.\frac{\bar{\varepsilon}_0}{F}\right|_{\delta_{ij}=\varepsilon_{eij}} = \left.\frac{\bar{\varepsilon}_0}{\sqrt{(C\bar{\varepsilon}_0)^2+(d\bar{\gamma}_0)^2}}\right|_{\delta_{ij}=\varepsilon_{eij}} = \left.\frac{\bar{\varepsilon}_0}{\sqrt{(C\bar{\varepsilon}_0)^2+(d\bar{\gamma}_0)^2}}\right|_{\delta_{ij}=k_1\cdot\varepsilon_{ij}}$$

$$= \left.\frac{k_1\bar{\varepsilon}_0}{k_1\sqrt{(C\bar{\varepsilon}_0)^2+(d\bar{\gamma}_0)^2}}\right|_{\delta_{ij}=\varepsilon_{ij}} = \left.\frac{\bar{\varepsilon}_0}{F}\right|_{\delta_{ij}=\varepsilon_{ij}} \qquad \text{(A-1-6)}$$

$$\left.\frac{\bar{\gamma}_0}{F}\right|_{\delta_{ij}=\varepsilon_{eij}} = \left.\frac{\bar{\gamma}_0}{F}\right|_{\delta_{ij}=\varepsilon_{ij}} \qquad \text{(A-1-7)}$$

Substituting Eq.(A-1-2), Eq.(A-1-5), Eq.(A-1-6) and Eq.(A-1-7) into Eq.(A-1-1), we obtain

$$dE \fallingdotseq \frac{C\bar{\varepsilon}_0}{F}\left.\frac{\partial\bar{\varepsilon}_0}{\partial\delta_{ij}}\right|_{\delta_{ij}=\varepsilon_{ij}}\cdot d\varepsilon_{ij} + \frac{d\bar{\gamma}_0}{F}\left.\frac{\partial\bar{\gamma}_0}{\partial\delta_{ij}}\right|_{\delta_{ij}=\varepsilon_{ij}}\cdot d\varepsilon_{ij} = \left.\frac{\partial F}{\partial\delta_{ij}}\right|_{\delta_{ij}=\varepsilon_{ij}}\cdot d\varepsilon_{ij}$$

$$E = \int\left.\frac{\partial F}{\partial\delta_{ij}}\right|_{\delta_{ij}=\varepsilon_{ij}}\cdot d\varepsilon_{ij} = \int dF = F(\varepsilon_{ij}) \qquad (36)$$

which is the strict solution in the isotropic biaxial compressive stress state.

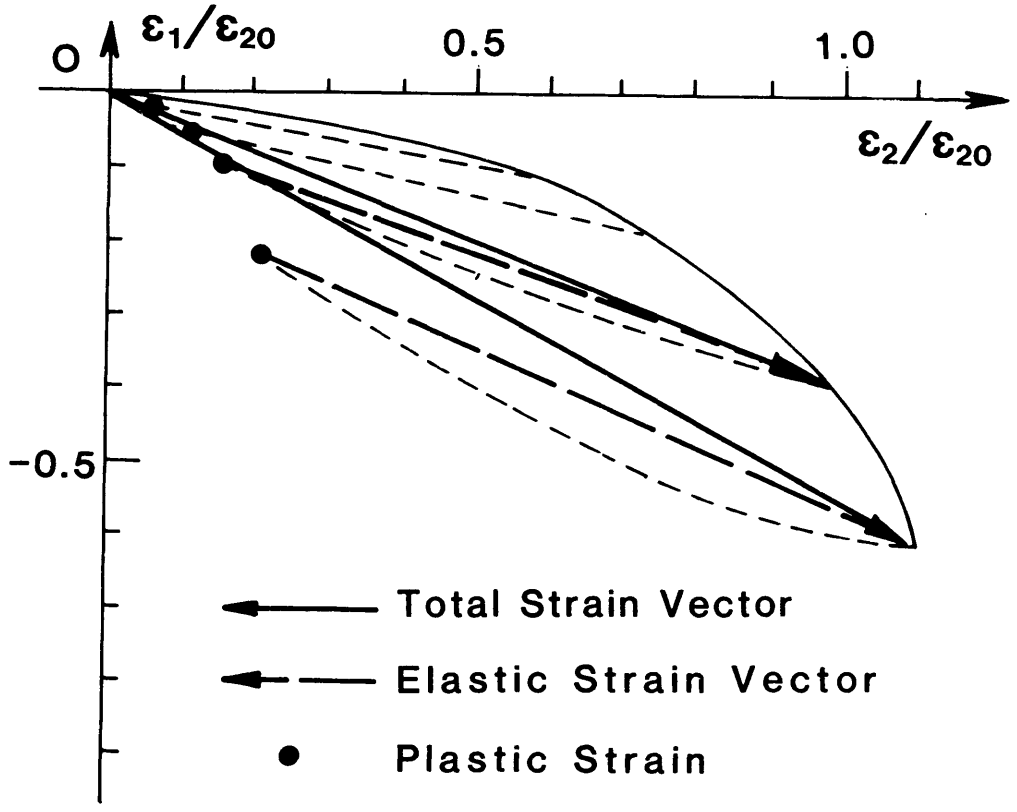

Fig.A1. Total and elastic strain vector under monotonic uniaxial compression stress state.

Appendix II Derivation of Constitutive Equations to Predict the Stress Invariant Vector in the Irreversible Process ---Derivation of Eq.(60)---

In differentiating Eq.(59), the neutral loading path (dE=dEmax=0) is chosen for integration path. As the reversible Poisson's ratio remains constant in this integration path, we have

$$d\left(\frac{1-\nu^*}{1+\nu^*}\right)=0 \tag{A-2-1}$$

Therefore, Eq.(59) is

$$\gamma_0 d\varepsilon_{on}-\varepsilon_0 d\gamma_{on}=\frac{1-\nu^*}{1+\nu^*}\left(\frac{\bar{\gamma}_0}{\bar{\tau}_0}\right)^2(\bar{\tau}_0 d\bar{\sigma}_{on}-\bar{\sigma}_0 d\bar{\tau}_{on}) \tag{A-2-2}$$

Substituting Eqs.(55) and (56) into Eq.(A-2-2), we find the unique ralationship between j and k as

dj = P1 dk

$$P1=\frac{1+\nu^*}{1-\nu^*}\left(\frac{\bar{\tau}_0}{\bar{\gamma}_0}\right)^2\left.\frac{\bar{\varepsilon}_0\dfrac{\partial F}{\partial\bar{\varepsilon}_0}+\bar{\gamma}_0\dfrac{\partial F}{\partial\bar{\gamma}_0}}{\bar{\tau}_0\dfrac{\partial S}{\partial\bar{\tau}_0}+\bar{\sigma}_0\dfrac{\partial S}{\partial\bar{\sigma}_0}}\right|_{\delta_{ij}=\varepsilon_{eij}} \tag{A-2-3}$$

Differentiating the elasto-plastic and fracture equation (35) with the irreversible criterion in Eq.(30), we have

$$dS=E_0\left\{K(E)\left(1-\frac{dE_p}{dE}\right)+\frac{dK}{dE}(E-E_p)\right\}dE \tag{A-2-4}$$

According to the definitions of the equivalent stress and the equivalent strain in Eq.(13) and Eq.(28) with definition in Eq.(45), the differentiations of these values are

$$dS=\frac{\partial S}{\partial\bar{\sigma}_0}d\bar{\sigma}_0+\frac{\partial S}{\partial\bar{\tau}_0}d\bar{\tau}_0 \tag{A-2-5}$$

$$dE=\left.\frac{\partial F}{\partial\delta_{ij}}\right|_{\delta_{ij}=\varepsilon_{eij}}\cdot d\varepsilon_{ij}=\left.\left(\frac{\partial F}{\partial\bar{\varepsilon}_0}d\bar{\varepsilon}_0+\frac{\partial F}{\partial\bar{\gamma}_0}d\bar{\gamma}_0\right)\right|_{\delta_{ij}=\varepsilon_{eij}} \tag{A-2-6}$$

Substituting Eqs.(A-2-5) and (A-2-6) into Eq.(A-2-4) with the flow rule No.2 and No.3 in Eqs.(55) and (56), we obtain

dl=(P2+P3)dm

$$P2 = E_0(E-E_p)\frac{dK}{dE_{max}}\cdot\left.\frac{(\bar{\varepsilon}_0-\alpha)\frac{\partial F}{\partial \bar{\varepsilon}_0}+(\bar{\gamma}_0-\beta)\frac{\partial F}{\partial \bar{\gamma}_0}}{\bar{\tau}_0\frac{\partial S}{\partial \bar{\tau}_0}+\bar{\tau}_0\frac{\partial S}{\partial \bar{\gamma}_0}}\right|_{\delta_{ij}=\varepsilon_{eij}}$$

$$P3 = E_0K\left(1-\frac{dE_p}{dE_{max}}\right)\cdot\left.\frac{(\bar{\varepsilon}_0-\alpha)\frac{\partial F}{\partial \bar{\varepsilon}_0}+(\bar{\gamma}_0-\beta)\frac{\partial F}{\partial \bar{\gamma}_0}}{\bar{\tau}_0\frac{\partial S}{\partial \bar{\tau}_0}+\bar{\sigma}_0\frac{\partial S}{\partial \bar{\gamma}_0}}\right|_{\delta_{ij}=\varepsilon_{eij}} \qquad \text{(A-2-7)}$$

Local coordinate values (dl,dm) can be determined by solving Eq.(56) under the arbitrary stress paths as

$$\begin{bmatrix} dl \\ dm \end{bmatrix} = [M]^{-1}\begin{bmatrix} d\bar{\varepsilon}_0 \\ d\bar{\gamma}_0 \end{bmatrix},\quad [M] = \left.\begin{bmatrix} -\frac{\partial F}{\partial \bar{\gamma}_0} & \bar{\varepsilon}_0-\alpha \\ \frac{\partial F}{\partial \bar{\varepsilon}_0} & \bar{\gamma}_0-\beta \end{bmatrix}\right|_{\delta_{ij}=\varepsilon_{eij}} \qquad \text{(A-2-8)}$$

As the envelope where equivalent total strain is conctant or in other words, Ee=const. is convex in the strain space (See Fig.50), two base vectors X1 and X2 are independent of each other when the convergence points Zc and Zt exist within the envelope (See Fig.54). The formulation of points Zc and Zt satisfies this condition. Accordingly, strain transformation matrix (M) whose column vectors are X1 and X2 become regular and the inverse of strain transformation matrix exists.

Parameter j and l are given by

$$\begin{bmatrix} dj \\ dl \end{bmatrix} = \begin{bmatrix} P1 & 0 \\ 0 & P2+P3 \end{bmatrix}\begin{bmatrix} dk \\ dm \end{bmatrix} \qquad \text{(A-2-9)}$$

The strain inveriant vector is calculated by Eq.(56) under an arbitrary strain path and parameters k and m are obtained by Eq.(A-2-8). Parameters j and l are determined by Eq.(A-2-9) and stress invariant vector is uniquely determined by Eq.(44).

These process is summarized in Eq.(60).

Appendix III Numerical Integration Method of Derived Plane Stress Constitutive Equations (r-minimum method)

Mathematical forms of constitutive equations in the reversible process is different from those in the irreversible process. Therefore, we must determine the integration ranges where reversible and irreversible constitutive equations can be applied in an integration step in the case where concrete is deformed from the reversible (elastic) to the irreversible process. The similar problems exist in the integration of the constitutive equations in the theory of plasticity.

This paper adopts the r-minimum method by Yamada(19) which was formulated in the stress space to the numerical analysis in the strain space. Let us consider the case where a strain point at time t (point A in Fig.A2) in the reversible area shifts to a new strain point at time $t+\Delta t$ (point B in Fig.A2) in the irreversible area due to the strain increment $\Delta\varepsilon_{ij}$. It is assumed that the strain state changes streightly from points A to B in the strain space as shown in Fig.A2. Ponint D is defined as a intersecting strain point between the reversible boundary (elasticity boundary) and the strain path from A to B, therefore, the strain state at D is expressed as $\varepsilon_{ij}^{t+r\Delta t}$ with the strain at A ε_{ij}^{t} and strain increment $\Delta\varepsilon_{ij}$ in the form

$$\varepsilon_{ij}^{t+r\Delta t} = \varepsilon_{ij}^{t} + r\Delta\varepsilon_{ij} \tag{A-3-1}$$

The strain at B is

$$\varepsilon_{ij}^{t} = \varepsilon_{ij}^{t} + \Delta\varepsilon_{ij} = \varepsilon_{ij}^{t+r\Delta t} + (1-r)\Delta\varepsilon_{ij} \tag{A-3-2}$$

where $0 \leqq r \leqq 1$.

Parameter r controls the integration interval. At the first stage, the stress $\sigma_{ij}^{t+r\Delta t}$ which corresponds to the strain at D can be calculated using the reversible constitutive equations with the strain increment $r\Delta\varepsilon_{ij}$. At the second stage, the stress at time $t+\Delta t$ can be calculated by the irreversible constitutive equations with the strain increment $(1-r)\Delta\varepsilon_{ij}$. We have

$$r = \frac{\left.\dfrac{\partial F}{\partial \delta_{ij}}\right|_{\delta_{ij}=\varepsilon_{eij}} \cdot r d\varepsilon_{ij}}{\left.\dfrac{\partial F}{\partial \delta_{ij}}\right|_{\delta_{ij}=\varepsilon_{eij}} \cdot d\varepsilon_{ij}} \fallingdotseq \frac{E^{t-r\Delta t} - E^{t}}{\Delta E} \tag{A-3-3}$$

From the definition of r as shown in Fig.A2, the inegration parameter is

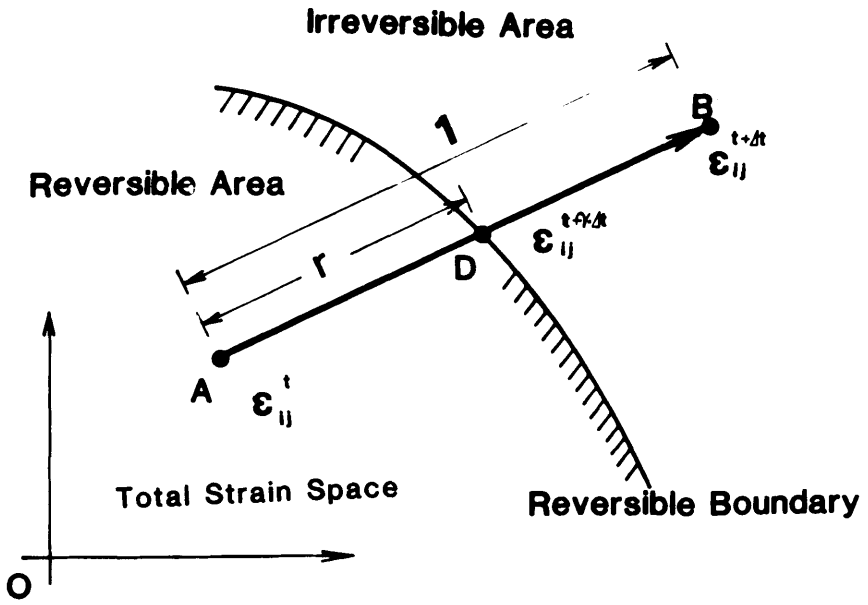

Fig.A2. Definition of control parameter for numerical integration.

$E^{t+\Delta t} = \quad Emax^{t}$

$$r = \frac{E^t_{max} - E^t}{\Delta E} = \frac{E^t_{max} - E^t}{F(\delta_{ij} = \varepsilon^t_{eij} + \Delta\varepsilon_{ij}) - E_e} \qquad \text{(A-3-4)}$$

The calculation flow of integrating the plane stress constitutive equations for FEM analysis is shown in Fig.A3 and Fig.A4. When the strain increment $\Delta\varepsilon_{ij}$ is given as input, $\sigma_{ij}^{t+\Delta t}$ can be calculated as output using σ_{ij}^{t}, ε_{ij}^{t}, ε_{pij}^{t}, E^t and $Emax^t$. The general process in Fig.A3 and Fig.A4 is equivalent to the simultaneous solution of the elasto-plastic and fracture constitutive equation (35) and flow rules No.1-No.4. in the difference forms of Eq.(40), Eq.(44), Eq.(49) and Eq.(63).

When the strain increment $\Delta\varepsilon_{ij}$ is inputed, the equivalent total strain at time $t+\Delta t$ is calculated by Eq.(31). If $E^{t+\Delta t}$ is smaller than $Emax^t$, this deformational process is the reversible one, therefore, the plastic strain at time $t+\Delta t$ is equal to the plastic strain at time t, and the stress at time $t+\Delta t$ is determined by Eq.(65).

If $E^{t+\Delta t}$ is larger than $Emax^t$, integration parameter r is calculated by Eq.(A-3-4). The stress point D at time $t+r\Delta t$ which corresponds to the strain increment $r\Delta\varepsilon_{ij}$ is calculated with the same flow as that in the reversible process. By resetting the strain increment $(1-r)\Delta\varepsilon_{ij}$ as the strain increment in the irreversible process, the stress invariant vector at time $t+\Delta t$ can be determined according to the calculation flow in Fig.A4. Then, the direction θ is calculated by Eq.(63). With the stress invariant vector and the direction of the maximum principal stress at time $t+\Delta t$, the total stress at time $t+\Delta t$ is calculated by Eq.(37).

The method to calculate the stress invariant vector in the irreversible process is explained in Fig.A4. According to Eq.(49), $(\Delta\bar{\varepsilon}_{on}, \Delta\bar{\gamma}_{on})$ is calculated in the arbitrary strain paths. Solving Eq.(44) and Eq.(47) simultaneously, the direction of the stress invariant vector is

$$\frac{\bar{\sigma}_0^{t+\Delta t}}{\bar{\tau}_0^{t+\Delta t}} = \frac{1+\nu^*}{1-\nu^*}\,\frac{\bar{\varepsilon}_0 + \Delta\bar{\varepsilon}_{on}}{\bar{\gamma}_0 + \Delta\bar{\gamma}_{on}} \qquad \text{(A-3-5)}$$

From the elasto-plastic and fracture equation (35), the equivalent stress at time $t+\Delta t$ is determined as the length of the stress invariant vector. Using the calculation processes above, we can get the direction and the degree of the stress invariant vector. Then, using the definition of equivalent stress, we can determine the stress invariant vector uniquely as Fig.A4.

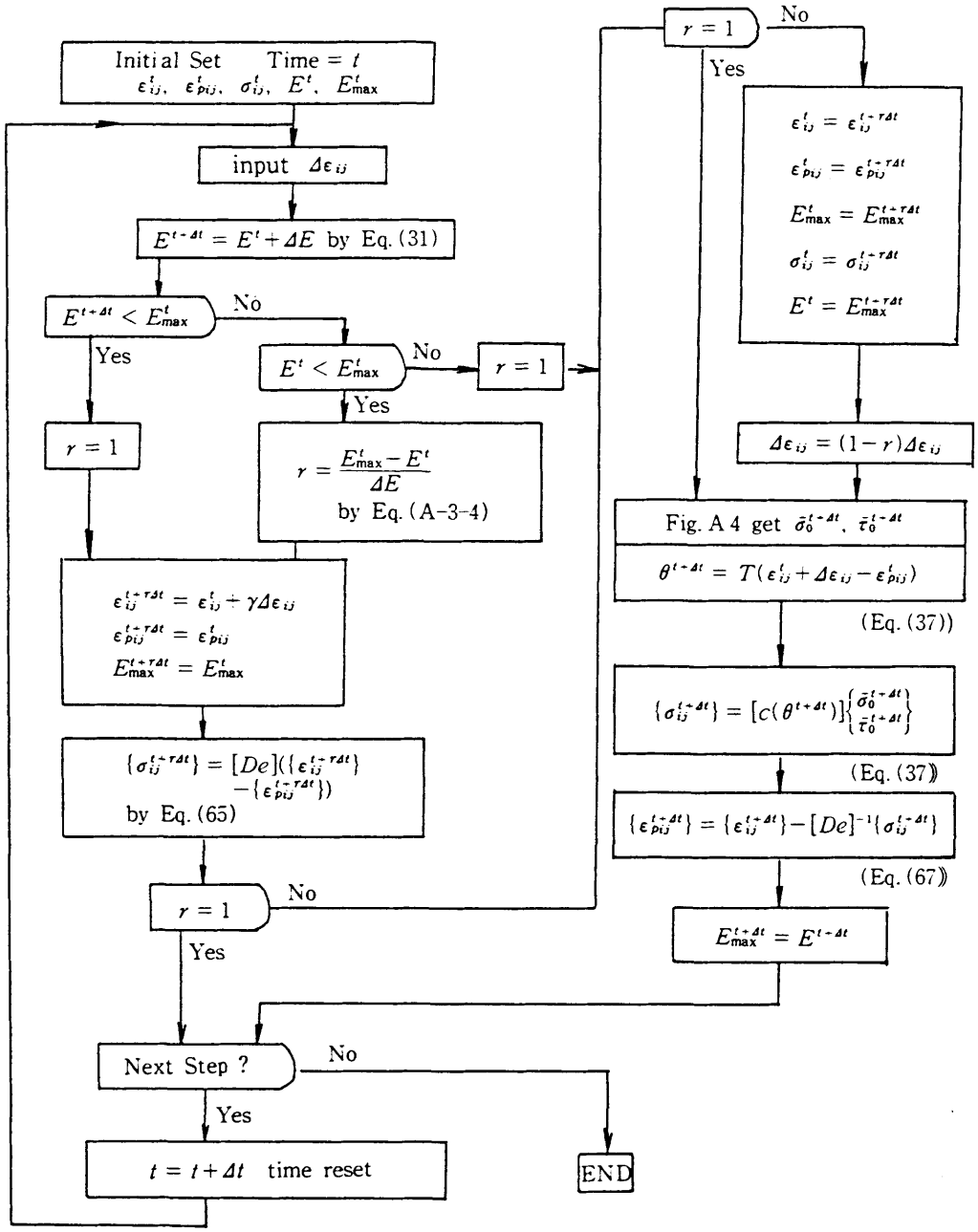

Fig.A3. Calculation flow of evaluating stress vector.

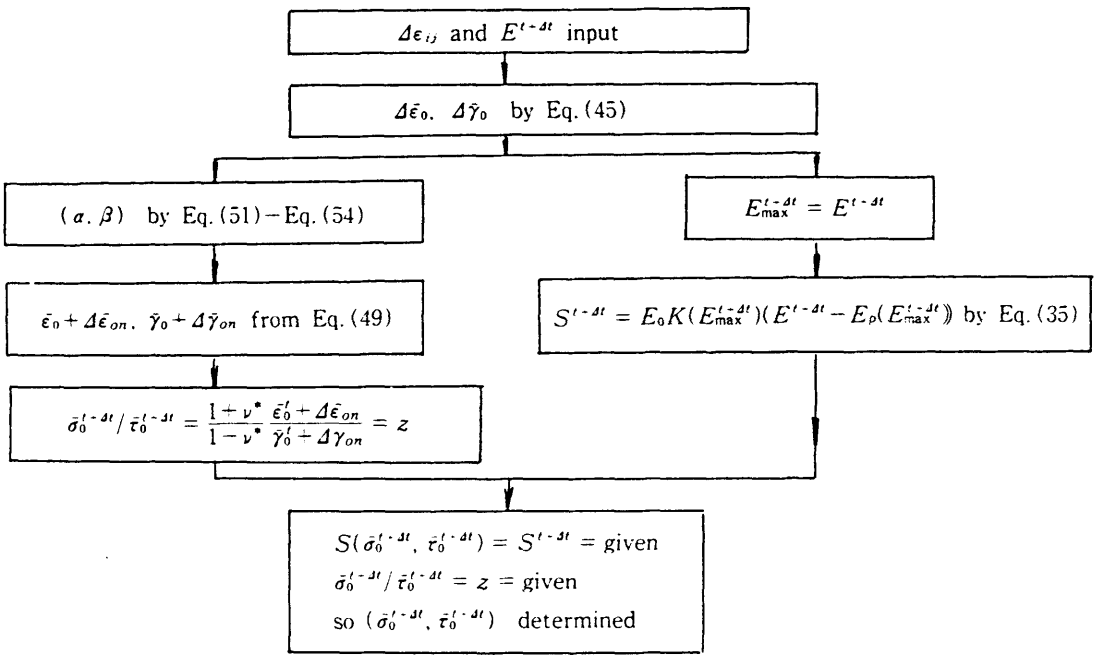

Fig.A4. Calculation method of evaluating stress invariant vector in the irreversible process.